Turbulence modelling and turbulent-flow computation in aeronautics

M. A. Leschziner
Imperial College of Science, Technology and Medicine, University of London, UK

D. Drikakis†
Queen Mary, University of London, UK

From time to time we invite acknowledged experts in a particular field to write a survey article for *The Aeronautical Journal*. Prof Leschziner is such an expert in turbulent flow. For many years he worked with Prof Brian Launder at UMIST before coming first to Queen Mary and Westfield College in London and then more recently to Imperial College. We are delighted to publish the very comprehensive survey article he and Prof Drikakis have prepared. It indicates the tremendous research effort that has gone into trying to understand and model turbulent flows in aeronautics. However, the paper also shows us that there is much, much more to be done before wide-ranging accurate prediction methods can be achieved. Comments on the article would be welcome.

John Stollery, Editor

ABSTRACT

Competitive pressures and economic constraints are driving aircraft manufacturers towards an ever-increasing exploitation of CFD for design, optimisation and prediction of off-design conditions. Such exploitation is favoured by rapid advances in meshing technology, numerical algorithms, visualisation tools and computer hardware. In contrast, the predictive capabilities of mathematical models of turbulence are limited — indeed, are often poor in regions of complex strain — and improve only slowly. The intuitive nature of turbulence modelling, its strong reliance on calibration and validation and the extreme sensitivity of model performance to seemingly minor variations in modelling details and flow conditions all conspire to make turbulence modelling an especially challenging component of CFD, but one that is crucially important for the correct prediction of complex flows.

This article attempts to provide a broad review of the current status of turbulence modelling for aeronautical applications, both from physical and numerical points of view. The review is preceded and underpinned by a discussion of key fundamental issues and processes, based on the exact equations governing the Reynolds stresses. The main body of the review begins with a discussion of all important model categories, starting with algebraic models and ending with Reynolds-stress-transport closures, with emphasis placed on a discussion of the underlying principles in the context of aerodynamic flows. This follows a review of key numerical issues pertaining to the incorporation of turbulence models into advanced computational schemes for compressible and incompressible flows, based on both time-marching and pressure-Poisson solution techniques. The performance of different classes of models is then reviewed by reference to major validation studies undertaken over the past two decades. A discussion of current capabilities in modelling unsteady turbulent flows, especially in the context of dynamic stall and transonic buffet, forms the final element of the review.

1.0 INTRODUCTION

John D. Anderson's fascinating book *A History of Aerodynamics*[1] contains a single substantive entry on turbulence, relating Osborne Reynolds' pioneering work on the 'criterion' for laminar-to-turbulent transition in pipe flow and on the statistical description of turbulence by way of what is now known as 'Reynolds decomposition and averaging'[2]. While the book deliberately avoids technical detail and covers, in the main, the 'pre-scientific' era of man's quest for powered flight, the almost invisible profile of turbulence in the book is not grossly unrepresentative of its position in main-stream aerodynamics, in which most efforts continue to be directed towards maximising lift and minimising drag. This is in stark contrast to fluid mechanics in the context of mechanical, hydraulic and chemical engineering, where turbulent mixing is often the mechanism of principal interest from an operational point of view.

Most aerodynamic flows are associated with fast-moving, slender, streamlined bodies. Such flows are characterised by low curvature, large irrotational ('inviscid') regions in which the motion is dictated by a balance between convection and pressure gradients and relatively thin rotational (sheared) layers. Turbulence is usually only important in the rotational parts — the boundary layers on the surface of the body and the wakes that combine the boundary layers following their separation from trailing edges. Any large-scale vortices shed from wing tips or swept leading edges are essentially

Paper No. 2729. Manuscript received 19 October 2001, revised version received 22 January 2002, accepted 29 January 2002.
This paper was originally published in *The Aeronautical Journal*, July 2002, **106**, (1061), pp 349-384.
As originally published it contained a number of printing errors, these have now been corrected.
†Now at Fluid Mechanics and Computational Science Group, Department of Aerospace Sciences, School of Engineering, Cranfield University.

non-turbulent, except perhaps within their cores which are formed by turbulent boundary-layer fluid. While the fundamental turbulence mechanisms at play might be (indeed, are) complex, the aeronautical engineer is usually only interested in a few global manifestations of turbulence: the skin friction, the displacement thickness of the boundary layer and its effect on the outer irrotational flow, and the momentum defect in the wake. These quantities are essentially dictated by a single statistical turbulence variable — the shear stress in the (local) streamwise direction. Although the determination of this stress is a non-trivial task, the focus on that single quantity, and the fact that the state of turbulence changes only slowly in the flow direction, allows highly simplified modelling approaches to be adopted, which side-step much of the fundamental physics and lean heavily on empirical correlations and calibration. Herein lies the reason for the prevalence and persistence of some especially simple turbulence models in aeronautical practice — models that reduce the turbulence-closure problem to the determination of a scalar eddy viscosity from an algebraic relationship or with the aid of a simple differential equation that takes into account the transport of a representative turbulence parameter.

Notwithstanding the above general categorisation, there are many aeronautical applications in which turbulence plays a much more influential role than in thin shear flows, and which require refined modelling techniques to provide an acceptably realistic predictive description. Many of these flows occur in off-design operational conditions and when the boundaries of the aerodynamic-performance envelope are approached or, indeed, breached. In many cases, separation and recirculation are the key features that require resolution. Specific examples are:

- shock-induced separation on transonic wings, afterbodies and concave ramps and ahead of fins in supersonic flight;
- high-lift and stalled aerofoils — especially multi-element configurations;
- wing-body–fin-body junctions which provoke strong horseshoe vortices and can included separation in the junction;
- vortical separation from streamlined bodies (e.g. fuselage) at high incidence;
- VSTOL flight with vectored jets;
- flow-control applications with vortex generators (e.g. fences or jets);
- dynamic stall in pitching and oscillating aerofoils; and
- under-expanded supersonic jets, with particular emphasis on spreading rate and infra-red visibility.

With the last example excluded, the major practical importance of turbulence arises from the fact that the sheared turbulent regions are sufficiently thick to cause appreciable changes to the irrotational flow around the load-bearing surfaces. In fact, in VSTOL applications, the highly turbulent impinging jets, the ensuing ground vortex and short-circuit associated with hot-gas reingestion are the features of primary concern to the operational performance and safety of the aircraft. In the case of transonic and high-lift wings, the shock or adverse pressure gradient acting on the suction-side boundary layers lead to strong fluid deceleration, rapid boundary-layer thickening and possibly separation, with consequent dramatic loss of lift and increase in drag. The key process in wing–body-junction and vortex-generator flows is the creation of a recirculation zone upstream of the wing or VG and the formation of a horseshoe vortex within which the transverse circulation redistributes streamwise momentum, thus inhibiting separation in the junction or downstream of the vortex generator.

The modelling challenges posed by the types of flow considered above are rooted in the complexity of the strain fields and the high-rates of change to which the flow as well as the turbulence fields are subjected. If attention is initially restricted to statistically steady, two-dimensional conditions, the complex flow features of primary concern are the strong streamwise straining provoked by an adverse pressure gradient (or a shock), separation, reattachment and post-reattachment recovery. All are affected by the details of the turbulence structure, not simply by a single shear stress. The response of the decelerating boundary layer to the adverse pressure gradient, and hence the location of separation, is dictated by the turbulent shear stress ($\rho\overline{uv}$) as well as the normal stresses ($\rho\overline{u}^2$, $\rho\overline{v}^2$). The importance of the normal stresses is due to two interactions: first, the normal stresses are dynamically active (i.e. unlike in thin shear flow, gradients of the normal stresses contribute to the momentum balance); second, the shear stress is sensitive to normal straining and streamline curvature, and, as will be shown later, this linkage occurs via the normal stresses which are themselves sensitive to streamwise, shear and curvature-related straining. Near a wall, turbulence is highly anisotropic, with $\overline{v}^2 << \overline{u}^2$. This anisotropy, induced by a combination of different production rates for the normal stresses and the kinematic blocking effect of the wall, needs to be correctly captured if the shear stress is to be evaluated accurately. As the flow approaches separation, the behaviour of the near-wall layer departs drastically from any universal law of the wall, and its detailed structure must be resolved, including that of the semi-viscous sublayer in which viscosity affects turbulence. Similar comments apply to recirculation and reattachment regions. Thus, here too, the turbulent normal stresses are dynamically active, and the turbulence is sensitive to streamline curvature. A further complication in relation to reattachment is that the turbulent state in this region depends sensitively on the evolution of turbulence in the separated shear layer about to reattach. Finally, the near-wall layer in the recovery region combines the reattached shear layer and a new boundary layer emanating from the reattachment point. This poses the problem of how to deal with component flows containing very different scales, reflecting the different history of these components.

Much of the above discussion also applies to three-dimensional flows, but a number of additional complications require consideration. Many three-dimensional flows feature skewed boundary layers in which the direction of the velocity vector changes rapidly as the wall is approached. Coupled with this 'rotation' are rapid variations in the shear-stress components associated with the shear strains formed with the wall-parallel velocity components (however, they are resolved within the chosen computational co-ordinate system) and the wall-normal co-ordinate. Hence, even in fully attached conditions, and even if the influence of the normal turbulent stresses may be ignored, the task is now one of devising a turbulence closure capable of returning two shear-stress components and their interaction with skewness and curvature. When, in addition, closed or open separation occurs — say, as a result of two boundary layers 'colliding' obliquely in the leeward side of a relatively thick curved body, a boundary layer interacting with a fin or wing or two interacting wall jets associated with twin-jet ground impingement — streamwise vortices are generated, the size of which can be substantially larger than the thickness of the boundary layers prior to their interaction. In such circumstances, the multi-faceted coupling among all stresses and strain components, as well as the interaction between turbulence and the curvature associated with the transverse circulation in the vortex, become influential.

Unsteadiness introduces a fundamental and profound uncertainty into the RANS framework. Reynolds-averaging, whether ensemble- or time-based, presupposes that the flow is statistically steady. At the very least, the time-scale associated with the organised unsteady motion must be substantially larger than the time-scale of the turbulent motion — or, in other words: the two time-scales must be well separated. This condition may be satisfied, say, in low-frequency dynamic stall, but perhaps not in flutter or buffet. From a purely formal point of view, phase-averaging offers a rigorously valid route to deriving a statistical framework for unsteady flow. However, in practice, closure of the (phase-averaged) correlations is necessarily identical or very similar to that adopted for the conventionally averaged correlations, and this inevitably leads to models which are formally identical to their steady counterparts.

Strictly, the only fundamentally secure approach to unsteadiness is via direct numerial simulation which resolves the entire spectrum of turbulent motions in all details. However, at Reynolds numbers perti-

nent to aerodynamic practice, the resource implications even of large eddy simulations is prohibitive. A decisive element in the resource equation is the fact that most turbulent aerodynamic flows occur close to walls and are therefore strongly affected by viscous processes. However, near a wall, the 'large', dynamically influential turbulent scales are small, so that very dense meshes are required for a reasonable resolution of the flow. To give an example, one conclusion emerging from the recent EU project LESFOIL[3], which investigated LES for high-lift aerofoils, is that the simulation of the marginally separated, transitional flow around a single-element, high-lift aerofoil at $Re = 2 \times 10^6$ (based on chord) would require of order 100 million nodes for a spanwise extent of only 10% of chord. These resources are dramatically beyond what is economically tolerable in practice.

On the assumption that conventional turbulence models may be applied to (a restricted range of) unsteady flows, the level of closure may have important implications to predictive accuracy. Unsteadiness increases the rate of change of all flow quantities and results, in particular, in a phase lag between the mean motion and the turbulence quantities. A relevant parameter to consider is the ratio of the time scales of the mean motion $\Omega k/\varepsilon$, where k is the turbulence energy and ε is its rate of dissipation and Ω is the frequency of the mean motion. As the boundary layer is traversed towards the wall, this ratio declines rapidly, given a fixed frequency of mean-flow oscillation. The implication is that the turbulence structure close to the wall will adjust rapidly to the external oscillation, so that a quasi-steady turbulence closure would be expected to be adequate. However, towards the outer part of the boundary layer, the turbulence field will not respond quickly to the oscillation, and the turbulent stresses would tend to 'freeze', with a consequent phase shift between the mean motion and the turbulence field. To take this into account, a turbulence model needs to include stress transport. Hence, unsteady flows can, in general, be expected to benefit from second-moment closure, which entails a reduced level of reliance on equilibrium assumptions.

The above considerations, while far from comprehensive, should suffice to justify the assertion that turbulence and turbulence modelling are important topics within the spectrum of subjects constituting modern aerodynamics. The increasing reliance of aerodynamic design and optimisation on accurate computational prediction methods, especially in multi-component configurations and high-load and off-design conditions, makes it imperative that appropriate turbulence models are used in combination with accurate and efficient numerical schemes which can cope with the complex, highly non-linear mathematical elements of some of these models. The adjective 'appropriate' is not necessarily synonymous with 'most advanced' or 'most general'. The essential point is that the capabilities and limitations of different models are understood and that their suitability for particular flows or classes of flows is appreciated. To this end, the very first step that needs to be made is to elucidate the fundamental interactions between turbulence and different flow features, especially in terms of statistical quantities.

The present paper aims to provide an up-to-date review of the current state-of-the-art of turbulence modelling for aeronautical applications. The elucidation of the links between the turbulent stresses and the mean flow is pursued in Section 2. This provides a foundation for a review, in Section 3, of major modelling methodologies and model categories, in terms of their rationale, calibration, range of application and limitations. Section 4 then considers numerical methodologies, with particular emphasis placed on the efficient implementation of turbulence models. Section 5 reviews model performance for a range of applications. In the case of statistically steady flow, the discussion is model-oriented; that is, the capabilities of different model classes are examined for different flow conditions and features. Unsteady flows are discussed separately, in view of their rather special position within the RANS field and the relative scarcity of related computational applications focusing on turbulence-model performance.

2.0 FUNDAMENTALS OF STRESS-STRAIN INTERACTIONS

The task of a turbulence model is to provide the Reynolds-averaged Navier-Stokes equations with closure relations for the Reynolds stresses $\rho\overline{u_i u_j} \equiv \{\rho\overline{u^2}, \rho\overline{v^2}, \rho\overline{w^2}, \rho\overline{uv}, \rho\overline{uw}, \rho\overline{vw}\}$, where the left-hand side is the Cartesian tensor representation of the stresses ($i, j = 1, 2, 3$)†. 'Closure' identifies the process by which the stresses are related to known or determinable quantities: geometric parameters, flow scales and strains. The strains play an especially prominent role in the closure process, for they are the primary agency by which turbulence is generated and sustained. An indication of the importance attached to this linkage is provided by the Boussinesq stress-strain relationship:

$$-\rho\overline{u_i u_j} = \mu_t\left(\frac{\partial U_i}{\partial x_j}+\frac{\partial U_j}{\partial x_i}-\frac{2}{3}\frac{\partial U_k}{\partial x_k}\delta_{ij}\right)-\frac{2}{3}\rho k\delta_{ij} \qquad \ldots (1)$$

in which μ_t is the eddy viscosity, $\mathbf{U_i} = \{U, V, W\}$ is the velocity vector, $\mathbf{x_i} = \{x, y, z\}$ are the spatial co-ordinates, ρ is the density, δ_{ij} is the Knoecker delta — a unit tensor with unit diagonal and zero off-diagonal elements — and $k = 0{\cdot}5(\overline{u^2} + \overline{v^2} + \overline{w^2})$ is the (kinematic) turbulence energy. The right-most term in Equation (1) is required to ensure that the normal stresses sum up to $2k$ in zero strain. For incompressible flow, $\partial U_k/\partial x_k = 0$. Although the relationship in Equation (1) has serious defects, as will emerge shortly, it expresses the basic fact that the level of turbulence activity (mixing) is intimately associated with straining. It must be said, however, that turbulence generally reacts slowly to external disturbances (including straining), a fact inconsistent with the proposal in Equation (1).

An excellent basis for illuminating the interactions between stresses and strains is the set of exact equations governing the evolution of the Reynolds stresses. This is also the best starting point for constructing turbulence models which hold some promise of generality — a subject considered later. The equations can be derived by a somewhat laborious, though otherwise straightforward, combination of the Navier-Stokes equations and their Reynolds-averaged forms. For present purposes, it is instructive to focus on simplified sets of equations applicable to two particular incompressible flows: simple shear, in which the only major strain is $\partial U/\partial y$, and homogeneous compression, in which $\partial U/\partial x = -2\partial V/\partial y = -2\partial W/\partial z$ is some prescribed (negative) value. Both are 'model flows' — the former representing any slowly evolving zero-curvature shear layer, and the latter a decelerating flow approaching a stagnation point. The effect of additional features, such as curvature, rotation and wall-blockage, will be considered later. The respective sets of equations for the relevant (kinematic) stresses and the turbulence energy k are Equations (2) and (3). In each equation, the left-handside is the evolution (rate-of-change) term, while the right-handside terms represent, in that order, generation, pressure-strain interaction, turbulent diffusion and dissipation by viscous destruction. One minor approximation which has been introduced into Equations (2) and (3) relates to the dissipation. This process occurs at the smallest scales of turbulence (the smallest eddies) and is assumed to be isotropic — that is: $\varepsilon_{\overline{u^2}} = \varepsilon_{\overline{v^2}} = \varepsilon_{\overline{w^2}} = {}^2/_3\varepsilon$, $\varepsilon_{\overline{uv}} = 0$, where ε is the rate of turbulence-energy dissipation.

†More generally, the model must also provide relations for turbelent heat and species fluxes which arise in the Reynolds-averaged energy and species-concentration equations.

$$\frac{D\overline{uv}}{Dt} = -\overline{v^2}\frac{\partial U}{\partial y} + \overline{\frac{p}{\rho}\left(\frac{\partial u}{\partial y}+\frac{\partial v}{\partial x}\right)} - \frac{\partial}{\partial y}\left(\overline{uv^2}+\frac{\overline{pu}}{\rho}\right) - 0$$

$$\frac{D\overline{u^2}}{Dt} = -2\overline{uv}\frac{\partial U}{\partial y} + 2\overline{\frac{p}{\rho}\frac{\partial u}{\partial x}} - \frac{\partial}{\partial y}\left(\overline{u^2v}\right) - \frac{2}{3}\varepsilon$$

$$\frac{D\overline{v^2}}{Dt} = 0 + 2\overline{\frac{p}{\rho}\frac{\partial v}{\partial y}} - \frac{\partial}{\partial y}\left(\overline{v^3}+\frac{2\overline{pv}}{\rho}\right) - \frac{2}{3}\varepsilon \qquad \ldots (2)$$

$$\frac{D\overline{w^2}}{Dt} = 0 + 2\overline{\frac{p}{\rho}\frac{\partial w}{\partial z}} - \frac{\partial}{\partial x}\left(\overline{vw^2}\right) - \frac{2}{3}\varepsilon$$

$$\frac{Dk}{Dt} = -\overline{uv}\frac{\partial U}{\partial y} + 0 - \frac{\partial}{\partial y}\left(\overline{uk}+\frac{\overline{pu}}{\rho}\right) - \varepsilon$$

$$\frac{D\overline{u^2}}{Dt} = \overline{2u^2}\frac{\partial U}{\partial x} + 2\overline{\frac{p}{\rho}\frac{\partial U}{\partial x}} - \frac{\partial}{\partial x}\left(\overline{u^3}+2\frac{\overline{pu}}{\rho}\right) - \frac{2}{3}\varepsilon$$

$$\frac{D\overline{v^2}}{Dt} = \overline{v^2}\frac{\partial U}{\partial x} + 2\overline{\frac{p}{\rho}\frac{\partial v}{\partial y}} - \frac{\partial}{\partial x}\left(\overline{uv^2}\right) - \frac{2}{3}\varepsilon \qquad \ldots (3)$$

$$\frac{D\overline{w^2}}{Dt} = \overline{w^2}\frac{\partial U}{\partial x} + 2\frac{p}{\rho}\frac{\partial w}{\partial z} - \frac{\partial}{\partial w}\left(\overline{uw^2}\right) - \frac{2}{3}\varepsilon$$

$$\frac{Dk}{Dt} = -\frac{1}{2}\left(\overline{2u^2}-\overline{v^2}-\overline{w^2}\right)\frac{\partial U}{\partial x} + 0 - \frac{\partial}{\partial x}\left(\overline{uk}+\frac{\overline{pu}}{\rho}\right) - \varepsilon$$

From set (2) it is observed first that, in simple shear, the only normal stress generated by the shear strain is $\overline{u}^2$. The other normal stresses are only finite because they receive a proportion of the turbulence energy contained in $\overline{u}^2$ via the redistributive pressure-strain process, which tends to steer turbulence towards isotropy, $\{\overline{u}^2, \overline{v}^2, \overline{w}^2\} \rightarrow {}^2/_3k$, and does not contribute to the turbulence energy. This 'rich-poor' relationship is the reason that sheared turbulence is strongly anisotropic, with $\overline{u}^2 = O(3\overline{v}^2) = O(2\overline{w}^2)$. Set (2) further shows that the shear stress — the quantity of primary interest — is generated by an interaction between the cross-flow normal stress $\overline{v}^2$ and the shear strain. This highlights the need to determine $\overline{v}^2$ accurately — that is, a good model will have to return a realistic description of anisotropy. Because of the assumption that turbulence is isotropic in the smallest scales (a good approximation at high Reynolds numbers, away from walls), there is no dissipative mechanism for the shear stress. However, the pressure-strain term provides a 'sink' for that stress, which counteracts generation in harmony with the isotropisation process; simple stress-balance considerations (analogous to Mohr's circle in Solid Mechanics) serve to show that the shear stress must decline and eventually vanish as the normal stresses approach a single value.

Here, it is interesting to note that the above relationship between $\overline{uv}$ and $\partial U/\partial y$ provides some justification for the eddy-viscosity relation (1), applied to the shear stress

$$-\overline{uv} = \nu_t\frac{\partial U}{\partial y} \qquad \ldots (4)$$

if ν_t is evaluated from $\nu_t \propto \overline{v}^2 \times$ (turbulent time scale) — a combination implying that the shear stress is proportional to its rate of generation, with the turbulent time scale (say, k/ε) providing dimensional consistency. The same cannot be said, however, for the eddy-viscosity relation applied to the normal stresses:

$$-\overline{u^2} = \nu_t\frac{\partial U}{\partial x} - \frac{2}{3}k, \quad -\overline{v^2} = \nu_t\frac{\partial V}{\partial y} - \frac{2}{3}k \qquad \ldots (5)$$

which are contrary to reality†, as expressed by set (2), and give identical values for the normal stresses, namely ${}^2/_3k$.

Set (3) shows first that stagnation (deceleration) tends to elevate the normal stress due to the (positive) generation $-2\overline{u}^2\partial U/\partial x$, and to diminish the other two stresses, due to negative generation rates $\overline{v}^2\partial U/\partial x$ and $\overline{w}^2\partial U/\partial x$, respectively, thus causing substantial anisotropy. Both effects are consistent, at least in principle, with the eddy-viscosity relations. However, in quantitative terms, these relations provide a far too rigid linkage between the stresses and strain. One reason is that the convective terms — the left-hand sides of the equations in set (3) — are substantial and tend to depress the rate of change in the stresses; in effect, there is a tendency for the stresses to be 'frozen' so that the rate of their generation is not far from linearly dependent on the strain. This is not an issue in simple shear strain for which stress convection is insignificant. As a consequence, the rate of turbulence-energy production is also close to being proportional to the strain. That this behaviour is incompatible with the eddy-viscosity concept becomes clear when the stresses in the production terms of set (3) are replaced by the eddy-viscosity relations:

$$P_{\overline{u^2}} = 4\nu_t\left(\frac{\partial U}{\partial x}\right)^2 - \frac{2}{3}k\frac{\partial U}{\partial x}$$

$$P_{\overline{v^2}} = \nu_t\left(\frac{\partial U}{\partial x}\right)^2 + \frac{1}{3}k\frac{\partial U}{\partial x}$$

$$P_{\overline{w^2}} = \nu_t\left(\frac{\partial U}{\partial x}\right)^2 + \frac{1}{3}k\frac{\partial U}{\partial x} \qquad \ldots (6)$$

$$P_k = 3\nu_t\left(\frac{\partial U}{\partial x}\right)^2$$

Set (6) reveals two major problems: first, the effect of the strain on all normal stresses is to elevate them, irrespective of the sign of the strain; second, as a result of the former, the production of turbulence energy is seriously overestimated because all contributions are unconditionally positive and quadratic in the strain. This constitutes a major defect in the eddy-viscosity framework and is responsible for serious predictive errors in normally straining flows — for example, a boundary layer approaching separation or an obstacle.

With some first lessons having been extracted from considerations for simple shear and normal strain, it is next instructive to broaden the range of flow features to include curvature and wall-blockage. The objective is to cover at least the majority of the key elemental interactions which combine to give practically relevant flows.

Considered first is the response of turbulence to the addition of curvature to shear. This is pertinent to a curved boundary layer, a curved shear layer following separation or a shear layer embedded in a vortex. In a two-dimensional, curved, thin shear layer, in which the primary shear strain is $\partial U/\partial y$, the Reynolds-stress transport equations yield the production rates of the shear stress and cross-flow normal stress, respectively, as:

$$P_{\overline{uv}} = -\overline{v^2}\frac{\partial U}{\partial y} - \overline{u^2}\frac{\partial V}{\partial x} \qquad \ldots (7)$$

$$P_{\overline{v^2}} - 2\overline{uv}\frac{\partial V}{\partial x}$$

where the secondary strain $\partial V/\partial x$ expresses streamline curvature. In any shear layer, normal-stress anisotropy is high, since the only normal stress generated by shear is that aligned with the streamwise direction. In a wall-bounded shear layer, $\overline{v}^2$ is especially low — typically, of order $0{\cdot}2\overline{u}^2$ — because of wall-blockage effects

†Note also that Equation (5) can yield negative normal stresses at high strains — an unphysical state which renders the approximations 'non-realisable'.

(see later). It is thus evident that curvature strain in a boundary layer has a disproportionately large influence on the level of shear-stress production and hence on the shear stress itself. In the case of a boundary layer on a convex wall, the curvature strain is negative, and the overall result is a considerable attenuation in the shear stress. This attenuation is further accentuated by the fact that convex curvature tends to reduce $\overline{v}^2$ relative to $\overline{u}^2$. This emerges from Equation (7) upon noting that the shear stress and the curvature strain are both negative in a convex boundary layer, so that the production $P_{\overline{v}^2}$ is negative. Precisely the opposite arises in concave boundary layers, in which turbulence is amplified by curvature. Dramatic demonstrations of the major changes curvature can cause, via turbulence, even to the primary mean-flow characteristics are given by Jones and Manners[4] and Lai[5], both in relation to the flow in a curved, faired diffuser.

The origin of anisotropy in a free shear layer has previously been identified by reference to the Equation set (2). It has also been stated, in relation to curvature effects, that wall-blockage tends to substantially increase the level of anisotropy at a wall. This may be demonstrated by using Taylor-series expansions, in terms of wall distance, for the turbulent velocity components

$$u_k = a_k(t)\,y + b_k(t)\,y^2 + c_k(t)\,y^3 \ldots \quad u_k = (u,v,w) \qquad \ldots (8)$$

and then by examining the asymptotic variation of the stresses formed by appropriate auto- or cross-multiplication of the appropriate Taylor series, followed by time-averaging. In Equation (8), the coefficients *a, b, c…* are functions of time corresponding to the time-dependence of the turbulent velocity components u_k. An additional constraint arising from the continuity principle is $\partial u_2/\partial y = 0$, so that, for the u_2 component, the lowest-order term in Equation (8) is quadratic in *y*. This then leads to:

$$\begin{aligned}
\overline{u^2} &= \overline{a_u(t)^2}\,y^2 + \ldots \\
\overline{v^2} &= \overline{b_v(t)^2}\,y^4 + \ldots \\
\overline{w^2} &= \overline{a_w(t)^2}\,y^2 + \ldots \\
\overline{uv} &= \overline{a_u(t)^2\,b_v(t)}\,y^3 + \ldots
\end{aligned} \qquad \ldots (9)$$

Hence, the wall-normal stress $\overline{v}^2$ must decay much faster than the other normal stresses (as well as *k*) — a process that increases the level of anisotropy. Typical wall-normal variations of the Reynolds stresses in a channel flow at a Reynolds number of 6,600, based on maximum velocity and channel height, are given in Fig. 1. The DNS data may safely be taken to represent the anisotropy faithfully. The figure also illustrates dramatic variations in the ability of different models to return the stresses correctly, especially the normal components. As might be expected, models based on the direct closure of set (2) — i.e. Reynolds-stress-transport models — perform especially well. At the other extreme, linear eddy-viscosity models return here identical normal stresses (= $^2/_3 k$, see Equation (5)), as does the '$k - \varepsilon$' model in Fig. 1. The subject of model performance will be considered later in the context of related closure strategies.

Equation (8) also allows a statement to be extracted on the variation of the turbulent viscosity, as well as quantities such as dissipation rate, pressure-strain correlations and diffusion terms, as given in sets (2) and (3). For example, for the viscosity, defined as

$$\nu_t \frac{\overline{uv}}{\partial U / \partial y} \qquad \ldots (10)$$

and with $\overline{uv}|_{y \to 0} = O(y^3)$, $(\partial u/\partial y)|_{y \to 0} = O(1)$, it follows that the viscosity must decay cubically as the wall is approached.

3.0 TURBULENCE MODEL CATEGORIES

3.1 General overview

There are three principal classes of models currently used in computations of practically relevant aerodynamic flows:

- linear eddy-viscosity models (LEVM);
- non-linear eddy-viscosity models (NLEVM);
- Reynolds-stress models (RSM).

Some models do not fall neatly into any one of the above categories, straddling two categories or containing elements from more than one category. Thus,

- explicit algebraic Reynolds-stress models (EARSM) combine elements of NLEVM and RSTM;
- the 'V2F' model of Durbin[6] (see also Parneix *et al*[7]) is essentially a LEVM, but incorporates a simplified transport equation for the normal stress perpendicular to streamlines (or the wall), which serves as the turbulent velocity scale in the eddy-viscosity, in preference to the turbulence energy.

Other model types exist, but have not been used to any significant extent for practical computations. These include:

- the 'Structure-Based Model' of Kassinos *et al*[8];
- various model proposals derived from two-point correlation functions (e.g. Cambon and Scott[9]).
- Multi-scale models which are based on a partitioning of the turbulence-energy spectrum, each partition associated with a different size range of eddies (e.g. Schiestel[10], Wilcox[11]).

Within any one of the above major categories, there are dozens of variants, and the LEVM category, being the simplest, contains several sub-categories (see Section 3.2 below) and is especially heavily populated with model variations, many differing from other forms by the inclusion of minor (though sometimes very influential) 'correction terms', or different functional forms of model coefficient, or even through slight differences in the numerical values of model constants. To a considerable degree, this proliferation reflects a trend towards adopting or adhering to simple (too simple) turbulence models for the modelling task at hand and then adding 'patches' so as to 'cure' specific ills for specific sets of conditions. Other not unimportant contributory factors are insufficiently careful and excessively narrow validation, yielding misleading statements on the predictive capabilities of existing models, and the fact that publishing a 'new' model, rather than a study quantifying the capabilities of an existing model, is not only easier, but also gives greater prominence to the originator whose name is customarily attached the model. The subsections to follow review models in the top five categories listed above.

3.2 Linear eddy-viscosity models

3.2.1 Introductory considerations

All models in this category are based on the linear stress-strain relationship (1). All are therefore afflicted with the defects identified in Section 2, almost irrespective of how the eddy viscosity is evaluated. Thus,

- they do not resolve normal-stress anisotropy (see Fig. 1);
- they do not account for transport of stresses (by convection and diffusion — see sets (2) and (3)), but link rigidly the stresses to the strain;
- they over-estimate the stresses at high strain rates;
- they do not respond correctly to curvature strain, normal straining and rotation (though *ad hoc* patches help in some circumstances);
- they are appropriate for flows in which a single shear stress is the dominant, dynamic link between turbulence and the mean-flow;
- they seriously misrepresent, when used in conjunction with eddy-diffusivity/gradient-diffusion approximations, the heat fluxes, except for the flux component normal to simple shear layers with a dominant cross-layer temperature gradient.

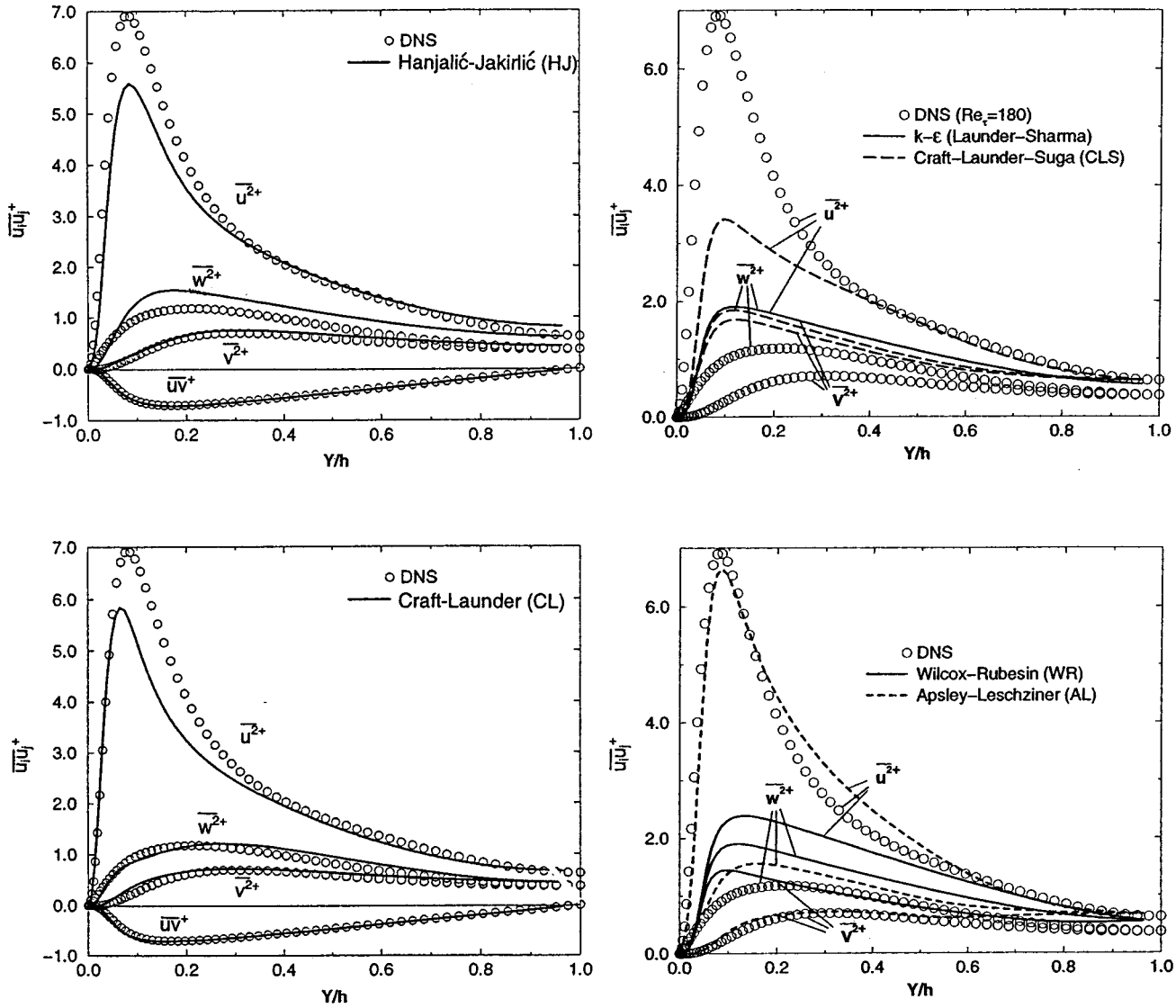

Figure 1. Turbulent stresses in fully-developed channel flow at mean-flow Reynolds number of 6,600; LHS: comparisons between DNS data and two Reynolds-stress-transport models (taken from Batten *et al*[77]); RHS: comparisons between DNS data and three non-linear eddy-viscosity models (taken from Loyau *et al*[141]).

The fact that many aerodynamic flows involve rather thin, slowly evolving shear layers, in which the shear stress is the only dynamically active component, has given strong impetus to the use of linear eddy-viscosity models in aerospace CFD. Indeed, the approaches adopted to determining the eddy viscosity have also been especially simple, often based on Prandtl's[12] and von Karman's[13] mixing-length theory, dating back to 1925:

$$\nu_t = l_m^2 \left| \frac{dU}{dy} \right|; \; l_m = \kappa y; \; \kappa = 0{\cdot}41 \qquad \ldots (11)$$

with the above particular form of l_m applicable to the fully turbulent near-wall (log-law) region. Within the semi-viscous sublayer ($y^+ \lesssim 50$), l_m needs to be multiplied by a 'van Driest damping function' of the form:

$$f_{\nu} = 1 - e^{-\frac{y^+}{A^+}}; \; y^+ \equiv \frac{y\sqrt{\tau_w/\rho}}{\nu} \qquad \ldots (12)$$

An important limitation of Equation (11) is that it implies negligible transport of turbulence — that is, the state of turbulence is implicitely held to be entirely dictated by a local balance between turbulence-energy production and dissipation (see last equation in set (2)):

$$-\overline{uv}\frac{\partial U}{\partial y} = \varepsilon \qquad \ldots (13)$$

which is referred to as 'local equilibrium'. The above equivalence can be elucidated upon noting that dimensional reasoning suggests:

$$\varepsilon \propto \frac{k^{3/2}}{l_m} \qquad \ldots (14)$$

while experiments show that in the log-law region:

$$-\overline{uv} \approx 0{\cdot}3k \qquad \ldots (15)$$

Substitution of Equations (14) and (15) into Equation (13) gives:

$$\left|\overline{uv}\right| \propto l_m^2 \left(\frac{\partial U}{\partial y} \right)^2 \qquad \ldots (16)$$

which is evidently consistent with Equation (11). Combining Equations (13) and (15) also yields,

$$\frac{k}{\varepsilon}\frac{\partial U}{\partial y} \approx 3 \cdot 3 \qquad \ldots (17)$$

Hence, local equilibrium implies that the turbulence time scale (k/ε) is a fixed factor of the mean-flow time scale.

Models closely related to Equation (11) are those of Cebeci and Smith[14] and Baldwin and Lomax[15]. The latter — an improvement of the former — has been especially popular for modelling attached aerodynamic flows, but has often been misused in separated shear layers. Differences relative to Equations (11) and (12), introduced in relation to the 'inner' near-wall layer, include the use of the mean vorticity in place of the strain (immaterial in simple shear) and the addition of an 'outer'-layer (wake) eddy-viscosity approximation of the form:

$$\nu_{to} = C F_{Kleb} F_{Wake} \qquad \ldots (18)$$

where C is a constant, F_{Kleb} is the Klebanoff intermittency function and F_{Wake} is the wake parameter which is related to the position at which the moment of absolute vorticity $y|\Omega|$ reaches a maximum. Switching between the inner- and outer-layer formulations is effected at the position at which the inner and outer eddy viscosities reach the same value. A correction to Baldwin and Lomax's outer-layer formulation was suggested by Granville[16]. An *ad hoc*, empirical patch to the Baldwin-Lomax model (or any other algebraic formulation), intended to account for separation, was proposed by Goldberg[17], but is entirely unrelated to any fundamental physics associated with the dynamics of separation.

As algebraic models of the above type are not appropriate for any but simple attached boundary layers, close to the state of equilibrium, and depend upon an explicit prescription of the viscosity on the basis of the distance from the wall, they are now regarded as outdated and are not considered further herein.

Algebraic models are also referred to as 'zero-equation' models. This designation identifies the fact that no transport equation is used to determine the turbulent viscosity. More advanced classes of eddy-viscosity models, referred to as 'one-equation' and 'two-equation' models, use, respectively, one differential equation or two to describe the evolution of related turbulence scales from which the eddy viscosity is evaluated. There is also a class designated 'one-half-equation' models, because they combine a mixing-length-type prescription across the flow with an ordinary differential equation describing the streamwise evolution of the cross-flow maximum shear stress to which the eddy-viscosity is related.

The relationship between the eddy viscosity and other scales emerges from dimensional considerations. Thus, dimensional analysis shows:

$$\nu_t \propto u' L \qquad \ldots (19)$$

where u' is a turbulent velocity scale and L is a turbulent length scale (eg the mixing length). The velocity scale is almost invariably chosen to be $k^{1/2}$ which is determined from a differential transport equation. Unless the length scale is prescribed algebraically — as is the case with one-equation models — a length-scale surrogate is usually used, rather than L itself, the most popular surrogate variables being the dissipation rate $\varepsilon = k^{3/2}/L$, the turbulent vorticity (or specific dissipation rate) $\omega = \varepsilon/k = k^{1/2}/L$ and the turbulence time scale $\tau = k/\varepsilon = L/k^{1/2}$. Other variables adopted include the turbulence enstrophy $\zeta = \omega^2$, the root of the turbulent time scale $g = \tau^{1/2}$, the turbulence Reynolds number $R_t = k^2/\nu\varepsilon$ and the groups $\varepsilon/k^{1/2}$ and kL. The rationale for choosing some of these variables in preference to others will be considered later.

3.2.2 One-equation models

One-equation models involve the solution of a single differential transport equation for a selected turbulence variable. In most models that variable is the turbulence energy, but other quantities chosen include the eddy viscosity, the turbulent Reynolds number (effectively, the ratio of turbulent-to-fluid viscosity) and even the shear stress itself. With isolated exceptions, one-equation models require, either directly or indirectly, a prescription of the length scale or a related quantity. This requirement is nearly as severe a limitation as that applicable to algebraic models, and one-equation models do not, therefore, generally display decisively superior predictive characteristics in wall flows departing substantially from equilibrium, unless specifically crafted by highly targeted calibration (e.g. via forcing functions) for such conditions. While accounting for non-equilibrium processes to some extent, models that rely on a length-scale prescription are not applicable to separated flows in which there is no general or known relationship between the length scale and the distance from the wall.

If k is chosen as the transported turbulence quantity, then the differential equation adopted is:

$$\frac{\partial k}{\partial t} + \frac{\partial U_j k}{\partial x_j} = \frac{\partial}{\partial x_j}\left(\nu + \frac{\nu_t}{\sigma_k}\right)\frac{\partial k}{\partial x_j} + P_k - \varepsilon \qquad \ldots (20)$$

This is a general form of the last equation in set (2) and arises upon a summation of the exact Reynolds-stress-transport equations (see later) for the normal stresses and a replacement of the exact diffusion term (which contains unknown triple correlations $\overline{u_j u_k u_k}$ and $\overline{u_j p}$) by a gradient-diffusion model, with σ_k being the turbulent Prandtl /Schmidt number for k.

Next, ε is replaced by $\varepsilon = k^{3/2}/L$ (see Equation (14)). It can readily be shown that a combination of $c_\mu \equiv (-\overline{uv}/k)^2 = 0{\cdot}09$ (see Equation (15)) and the equilibrium relations imply:

$$\varepsilon = \frac{k^{3/2}}{c_\mu^{-3/4} l_m} \qquad \ldots (21)$$

$$\nu_t = c_\mu^{1/4} k^{1/2} l_m \qquad \ldots (22)$$

There is no compelling reason, however, why the length scale in Equations (21) and (22) need to be identical. Specific variations were adopted by different modellers on the basis of calibration against experimental data for key flows, such as channel and boundary-layer flows. Thus, in Wolfshtein's model[18]:

$$l_\nu = \kappa y\left(1 - e^{-0{\cdot}016\, y^*}\right), \quad l_\varepsilon = \kappa y\left(1 - e^{-0{\cdot}263 y^*}\right) \qquad \ldots (23)$$

while Norris and Reynolds[19] propose:

$$l_\nu = \kappa y\left(1 - e^{-0{\cdot}0198\, y^*}\right), \quad l_\varepsilon = \kappa y_n \frac{y^*}{y^* + 2\kappa / c_\mu^{3/4}} \qquad \ldots (24)$$

where $y^* \equiv (y c_\mu^{1/4} k^{1/2})/\nu$. The use of y^* instead of y^+ in Equations (23) and (24) is not a trivial matter. This replacement is enabled by the availability of k and use of Equation (13) in conjunction with the replacement $u_\tau \leftarrow (\overline{uv})^{1/2}$. The advantage arising therefrom is that, in non-equilibrium conditions (e.g. adverse pressure gradient), the state of the semi-viscous sublayer does not scale well with u_τ, but does so much better with $k^{1/2}$.

A third model of the above type is that of Hassid and Poreh[20]. This is, essentially, a corrected version of the Wolfshtein model and reflects the recognition that, at the wall, the rate of dissipation must be balanced by viscous diffusion of turbulence energy:

$$\varepsilon\big|_{y\to 0} = \nu \left.\frac{\partial^2 k}{\partial y^2}\right|_{y\to 0} \qquad \ldots (25)$$

As k varies quadratically as the wall is approached (see Equation (9)), it follows that ε is finite at the wall, namely $\varepsilon|_{y\to 0} = (2k\nu/y^2)|_{y\to 0}$.

A model by Mitcheltree *et al*[21] is yet another form closely akin to that of Wolfshtein, but includes an extension intended to accommodate separation. The extension leans heavily on experimental observations of some similarity characteristics of the velocity profile within the separated region. These are used to derive length-scale prescriptions for the separated region equivalent to Equations (23) and (24) (though without the damping terms) with pre-multiplying coefficients which vary with the streamwise direction and depend upon the (y-wise) maximum turbulence energy, the maximum strain rate (or rather vorticity), the y-location of this maximum and the y-location of the shear-stress maximum. When applied to the computation of shock-induced separation over the RAE 2822 aerofoil (Cook *et al*[22], Case 10, the model is not found to give adequate results for either shock location or pressure coefficient.

Models by Baldwin and Barth[22], Spalart and Allmaras[24], Menter[25] and Goldberg[26] are based on the solution of transport equations for the turbulent Reynolds number $R_t = k^2/\nu\varepsilon$ or the turbulent viscosity, both quantities being closely related to each other. The model of Menter will be considered at the very end of this section, for reasons that will transpire in due course. The first model is derived by a combination of the k- and ε-transport equations (see next section), followed by simplifications applicable to equilibrium conditions (Equation (13)) and some calibration by reference to the algebraic Cebeci-Smith model. The result is an equation of the form:

$$\frac{\partial \nu R_t}{\partial t} + \frac{\partial U_j \nu R_t}{\partial x_j} = C_1\sqrt{\nu R_t P_k} + \left(\nu + \frac{\nu_t}{\sigma_R}\right)\frac{\partial^2(\nu R_t)}{\partial x_j^2} - C_2\frac{\partial \nu_t}{\partial x_j}\frac{\partial \nu R_t}{\partial x_j} \quad \ldots (26)$$

from which the viscosity is then evaluated as:

$$\nu_t = c_\mu \nu R_t f_{\mu 1} f_{\mu 2} \quad \ldots (27)$$

where $f_{\mu 1}$ and $f_{\mu 2}$ are van Driest damping functions involving y^+. One advantage of this model is that it avoids an explicit prescription of the length scale, although it does involve, explicitely, the distance from the wall in the damping functions. This last restriction was removed by Goldberg[27] who proposed a point-wise ('local') version of the model which, for high Reynolds-number flows, is identical to Baldwin and Barth's parent form.

Spalart and Allmaras derived their model along much more intuitive, less formal lines than Baldwin and Barth, and rely heavily on calibration by reference to a wide range of experimental data. The model is built up in several stages, starting from a version for free flows and extending this to near-wall flows at high and then low Reynolds numbers, each stage involving calibration by reference to key flows (mixing layers, wakes, flat-plate boundary layers). The high-Reynolds-number version of the viscosity equation for near-wall flows has the form:

$$\frac{\partial \nu_t}{\partial t} + \frac{\partial U_j \nu_t}{\partial x_j} = C_1 \nu_t S + \frac{1}{\sigma}\frac{\partial}{\partial x_j}\left(\nu_t \frac{\partial \nu_t}{\partial x_j}\right) + \frac{C_2}{\sigma}\left(\frac{\partial \nu_t}{\partial x_j}\right)^2 - C_w f_w \left(\frac{\nu_t}{d}\right)^2 \quad \ldots (28)$$

where S is the strain rate (for which Spalart and Allmaras actually use the vorticity), d is the distance from the wall and f_w is a function calibrated by reference to a range of data for equilibrium, adverse- and favourable-pressure-gradient boundary layers. The function f_w is of particular importance because it controls the 'destruction' of ν_t at the rate calibrated to give the correct behaviour in conditions departing from equilibrium. The extension to low Reynolds numbers involves the introduction of additional damping functions with argument ν_t/ν (in effect, a turbulent Reynolds number).

It may be argued that Spalart and Allmaras' model, while having a rather weak formal foundation, contains an especially rich body of empirical information, which is likely to make it applicable to a fair range of attached and thin free-shear flows, including those subjected to adverse and favourable pressure gradient. Indeed, this has been the observation made by users of the model, and the model has therefore gained significant popularity among CFD practitioners whose main concern is with attached boundary-layer flows and thin free shear flows. Spalart and Allmaras demonstrate themselves that their model is able to provide a fair representation of shock-induced separation on the RAE 2822 (Case 10) aerofoil. While the model is not intended for separated flows, the fact that it captures the behaviour of the boundary layer as it approaches separation is crucial to the prediction of the separation point and hence shock location. It is noted, however, that the model returns poor results, in common with many other models, in the post-shock region of the RAE 2822 aerofoil. There are also indications that the response of the model to mild adverse pressure gradient is too strong.

An early one-equation model of Bradshaw *et al*[28] for the transport of the shear-stress is considered next, mainly for its relevance to Menter's[25] one-equation eddy-viscosity-transport model and to his related two-equation model (Menter[29]) used extensively in computational aerodynamics and discussed in the next section. The model is based on Bradshaw *et al*'s observation that the shear stress in shear flows is more closely connected to other turbulence parameters, especially the turbulence energy, than to the mean-velocity profile. An implication of this observation is that the eddy-viscosity relation (4) is not a good approximation of reality. Instead, Bradshaw *et al* propose:

$$-\overline{uv} = ak \quad \ldots (29)$$

with a expected to be a function of y/δ, but chosen to be a constant (= 0·15). In fact, this relationship has been used already, Equation (15), but only in relation to the log-law region, in which case $a = c_\mu^{1/2} = 0{\cdot}3$. Bradshaw *et al* suggest that this should be used more generally. They then proceed to derive a shear-stress-transport equation by inserting Equation (29) into the turbulence energy equation (a general form of the last equation in set (2)), approximating the diffusion of the shear stress to be in proportion to the diffusion of k and replacing the dissipation by u_τ^3/L ($u_\tau \equiv \sqrt{-\overline{uv}}$), a substitution equivalent to Equations (14) and (15).

It is instructive, at this stage, to juxtapose Equations (4) and (29). Eliminating l_m from Equations (21) and (22) gives:

$$\nu_t = c_\mu \frac{k^2}{\varepsilon} \quad \ldots (30)$$

which is, in fact, the expression used in conjunction with two-equation $k-\varepsilon$ models, covered later. Eliminating, for thin shear flow, the shear strain from

$$P_k = -\overline{uv}\frac{\partial U}{\partial y} \quad \ldots (31)$$

$$-uv = c_\mu \frac{k^2}{\varepsilon}\left(\frac{\partial U}{\partial y}\right) \quad \ldots (32)$$

gives:

$$-\overline{uv} = c_\mu^{1/2}\sqrt{\frac{P_k}{\varepsilon}}k \quad \ldots (33)$$

This demonstrates that the eddy-viscosity framework tends to return high levels of shear stress in strong straining in which the production-to-dissipation ratio is high — a consequence of the rigid linkage of the shear stress to the strain. In contrast, Equation (29) suggests that the shear stress is not sensitive to the production-to-dissipation ratio. This relationship is exploited in Menter's[25] model which is considered last.

Following Baldwin and Barth[23], Menter derived an equation for the eddy viscosity, Equation (30), by combining the transport equa-

tion for k and ε. Insertion of Equation (30) into the result allows the replacement of ε, which leaves k and ν_t as unknowns. The former is then eliminated using Bradshaw's relation in Equation (29), with $\overline{uv}$ being related to the eddy viscosity via (4). The coefficients are determined from those of the parent two-equation $k - \varepsilon$ model of Jones and Launder[30] (see next section), with an extension to low-Reynolds-number flows effected by the provision of 'pragmatic' damping functions pre-multiplying the eddy viscosity and the turbulence-production terms. Because of the use of Equation (29), there is no need to prescribe a length scale, and the model would appear to be valid for any flow. Indeed, Menter provides the following generalisation of the thin-shear-flow form:

$$\frac{D\nu_t}{Dt} = C_1 f_{v1} \nu_t S - C_2 \frac{\nu_t^2}{S^2}\left(\frac{\partial S}{\partial x_j}\right)^2 + \frac{\partial}{\partial x_j}\left(\left(\nu + \frac{\nu_t}{\sigma}\right)\frac{\partial \nu_t}{\partial x_j}\right) \quad \ldots (34)$$

in which

$$S = \sqrt{\frac{\partial U_i}{\partial x_j}\left(\frac{\partial U_i}{\partial x_j} + \frac{\partial U_j}{\partial x_i}\right)}$$

However, it needs to be born in mind that the key relation in Equation (29), used by Menter to close the eddy-viscosity-transport equation, is rooted in thin-shear-flow considerations, so that the generalisation in Equation (34) has unclear physical implications in non-equilibrium conditions. Nevertheless, Menter demonstrates that the equation performs as well as (indeed, slightly better than) the equivalent two-equation $k - \varepsilon$ model for two particular separated flows.

3.2.3 Half-equation models

Half-equation models combine algebraic eddy-viscosity prescriptions of the type considered in Section 3.2.2 with an ordinary differential Equation which describes the streamwise evolution (i.e. transport) of a scale to which the algebraic cross-flow prescription is sensitised. Although less general than the previous category, half-equation models are considered at this point because they make use of Bradshaw's concept of shear-stress transport, as described by the turbulence-energy transport equation (20) incorporating Equation (29).

The most widely used formulation is than of Johnson and King[31]. In common with algebraic models, such as that by Cebeci and Smith[14], a two-(inner/outer) layer algebraic prescription is adopted for the eddy viscosity (see Equations (11), (12) and (18)), with the effective eddy viscosity evaluated from the exponential blending function:

$$\nu_t = \nu_{to}\left[1 - \exp\left(\frac{-\nu_{ti}}{\nu_{to}}\right)\right] \quad \ldots (35)$$

rather than by hard switching between the two layers. The key new feature is the evaluation of the inner-layer viscosity from:

$$\nu_{ti} = f_\mu^2 \kappa y \left(-\overline{u}\overline{v}_m\right)^{1/2} \quad \ldots (36)$$

which arises, in principle, from the eddy-viscosity relation, Equation (22), and Bradshaw's relation in Equation (29), combined with a van Driest damping function. In Equation (36) the shear stress is the cross-flow *maximum* value, hence a one-dimensional function varying in the streamwise direction. This maximum is determined from an ordinary differential equation for the maximum turbulence energy into which Equation (29) is inserted. In principle, this is analogous to the process adopted by Bradshaw *et al*[28] for deriving their one-equation shear-stress-transport model (see Section 3.2.1). The outer eddy viscosity is also sensitised to $\overline{uv}_m$ via a non-equilibrium function.

The above model has been effective in predicting decelerating and incipiently separating boundary layers, shock–boundary-layer interaction, especially shock-induced separation, and the flow around high-lift aerofoils (e.g. NACA 4412[32] and Aerospatiale A[33]) where it has been found to give a good representation of the separation point, the effect of separation on the surface pressure and the boundary-layer profiles (see Section 5.3). However, the model has also been observed to display deficiencies in near-equilibrium conditions in which it responds too sensitively to adverse pressure gradient. These weaknesses motivated the introduction of modifications into the model by Johnson and Coakley[34], while a three-dimensional extension was formulated by Abid *et al*[35].

3.2.4 Two-equation models

In complex strain, away from the immediate vicinity of a wall, the turbulent length scale does not, nor is expected to, scale with the wall distance. Neither is there, in general, any other global flow quantity (e.g. shear-layer thickness) which offers itself for scaling. Rather, the length scale must be expected to be governed by local turbulence mechanisms which evolve in space and time. This implies the need to determine the length scale from its own transport equation. This is, as it turns out, no mean task — one that is generally regarded as a major, if not the principal, obstacle to improving the predictive realism of turbulence models, not only within the eddy-viscosity framework, but also in the context of more elaborate closure approaches.

The foundation for a closed equation for the length scale is an exact transport equation that can be derived for the dissipation rate

$$\varepsilon = \overline{\frac{\partial u_i}{\partial x_j}\frac{\partial u_i}{\partial x_j}} \quad \ldots (37)$$

or any other quantity of the form $\xi \equiv k^a \varepsilon^b$. This derivation involves a laborious combination of derivatives of the Navier-Stokes equations (see Davidov[36]), and results in an equation of the form:

$$\frac{\partial \varepsilon}{\partial t} + \frac{\partial U_j \varepsilon}{\partial x_j} = \sum_{k=1,4} P_{\varepsilon,k} + \sum_{l=1,3} D_{\varepsilon,l} - \varepsilon_\varepsilon \quad \ldots (38)$$

which contains numerous groups of correlations interpretable as production (P_ε), diffusion (D_ε) and destruction (ε_ε). The left-hand side represents convection and arises precisely as written in Equation (38). Term-by-term modelling of this equation has been attempted by Rodi and Mansour[37] on the basis of DNS data, but has not been really productive in terms of creating a working model superior to more established forms. A key problem with Equation (38) is that the processes on the right-hand side occur in the smallest scales of turbulence which interact with fluid viscosity. At high Reynolds numbers, these scales are very far from the energetic scales associated with the turbulent stresses and the energy. Yet, the behaviour of the dissipation generally follows closely that of the large scale processes (see, for example, the equilibrium relation in Equation (13)), the implication being that the modelling of the dissipation equation must be based on those adopted for the large-scale processes.

A concept that is central to a rational closure of the ε-equation, on the basis of large-scale dynamics, is that the turbulence energy generated by the interaction between the energetic eddies and the mean flow 'cascades' down the 'inertial scale range' towards the dissipative range†. This 'pipeline' concept thus allows us to model, if only intuitively and globally, the rate of change of dissipation as an

†Richardson, in 1922[38], gave the following witty, though imprecise, description of this process: "Great whirls have little whirls that feed on their velocity and little whirls have lesser whirls and so on to viscosity."

imbalance of terms associated with the large-scale energy that flows into the 'pipeline'.

The first practical forms of a dissipation equation were proposed by Harlow and Nakayama[39] and Hanjalic[40]. The basic form (Jones and Launder[30]) used in conjunction with the k-equation (20) and expression (30) for the eddy viscosity is:

$$\frac{\partial \varepsilon}{\partial t}+\frac{\partial U_j \varepsilon}{\partial x_j}=C_{\varepsilon 1}\frac{\varepsilon}{k}P_k+\frac{\partial}{\partial x_j}\left(\left(\frac{\nu_t}{\sigma_\mu}+\nu\right)\frac{\partial \varepsilon}{\partial x_j}\right)-C_{\varepsilon 2}\frac{\varepsilon^2}{k} \qquad \ldots (39)$$

Its applicability to low-Reynolds-number near-wall flows necessitates the introduction of damping functions and additional terms that procure the correct near-wall behaviour, and it is the need for this (non-trivial) extension that has spawned numerous model variations (Jones and Launder[30], Launder and Sharma[41], Hoffman[42], Lam and Bremhurst[43], Chien[44], Nagano and Hishida[45], Myong and Kasagi[46], So *et al*[47], Huang and Coakley[48], Orszag *et al*[49], Kawamura and Kawashima[50] and Lien and Leschziner[51]). It is informative, ahead of reviewing some of these extended models, to comment on a few fundamental aspects of modelling the dissipation rate.

First, the Taylor-series analysis that led to relations in Equation (9), can readily be applied to Equation (37) to show that the wall-asymptotic behaviour of the dissipation is $\varepsilon = O(1)$. This has already been demonstrated through Equation (25). In fact, DNS simulations for channel flow by Moser *et al*[52] and others show that ε reaches a maximum at the wall ($\varepsilon\nu/u_\tau^3 \approx 0{\cdot}16$). The fact that the wall value is unknown, but needs to be determined via the compatibility condition Equation (25) is numerically disadvantageous and has led to the adoption of the 'homogeneous' dissipation

$$\tilde{\varepsilon} \equiv \varepsilon - 2\nu\left(\frac{\partial k^{1/2}}{\partial x_j}\right)^2 \qquad \ldots (40)$$

as the dependent variable, with its wall-asymptotic variation arising as $O(y^2)$. This is the variable used in the models of Jones and Launder[30], Launder and Sharma[41] and Chien[44]. Second, it is noted that the turbulent viscosity, as defined by Equation (30), has the asymptotic behaviour $\nu_t = O(y^4)$, but should vary as $\nu_t = O(y^3)$ (see Equation (10)). It follows that Equation (30) must be multiplied by a function $f_\mu = O(y^{-1})$. If $\tilde{\varepsilon}$ is used instead of ε in the eddy-viscosity relation (10) then $k^2/\tilde{\varepsilon}$ varies as $O(y^2)$, so that $f_\mu = O(y)$. Third, the exact destruction term in the dissipation equation

$$\varepsilon_\mu = 2\overline{\left(\nu\frac{\partial^2 u_i}{\partial x_j \partial x_k}\right)} \qquad \ldots (41)$$

can be shown to vary as $\varepsilon_\varepsilon = O(1)$. However, its model in Equation (39) varies as $\varepsilon_\varepsilon = O(y^{-2})$. Hence, this term must be multiplied by a function $f_{\varepsilon 2} = O(y^2)$. If $\tilde{\varepsilon}$ is used, then the near-wall simplification of Equation (39),

$$\frac{\partial}{\partial y}\left(\nu\frac{\partial \tilde{\varepsilon}}{\partial y}\right)-C_{\varepsilon 2}\frac{\tilde{\varepsilon}^2}{k}=0 \qquad \ldots (42)$$

implies the need for $f_{\varepsilon 2} = O(y^{-2})$. Some model variants use the product $\varepsilon\tilde{\varepsilon}$ in the destruction term, in which case consistency in the wall-asymptotic behaviour implies $f_{\varepsilon 2} = O(1)$. Finally, the exact production of dissipation can be shown to vary as $O(y)$. Its modelled form in Equation (39) is also $O(y)$, implying that any corrective function appended to this term should vary as $f_{\varepsilon 1} = O(1)$ if ε is retained as the subject of Equation (39). However, use of $\tilde{\varepsilon}$ clearly implies $f_{\varepsilon 1} = O(y^{-2})$. It is seen, therefore, that the particular choice of the dissipation variable has substantial implications to the nature of the damping functions which need to be used to ensure wall-asymptotic consistency between the exact and modelled terms.

The approximately 20 variants of the $k - \varepsilon$ model documented in the literature differ in respect of the following features:

- the use of ε or $\tilde{\varepsilon}$ or a mixture of both;
- the details of the damping functions f_μ and f_ε;
- the precise numerical values of the constants c_μ, $C_{\varepsilon 1}$, $C_{\varepsilon 2}$, σ_k and σ_ε;
- the presence or absence of additive correction terms on the right-hand side of Equation (39).

It is not possible to give here a detailed account of the many existing model variants, and only some general distinguishing characteristics are indicated below. Detailed reviews can be found in Patel *et al*[53], Michelassi *et al*[54] and Mansour *et al*[55].

The adoption of $\tilde{\varepsilon}$ necessitates the replacement $\varepsilon = \tilde{\varepsilon} + 2\nu(\partial k^{1/2}/\partial x_j)^2$ (see Equation (40)) in the k-equation. Some models use the equivalent corrections $2\nu k/y^2$ or $(\nu/y)(\partial k/\partial y)$ which are numerically more benign, but require the valuation of the wall distance (i.e. are 'non-local').

There are significant differences in respect of the damping functions $f_\mu, f_{\varepsilon 2}$ among different model variations, although almost all are based on exponential-decay laws of the form $(1 - \alpha\exp(-\beta Arg_\mu))$, where $Arg_\mu = \{y^+ = yu_\tau/\nu,\ y^* = yk^{1/2}/\nu,\ R_t = k^2/\nu\tilde{\varepsilon}\}$. Some models also include exponential functions $f_{\varepsilon 1}$, although most adopt $f_{\varepsilon 1} = 1$. Several (indeed, most) models do not obey the limiting behaviour in all respects (not even for $\overline{uv}$) indicated above by reference to exact constraints (see the review of Patel *et al*[53] where eight models are reviewed in detail). Rather, damping functions are designed and optimised by calibration against experimental behaviour. For example, $f_{\varepsilon 2}$ is calibrated to return the correct decay law for isotropic turbulence at low Reynolds numbers — a rate twice as high as that used to initially calibrate $C_{\varepsilon 2}$. Another example is the model of Lien and Leschziner[51] in which the asymptotic near-wall behaviour is made to mimic the length-scale variation prescribed as part of the Norris-Reynolds[19] one-equation model. One important distinction between different forms of Arg_μ is their 'locality' or 'non-locality'. The first two forms involve the distance from the wall, while the third does not, thus offering particular advantages in complex geometries and non-orthogonal or unstructured numerical grids.

In terms of predictive quality, there are rarely dramatic differences among aerodynamic quantities predicted by different variants of the $k - \varepsilon$ model (unless some of the fixes indicated below are added). Perhaps the message contained in this observation is that the wall-asymptotic behaviour of a model is not of great importance to the principal mean-flow quantities in comparison to other issues. In contrast, the skin-friction and heat-transfer coefficients and the behaviour of relaminarising flows are materially sensitive to the details in the viscous sublayer.

The precise numerical values of the coefficients, especially $C_{\varepsilon 1}$ and $C_{\varepsilon 2}$, are of major importance to the predictive performance of two-equation models, and this has been the source of much uncertainty when trying to assess the inherent qualities of some model variations relative to others. In the large majority of models $c_\mu = 0{\cdot}09$, $\sigma_k = 1{\cdot}0$, $\sigma_\varepsilon = 1{\cdot}3$. All models should obey the compatibility condition:

$$C_{\varepsilon 1} = C_{\varepsilon 2} - \frac{\kappa^2}{\sigma_\varepsilon\sqrt{c_\mu}} \qquad \ldots (43)$$

which can be derived upon the insertion of the log-law and equilibrium constraints into the ε-equation. Not all do so, however, and a 1% deviation from Equation (43) leads to a 5-7% change in the spreading rate of a shear layer. The constant $C_{\varepsilon 2}$ is determined, from experimental data for the decay of turbulence behind a grid ($k \propto x^{-1{\cdot}25}$ at high turbulent Reynolds number), to be around 1·92, which then gives $C_{\varepsilon 1} = 1{\cdot}44$ from Equation (43), but there is some uncertainty about the correct decay rate, and other values have been used. The final choice of the constants, subject to the constraint of Equation (43), is a compromise, based on computer optimisation, and can change the performance of the model considerably.

Several models include additive correction terms in Equation (39), designed either to procure the requisite near-wall variation of ε or to force the equation to yield variations which improve agreement with experimental data. The most influential correction is one that counteracts the seriously detrimental tendency of the ε-equation to return, in adverse pressure gradient, excessive length scale values $k^{1.5}/\varepsilon$ — much larger than correspond to the equilibrium variation ($\kappa c_\eta^{-3/4} y$) in the log-law region. Two alternative correction forms proposed by Yap[56] and Jakirlic and Hanjalic[57], respectively, are:

$$E = \max\left[\left(\frac{l}{\kappa c_\mu^{-3/4} y} - 1\right)\left(\frac{l}{\kappa c_\mu^{-3/4} y}\right)^2 \frac{\tilde{\varepsilon}^2}{k}, 0\right] \quad \ldots (44)$$

$$E = \max\left[\left(\frac{l}{\kappa c_\mu^{-3/4}} \frac{\partial l}{\partial y} - 1\right)\left(\frac{l}{\kappa c_\mu^{-3/4}} \frac{\partial l}{\partial y}\right)^2 \frac{\tilde{\varepsilon}\varepsilon}{k}, 0\right] \quad \ldots (45)$$

The latter is again 'local', in that it does not require the wall distance to be determined. In both, $l = k^{1.5}/\varepsilon$, and both are 'source' terms in the ε-equation, which force a reduction (or moderation) in the deviation of the length scale from its equilibrium value. A form closely akin to Equation (45) has been proposed by Iacovides and Raisee[58] in the context of second-moment closure. Other corrections include one by Hanjalic and Launder[59], designed to conteract the erroneously high production of turbulence energy in irrotational straining (see Equation (6)), and a correction by Yakhot *et al*[60], in the context of a RNG-theory-based $k - \varepsilon$ model, which has the form of a strain-dependent source term in the ε-equation, resulting in a reduction of the length scale at high strain rates. A 'harsh' correction by Kato and Launder[61], also designed to alleviate the excessive production of turbulence energy, entails the replacement:

$$P_k = \nu_t S^2 \leftarrow \nu_t S\Omega \quad \ldots (46)$$

where S is the strain rate and Ω is the vorticity. This correction aims specifically at stagnation flows in which S is large while Ω is low, in which case turbulence production is suppressed. However, the correction is not valid for general shear flow (except in thin layers, where $S \approx \Omega$), and is also formally inconsistent with the eddy-viscosity relation which inevitably leads to $P_k = \nu_t S^2$. A more well-founded correction, aiming to address both the wrong response to normal straining as well as the excessive turbulence generation in high strain rates (reflected by the disparity between Equations (29) and (33)), is that proposed by Liou *et al*[62]. Based on realisability constaints, c_μ is sensitised to invariants of the strain and vorticity tensors (see Equation (78) below) in such a way that c_μ declines progressively beyond a strain corresponding to the turbulence-equilibrium condition $P_k = \varepsilon$. While this correction is different, in principle, from that of Menter[25], the objective is the same, in terms of predictive performance, and Liou *et al* demonstrate its effectiveness by reference to computations for transonic bump and supersonic ramp flows.

Yet another type of *ad hoc* correction is that designed to sensitise the eddy viscosity to curvature. It was shown in Section 2, by reference to Equation (7), that sensitivity of turbulence to curvature is rooted in normal-stress anisotropy and its selective interaction with particular strain components. None of this is represented within the eddy-viscosity framework. Curvature was shown to stabilise or destabilise turbulence, depending on the sense of curvature relative to the principal shear strain. Parameters that can be used to mimic the effects of curvature are the 'gradient' and 'flux' Richardson numbers (Launder *et al*[63], Rodi[64], Rodi and Scheuerer[65]), defined respectively as:

$$Ri_g = \frac{k^2}{\varepsilon^2} \frac{U}{R^2} \frac{\partial(RU)}{\partial y} \quad \ldots (47)$$

$$Ri_f = \frac{2\nu_t U \dfrac{\partial U/R}{\partial y}}{P_k} \quad \ldots (48)$$

in which R is the radius of streamline curvature. The latter parameter represents the ratio of curvature-related turbulence-energy production to the total production. The parameters have been used to introduce additional source/sink term of the form

$$\begin{aligned} C_{\varepsilon 2} &\leftarrow C_{\varepsilon 2}\left(1 - C_{\varepsilon 3} Ri_g\right) \\ C_{\varepsilon 1} &\leftarrow C_{\varepsilon 1}\left(1 + C_{\varepsilon 3} Ri_f\right) \end{aligned} \quad \ldots (49)$$

into the ε-equation. However, both corrections are only tenable in curved boundary layers or swirling flows, in which the local radius of curvature can be readily estimated from the curvature of the wall and the radial distance from the vortex centre, respectively. In more complex flows, neither is a practical or promising patch. An alternative type of curvature correction by Leschziner and Rodi[66] is based on a modification of the coefficient c_μ, derived from a simplified form of an algebraic Reynolds-stress model. This has been successfully used to calculate recirculating flows, but is difficult to extend to complex three-dimensional flows.

Two-equation $k - \varepsilon$ models are appropriate, in principle, to complex flows, do not involve fundamental restrictions in respect of flow features, including separation, and have been used extensively in aerodynamic computations (see Section 5). However, the overall conclusion emerging from extensive application experience has been that they not return high-quality results for conditions that are considerable more challenging than those in thin-shear-layer flows. In particular, the models have been observed to be too diffusive in stagnating flow, in boundary layers subjected to adverse pressure gradient and in the presence of stabilising curvature — defects that result from a combination of the limitations of the eddy-viscosity concept and the tendency of the ε-equation to seriously overestimate the turbulent length scale and hence viscosity in decelerating near-wall flows. In consequence, separation from continuous surfaces tends to be seriously inhibited or delayed, recirculation regions are too short, skin friction is excessive and the wall-pressure variation is misrepresented. The many corrections and fixes proposed, none of which is general, bear witness to the inescapable conclusion that $k - \varepsilon$ models constitute an insufficiently refined modelling framework for complex strain. On the other hand, for relatively simple thin shear flows, one- or even half-equation models can give results as good as, if not better, than $k - \varepsilon$ models at a considerably lower level of mathematical and numerical elaboration. Indeed, as shown in the previous section, Menter's[25] one-equation model provides a slightly superior representation even in the presence of separation.

The difficulties experienced with $k - \varepsilon$ models, in terms of predictive weaknesses and also numerical difficulties arising from the viscosity-affected near-wall properties of the ε-equation, have motivated efforts, especially in the 1990s, to formulate, test and improve models that use alternative length-scale variables. In computational aerodynamics, the most popular alternative to ε has been the turbulent vorticity $\omega \equiv \varepsilon/k$ (Wilcox[66, 67]) and, to a lesser extent, its inverse, the turbulent time scale τ (Speziale *et al*[69]) and its root (Kalitzin *et al*[70]). These models are reviewed below. Models based on other length-scale equations include the $k^{1/2} - \xi$ ($\xi = \varepsilon/k^{1/2}$) model of Gibson and Daffa'Alla[71], the $k - R_t$ model of Goldberg[72] and the $k - L$ (or $k - \sigma$) model of Benay and Servel[73].

The choice of ω is initially curious, for its asymptotic variation is

$$\omega \rightarrow \left.\frac{2\nu k / y^2}{k}\right|_{y \rightarrow 0} \rightarrow \infty \quad \ldots (50)$$

a behaviour which requires the boundary condition to be specified at some finite distance from the wall. In contrast, its inverse has the

natural and benign behaviour

$$\tau \to \left.\frac{y^2}{2\nu}\right|_{y\to 0} \to 0 \qquad \ldots (51)$$

Speziale *et al*[69] show, by reference to the exact equation for τ, corresponding to Equation (38), that the exact balance of terms at the wall involves only viscous contributions that include derivatives of τ and k, i.e. no correlations explicitly dependent on modelling assumptions. This is in contrast to the ε-equation the near-wall balance of which includes a whole range of higher-order correlations. Furthermore, the near-wall balance is satified by Equation (51) in conjunction with the quadratic decay of k. This is argued to give τ distinct advantages over ε in terms of near-wall modelling and behaviour.

An exact transport equation for ω can be derived along analogous lines to those for τ. At the wall, the balance of terms reduces to:

$$\frac{2\nu}{k}\frac{\partial\omega}{\partial y}\frac{\partial k}{\partial y}+\nu\frac{\partial^2\omega}{\partial y^2}+\omega^2=0 \qquad \ldots (52)$$

which, again, does not contain higher-order turbulence correlations dependent on modelling assumptions. Substitution of Equation (50) and $\partial k/\partial y = 2k/y$ into Equation (52) also shows wall-asymptotic consistency. Hence, ω also appears to be preferable to ε.

An early modelled equation for ω proposed by Wilcox[67] is:

$$\frac{\mathrm{D}\omega}{\mathrm{D}t}=C_{\omega 1}\frac{\omega}{k}P_k+\frac{\partial}{\partial x_j}\left(\left(\nu+\frac{\nu_t}{\sigma_\omega}\right)\frac{\partial\omega}{\partial x_j}\right)-C_{\omega 2}\omega^2 \qquad \ldots (53)$$

with $C_{\omega 1} = 5/9$, $C_{\omega 2} = 5/6$, $\sigma_\omega = 2$. Wilcox advocates the use of this equation (irrespective of the Reynolds number) for its freedom from wall-correction terms. However, the wall-asymptotic balance implied by Equation (53) is

$$\nu\frac{\partial^2\omega}{\partial y^2}+C_{\omega 2}\omega^2=0 \qquad \ldots (54)$$

which, with $C_{\omega 2} = 5/6$, is inconsistent with Equation (52) and leads to the wrong decay of k at the wall. This then led Wilcox[68] to introduce damping functions pre-multiplying the eddy viscosity, the destruction term in the k-equation and $C_{\omega 1}$ in Equation (53).

In terms of predictive performance, it has often been reported or claimed that the $k-\omega$ model gives distinctly better results for near-wall flows, especially in boundary layers subjected to adverse pressure gradient. While the asymptotic near-wall behaviour may play a role in these differences, another likely source is the representation of the length scale in the turbulent layer. In an effort to elucidate the origin of any differences, it is informative to compare the modelled forms of the ε- and the ω-equations. One of the two equations needs to be transformed in terms of the length-scale variable of the other.

Starting from

$$\frac{\partial k}{\partial t}+\frac{\partial U_j k}{\partial x_j}=\frac{\partial}{\partial x_j}\left(\frac{\nu_t}{\sigma_k}\frac{\partial k}{\partial x_j}\right)+P_k-\varepsilon \qquad \ldots (55)$$

$$\frac{\partial\varepsilon}{\partial t}+\frac{\partial U_j\varepsilon}{\partial x_j}=C_{\varepsilon 1}\frac{\varepsilon}{k}P_k+\frac{\partial}{\partial x_j}\left(\frac{\nu_t}{\sigma_k}\frac{\partial\varepsilon}{\partial x_j}\right)-C_{\varepsilon 2}\frac{\varepsilon^2}{k} \qquad \ldots (56)$$

one can derive an equation for ω by inserting $\omega = \varepsilon/k$ into the ε equation, differentiating this and combining the result with the k-equation. Subject to the simplification $\sigma_k = \sigma_\varepsilon$, the outcome is:

$$\frac{\mathrm{D}\omega}{\mathrm{D}t}=(C_{\varepsilon 1}-1)\frac{\omega}{k}P_k+\frac{\partial}{\partial x_j}\left(\frac{\nu_t}{\sigma}\right)\frac{\partial\omega}{\partial x_j}-(C_{\varepsilon 2}-1)\omega^2+\frac{2}{\omega\sigma}\frac{\partial k}{\partial x_j}\frac{\partial\omega}{\partial x_j} \qquad \ldots (57)$$

Comparison of Equation (57) with Equation (53) reveals the following differences:

- the ω-equation lacks the mixed term in the transformed ε-equation;
- the coefficients of the production and destruction terms are 0·55 *vs* 0·44 and 0·83 *vs* 0·92, respectively;
- the Prandtl/Schmidt number in Equation (57) is $\sigma = O(1{\cdot}3)$, while $\sigma_\omega = 2$.

In addition, the Prandtl/Schmidt number in Wilcox's k-equation is 2, relative to 1 in the $k-\varepsilon$ model. Hence, there are several potentially influential sources for the different performance of the $k-\varepsilon$ and $k-\omega$ models. Although the coefficients of Equation (53) satisfy the equilibrium constraint, Equation (43), the differences in the values can, on their own, be very influential. This is illustrated, for example, by Apsley and Leschziner[74] for the case of a separated diffuser flow. For that same case, the $k-\omega$ model was found to perform almost as poorly as the $k-\varepsilon$ model.

While the $k-\omega$ model may have some marginal advantages over the $k-\varepsilon$ model (see discussion in Section 5), a serious and well-proven defect of the former (Menter[75], Bardina *et al*[76]) is its extreme sensitivity to the free-stream value of ω at irrotational boundaries of shear flows. Menter shows, for example, that the viscosity within a boundary layer can change by a factor of two or more by varying the free-stream value within reasonable bounds. With the $k-\varepsilon$ model, the usual practice is to prescribe (unless known) low free-stream values for k and ε. The shear flow is virtually insensitive to these values, provided the associated eddy viscosity is kept realistically low (say, O(10-50ν)). The above observations have led Menter[29] to formulate a hybrid model which blends the $k-\omega$ model near the wall with the $k-\varepsilon$ model in wall-remote regions. Computationally, this is achieved through a weighted average formula operating on corresponding $k-\varepsilon$ and $k-\omega$ model coefficients:

$$C_{eff}=FC_{k-\omega}+(1-F)C_{k-\varepsilon} \qquad \ldots (58)$$

with the k-ε coefficients arising from Equation (57) and F being a prescribed blending function which ensures a dominance of the $k-\omega$ model in the region $y^+ < 70$ and the dominance of the $k-\varepsilon$ model beyond. This hybridisation, on its own, does not yield significant improvements relative to the $k-\varepsilon$ model — nor is it expected to, in view of the comments made earlier. However, a far more influential addition to the hybrid model is a correction which limits the shear stress in accordance with Bradshaw's relation (29) which has also been used to construct the one-equation model (34). Here again, the basic idea is rooted in the difference between (29), reflecting experimental observation for shear layers, and relation (33) which is consistent with the $k-\varepsilon$ model. Thus a shear-stress limiter is introduced via:

$$\nu_t=\frac{ak}{\max\left(\omega/a,\alpha\,\partial U/\partial y\right)} \qquad \ldots (59)$$

where $a = c_\mu^{1/2}$ and α is a function with extrema of 1 for boundary-layer flow and 0 for free shear flow (Menter actually uses the vorticity Ω in place of the velocity gradient; these are identical in thin shear flow). The switch occurs at:

$$c_\mu^{-1/2}\omega=\frac{\partial U}{\partial y}\to c_\mu^{1/2}=c_\mu\frac{k}{\varepsilon}\frac{\partial U}{\partial y}=-\frac{\overline{uv}}{k} \qquad \ldots (60)$$

which corresponds to the equilibrium condition P_k/ε (see Equation (33)). Hence, in high strain, beyond the equilibrium state, Equation (59) yields:

$$\nu_t=\frac{c_\mu^{1/2}k}{\partial U/\partial y}\to -\overline{uv}=c_\mu^{1/2}k \qquad \ldots (61)$$

This composite formulation — termed "shear-stress-transport" (SST) model — has enjoyed significant popularity in aerodynamic computations because of its favourable response to adverse pressure gradients. In a decelerating boundary layer, Equation (61) comes into action and reduces the shear-stress level relative to that of the non-limited $k - \omega$ model, and this is extremely effective in promoting separation, including shock-induced separation (Batten *et al*[77], Leschziner *et al*[78]). In fact, it has been observed to be excessively effective in some separated flows, both subsonic (Apsley and Leschziner[73, 78]) and trans/supersonic flows (Liou *et al*[62]) in which it gave too early separation and excessively long recirculation regions.

One difficulty highlighted earlier in relation to the ω-equation is that ω increases steeply towards infinity at solid boundaries. This is numerically disadvantageous and also requires the boundary condition to be specified at some finite distance from the wall. The alternative of using τ has been noted, and Equation (51) shows that this quantity tends to zero at the same rate as k, which offers numerical advantages. A potentially even better variable is $\tau^{1/2}$ which decays linearly. Although the use of τ as the length-scale variable goes back to the 1980s (e.g. Zeierman and Wolfshtein[80]), the first well-founded $k - \tau$ model was proposed by Speziale *et al*[69] in 1992. The details of the model are not given here. Suffice it to say that the modelled τ-equation is closely related to both the ε- and the ω-equations. In fact, for an identical value of all turbulent Prandtl/Schmidt numbers, the τ-equation reduces to the ε-equation. Moreover, the τ-equation is similar to the ω-equation, but contains a mixed term proportional to $(\partial k/\partial x_j)(\partial \tau/\partial x_j)$ which, if the equation is transformed in terms of ω, gives rise to a mixed term proportional to $(\partial k/\partial x_j)(\partial \omega/\partial x_j)$, as appearing in Equation (57). Finally, there are differences in the way viscous damping is handled.

A model based on $\tau^{1/2}$ (termed 'g') was proposed by Kalitzin *et al*[70]. In its basic form, this is formally identical to the $k - \omega$ model, with the equation for g derived by inversion of the ω-equation, first in terms of τ and then in terms of g. However, the final working version of the model contains a limiter designed to suppress the tendency of the model to generate high levels of τ at free-stream boundaries. In terms of predictive performance, illustrated by Kalitzin *et al* for a three-element high-lift aerofoil and the transonic RAE 2822 (Case 9) aerofoil, the model generates solutions which do not differ greatly from its $k - \omega$ and $k - \varepsilon$ relatives. Apsley and Leschziner[74] also show that its performance for separated flow is close to that of the $k - \omega$ and $k - \varepsilon$ models.

All models reviewed above use the turbulence energy k as the velocity scale in the eddy-viscosity relation. This might be a convenient co-ordinate-invariant parameter, but is certainly not ideal, as has been shown in Section 2 by reference to Equation (2), Equation (4) and arguments following the latter. The essential argument is that the shear stress in a shear layer $\overline{uv}$ is driven by the normal stress across the flow, $\overline{v}^2$. As turbulence is highly anisotropic, especially at a wall, k is not a particularly good representative of the turbulence scale in the eddy-viscosity relation. This disparity is, in part, the reason for having to attach heavy damping to the eddy-viscosity, via the damping function f_μ, in two-equation models applicable down to the wall. As the wall is approached, anisotropy increases progressively, because the wall-normal intensity decays far more rapidly than the turbulence energy (see Equation (9)), with consequent rapid decline in shear-stress generation. This is a purely kinematic process, but one that cannot be captured properly via k, which decays far more slowly than $\overline{v}^2$. The damping function is introduced in compensation. However, its argument is the Reynolds number — that is, damping is assumed to be purely viscous, which is not consonant with reality. While viscous damping is effective, it is far weaker and occurs over a thinner region than is implied by the usual damping functions. These arguments form the basis for the '$\overline{v}^2 - f$' model of Durbin[6], which includes a transport equation for instead of k and an additional wall-related 'relaxation' equation which 'relaxes' $\overline{v}^2$ towards k away from the wall. As the model leans heavily on closure ideas pertaining to Reynolds-stress-transport modelling, it will be reviewed later in the context of anisotropy-resolving models.

3.3 Anisotropy-resolving models

3.3.1 Introductory remarks

It has been demonstrated in Section 2 that the anisotropy of turbulence plays a crucial role in the processes through which the flow and turbulence fields respond to a whole range of specific strain types. In particular, the response of turbulence to curvature, normal straining and wall-blocking has been highlighted. Thus, even if the normal stresses are not dynamically active (they *are* in complex separated and highly 3D flows), the resolution of anisotropy is important, for its effects on the shear stress. A failure to resolve anisotropy — as is the case with any linear eddy-viscosity model — poses the need to introduce a whole range of *ad hoc* corrections, which usually only mimic particular processes that are not represented due to missing model elements. Another process which eddy-viscosity models fail to resolve is shear-stress transport. Implicitly, this transport is represented by the linkage shown in Equations (33) or (29), in conjunction with the transport equation for k. However, set (2) shows that the shear stress is governed by a radically different balance than that pertaining to the normal stresses. Hence, the link implied by the eddy-viscosity model is unrealistic.

The natural modelling step beyond the eddy-viscosity framework is second-moment closure — that is, a model which consists of transport equations for all Reynolds stresses, without recourse to the artefact termed 'eddy viscosity'. Simple (exact) forms of these equations applicable to particular flow conditions have already been given in sets (2) and (3). A key advantage of second-moment closure is that the stress-generation terms do not require approximation, for they only involve products of stresses and strains. It is recalled that the stress-generation terms are primarily responsible for the anisotropy and the selective response of turbulence to different strain types. Another advantage is that convective stress transport is represented exactly. Other processes require modelling, however, and this continues to be an active and challenging area of research.

A drawback of second-moment closure is its mathematical complexity and, arising from this, numerical difficulties (see Section 4) and higher computational costs. In three-dimensional flow, the model consists of six highly coupled, non-linear partial differential equations, to which must be added at least one further equation for the rate of turbulence dissipation. If heat transfer or scalar transport is included, a consistent modelling framework entails the solution of (at least) three further equations for flux transport. In addition, the absence of an eddy-viscosity and associated second-order gradient terms from both the mean-flow and Reynolds-stress equations tends to reduce the iterative robustness of most solution algorithms and adds to the computational costs. Finally, additional boundary conditions are required for the stresses (because they are transported). These are rarely available from experimental data and need to be inferred from other quantities. Yet, the above challenges can be and have been met for over a decade, and it is now possible to compute very complex 3D flows, both compressible and incompressible, with the most advanced forms of second-moment closure, incorporating non-linear models for the pressure-strain redistribution process and applicable down to the wall without Reynolds-number restrictions. Examples of the type of compressible flows recently computed with second-moment closure are given in Fig. 2.

The complexities associated with second-moment closure have motivated efforts in recent years to construct simpler model forms which retain the principal advantages of the former over linear eddy-viscosity models. These have led to the formulation of a whole range of non-linear eddy-viscosity and explicit algebraic Reynolds-stress models, both consisting of sets of explicit algebraic relations for the stresses in terms of strains. These model are not as fundamentally firm as second-moment closure, but easier to implement and cheaper to apply.

In what follows, both modelling frameworks are reviewed, with particular relevance to aerodynamic computations.

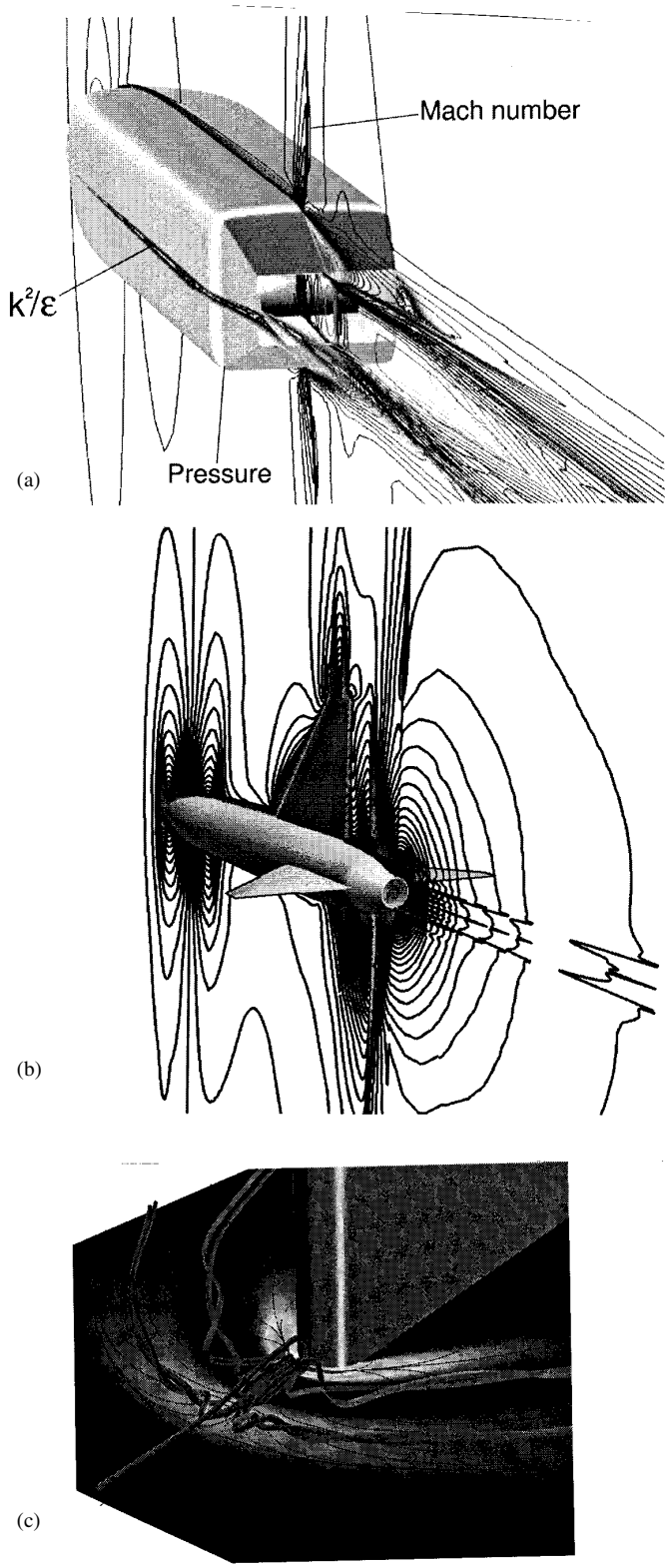

Figure 2. Compressible flows featuring strong shock–boundary-layer interaction, computed with a low-Re Reynolds-stress-transport model incorporating a cubic pressure-strain model; (a) jet-afterbody flow (from Leschziner *et al*[78]); (b) AGARD B2 generic fighter configuration (from Leschziner *et al*[78]); (c) Mach-2 flow around fin-plate assembly (taken from Batten *et al*[77]).

3.3.2 Reynolds-stress models (RSTM)

The foundation of all RSTMs is the exact set:

$$\underbrace{\frac{\mathrm{D}\overline{u_i u_j}}{\mathrm{D}t}}_{C_{ij}} = \underbrace{-\left\{\overline{u_i u_k}\frac{\partial U_j}{\partial x_k} + \overline{u_j u_k}\frac{\partial U_i}{\partial x_k}\right\}}_{P_{ij}} + \underbrace{\left(\overline{f_i u_j} + \overline{f_j u_i}\right)}_{F_{ij}} \underbrace{- 2\nu\overline{\frac{\partial u_i}{\partial x_k}\frac{\partial u_j}{\partial x_k}}}_{\varepsilon_{ij}}$$
$$+ \underbrace{\overline{\frac{p}{\rho}\left(\frac{\partial u_i}{\partial x_j} + \frac{\partial u_j}{\partial x_i}\right)}}_{\Phi_{ij}} \underbrace{- \frac{\partial}{\partial x_k}\left\{\overline{u_i u_j u_k} + \overline{\frac{pu_j}{\rho}}\delta_{ik} + \overline{\frac{pu_i}{\rho}}\delta_{jk} - \nu\frac{\partial\overline{u_i u_j}}{\partial x_k}\right\}}_{d_{ij}} \quad \ldots (62)$$

in which C_{ij}, P_{ij}, F_{ij}, Φ_{ij}, ε_{ij} and d_{ij} represent, respectively, stress convection, production by strain, production by body forces (e.g. buoyancy $f_i = g_i\beta T'$), dissipation, pressure-strain redistribution and diffusion. The last three processes require modelling, and there is a large body of literature in this respect, of which only a small proportion is covered herein.

At high Reynolds numbers, dissipation is usually assumed to be isotropic, because it occurs at eddy length scales which tend to be very much smaller than the scales of the large energetic eddies which are sensitive to the mean strain (and hence to its orientation), the ratio of the scales being of order $\mathrm{Re}^{3/4}$. Isotropy in the dissipative scales implies:

$$\varepsilon_{ij} = \frac{2}{3}\varepsilon\delta_{ij} \quad \ldots (63)$$

in which ε is the dissipation rate of turbulence energy. This approximation is inadequate close to the wall where length scales are generally small and anisotropy is large. Proposals have thus been made (e.g. in Gilbert and Kleiser[81], Launder and Tselepidakis[82], Hallbaeck *et al*[83] and Hanjalic and Jakirlic[84]) to sensitise ε_{ij}, in an algebraic fashion, to invariants of the stress anisotropy $a_{ij} = (\overline{u_i u_j}/k - 2/3\delta_{ij})$:

$$A_2 = a_{ij}a_{ij}; \quad A_3 = a_{ij}a_{jk}a_{ki}; \quad A = 1 - \tfrac{9}{8}\left(A_2 - A_3\right) \quad \ldots (64)$$

of the dissipation anisotropy $e_{ij} = (\varepsilon_{ij}/\varepsilon - 2/3\delta_{ij})$:

$$E_2 = e_{ij}e_{ij}; \quad E_3 = e_{ij}e_{jk}e_{ki}; \quad E = 1 - \tfrac{9}{8}\left(E_2 - E_3\right) \quad \ldots (65)$$

From a physical point of view, A_2, A_3 and A may be related, if only tentatively, to structural features of turbulence. Thus, $A = 1$ identifies isotropic turbulence ('spherical' eddies), while $A = 0$ characterises two-component turbulence ('flat' eddies — say, near a wall or sharp fluid–fluid interface). Moreover, negative values for A_3 characterise 'saucer'-shaped eddies, while positive values indicate 'sausage'-shaped structures.

A model widely used to represents the anisotropic dissipation is:

$$\varepsilon_{ij} = \frac{2}{3}f_\varepsilon\delta_{ij}\varepsilon + \left(1 - f_\varepsilon\right)\varepsilon^*_{ij} \quad \ldots (66)$$

where ε^*_{ij} are the wall-limiting values of ε_{ij}, which can be readily obtained by applying the Taylor-series expansions in Equation (8) to the dissipation tensor in Equation (62) (see Launder and Reynolds[85]). The 'blending' function f_ε varies from model to model — there are at least five forms (see Hanjalic[86]) — and its subjects are A and/or E and/or R_t. Apart from securing the correct wall-limiting behaviour of ε_{ij} and introducing shear-stress dissipation, Equation (66) also ensures that dissipation of the wall-normal intensity is 'shut off' as turbulence approaches the two-component near-wall limit. This is an important element of any model designed to satisfy realisability, a property which includes the unconditional satisfaction of $\overline{u}^2_\alpha \geq 0$

(with α denoting the principal directions). More recent efforts (e.g. Oberlack[87]) have focused on the derivation of transport equations for the dissipation components, based on two-point correlation arguments, but such equations have not been used in aerodynamic practice.

The determination of the dissipation rate ε, required by Equation (66), has been the subject of an extensive discussion in Section 3.2 in relation to eddy-viscosity models. Much of what was said therein applies here too: the length-scale equation remains a major source of model weaknesses. With few exceptions, ε is determined from variants of the transport Equation (39), with or without corrections. The only major difference is the replacement:

$$\frac{\partial}{\partial x_j}\left(\left(\frac{\nu_t}{\sigma_\mu}+\nu\right)\frac{\partial \varepsilon}{\partial x_j}\right) \leftarrow \frac{\partial}{\partial x_j}\left(c_\varepsilon \overline{u_j u_k}\frac{k}{\varepsilon}\frac{\partial \varepsilon}{\partial x_k}\right) \quad \ldots (67)$$

which implies that the diffusive flux of dissipation in any one direction is not simply associated with the gradient of the dissipation in that direction (a form of the Fourier-Fick law), but is a weighted sum of the gradients of the dissipation in all directions, each weighted by the appropriate Reynolds stress. This is referred to a 'generalised gradient diffusion hypothesis' (GGDH), and its rationale will be indicated below by reference to modelling stress diffusion.

A problem with the dissipation-rate equation, already addressed in Section 3.2, is that it returns excessive levels of turbulent length scale in boundary layers subjected to adverse pressure gradient. This defect is common to both two-equation eddy-viscosity and Reynolds-stress models, and requires a correction analogous to Equations (44) and (45). Here again, the usual practice is to add a 'Yap-type' correction (Yap[56]) which forces the ε-equation to return a length scale close to the local-equilibrium value. An example is the recent variant of Jakirlic and Hanjalic[57],

$$E = \max\left(\left[\left(\frac{1}{c_\mu^{-3/4}\kappa}\frac{\partial l}{\partial y}\right)^2 - 1\right]\left(\frac{1}{c_\mu^{-3/4}\kappa}\frac{\partial l}{\partial y}\right)^2 A\frac{\varepsilon\tilde{\varepsilon}}{k}, 0\right) \quad \ldots (68)$$

which is very similar to Equation (45) and involves the anisotropy invariant A, determined from Equation (64).

Alongside dissipation, the redistribution or 'pressure-strain' term Φ_{ij} presents the modeller with the biggest challenge in the context of second-moment closure. This term vanishes upon the contraction $k = 0{\cdot}5\overline{u_i u_j}\delta_{ij}$ (strictly, in incompressible flow only) and thus becomes irrelevant in closures based on the turbulence energy or a surrogate scalar. In second-moment closure, however, this term controls the redistribution of turbulence energy among the normal stresses — a process driving turbulence towards a state of isotropy — as well as the reduction in the shear stresses in harmony with the isotropisation process (recall Mohr's circle in solid mechanics). It only requires reference to Equation (2) to appreciate that the pressure-strain process is of crucial importance in the context of second-moment closure. In simple shear flow, the shear stress is driven by $\overline{v^2}$, a (kinematic) stress that is not generated and is only finite because of the redistribution process effected by Φ_{22}. Moreover, Φ_{12} is the only term which balances the generation of shear stress and hence avoids that stress rising indefinitely.

It can be shown analytically that the redistribution process consists of two major constituents, one involving an interaction between turbulent quantities only (Φ_{ij1} and referred to as the *slow* or the *Rotta* term) and the other involving an interaction between mean strain and turbulence fluctuations (Φ_{ij2} and termed *rapid*). This fact has led most modellers to make separate proposals for these two fragments. The simplest proposal forms, used for most complex-flow computations, are the linear relations by Rotta[88] and Gibson and Launder[89]:

$$\Phi_{ij1} = \frac{-C_1\varepsilon}{k}\left(\overline{u_i u_j} - \frac{1}{3}\delta_{ij}\overline{u_k u_k}\right); \quad \Phi_{ij2} = -C_2\left(P_{ij} - \frac{1}{3}\delta_{ij}P_{kk}\right) \quad \ldots (69)$$

Fu *et al*[90] have shown, by reference to swirling flow, that the above form of Φ_{ij2} is not frame-invariant, but that invariance is assured if the body-force-related production terms Φ_{ij} and the convection tensor are included to give the form:

$$\Phi_{ij2} = -C_2\left(\left[P_{ij} + F_{ij} - \frac{1}{3}\delta_{ij}\left(P_{kk} + F_{ij}\right)\right] - \left(C_{ij} - \frac{1}{3}\delta_{ij}C_{kk}\right)\right) \quad \ldots (70)$$

Although this combined 'linear' model satisfies the basic requirement of steering turbulence towards isotropy, the isotropisation process is far too intense at the high levels of anisotropy prevailing near the wall or free liquid surface. As the wall is approached, turbulence tends towards a two-component state ($A = 0$), and redistribution must vanish to allow this state to be achieved. By intensifying the isotropisation process as the wall is approached, the linear model does not merely fail to represent the physical process correctly, but can lead to one of the principal normal stresses becoming negative — a condition violating realisability.

Correcting the above weakness, within the linear framework, relies on the introduction of elaborate and influential *ad hoc* terms (Shir[91], Gibson and Launder[89], Craft and Launder[92]) which counteract the isotropisation process in proportion to the distance from the wall, normalised by the turbulent length scale $k^{3/2}/\varepsilon$. For example, for a shear layer along a single horizontal wall, the correction terms damping the linear isotropisation of the wall normal stress $\overline{v^2}$ are:

$$\Phi^w_{22,1} = -C_1^w\frac{4}{3}\frac{\varepsilon}{k}\overline{v^2}\frac{k^{3/2}/\varepsilon}{c_\mu^{-3/4}\kappa y}; \quad \Phi^w_{22,2} = 2C_2^w\left(P_{22} - \frac{2}{3}P_k\right)\frac{k^{3/2}/\varepsilon}{c_\mu^{-3/4}\kappa y} \quad \ldots (71)$$

In addition, the redistribution process needs to be sensitised to inhomogeneity, associated with large strain gradients, and to anisotropy invariants, especially in low-Re forms which allow the model to be used down to the wall (Launder and Shima[93], So *et al*[94], Ince *et al*[95], Jakirlic and Hanjalic[57], Craft and Launder[96]). An example of the latter practice is that of Jakirlic and Hanjalic who made extensive use of DNS data to calibrate their linear low-Re model and use:

$$C_1 = 2{\cdot}5A\left(\min\left(0{\cdot}6, A_2\right)\right)^{1/4} f + \sqrt{A}E^2; \quad C_2 = 0{\cdot}8A^{1/2} \quad \ldots (72)$$

where f is a function of the turbulent Reynolds number R_t. Similarly, C_1^w and C_2^w in Equation (71) are sensitised to A, A_2 and R_t.

An alternative, proposed by Durbin[97], introduces an elliptic relaxation equation of the form:

$$L^2\nabla^2\frac{\Phi^c_{ij}}{k} - \frac{\Phi^c_{ij}}{k} = \frac{\Phi_{ij}}{k} \quad \ldots (73)$$

where Φ^c_{ij} is the wall-corrected form of the standard (uncorrected) Φ_{ij}, L is the turbulence length scale and ∇^2 is the elliptic operator. Equation (73) steers Φ_{ij} towards the correct wall values, prescribed as boundary conditions. Although this approach has been shown to perform well for several challenging flows (Durbin[97]), it requires the solution of the six additional differential equations (73), which obviously adds to the resource requirements. A simplified variant of Equation (73), intended for near-wall shear flows, is adopted as part of Durbin's[6] so-called $v^2 - f$ model and has already been mentioned at the end of Section 3.2. The model involves a single Reynolds-stress equation for $\overline{v^2}$, essentially the stress normal to the wall or the streamlines. This stress is also the velocity scale used in the eddy viscosity with which the mean flow is computed. The Reynolds-stress equation is solved in conjunction with the $i, j = 2, 2$ component of Equation (73) (f denotes the ratio Φ_{22}/k) and the k-equation.

From a fundamental point of view, as well as on practical grounds, the use of wall corrections is unsatisfactory, not only because of their non-general nature, but also because they rely

heavily on the wall distance (y in Equation (71)). The latter is especially disadvantageous in complex geometries, where the influence of more than one wall needs to be taken into account, and when general non-orthogonal numerical grids are used. Hence, much of the recent fundamental research in the area of turbulence modelling has been concerned with the construction of non-linear pressure-strain models which satisfy the realisability constrains and do not require wall corrections. Non-linear models or variants have been proposed by Shih and Lumley[98], Fu *et al*[99], Speziale *et al*[100], Launder and Tselepidakis[82], Craft *et al*[101], Craft[102], Craft and Launder[96], Pfunderer *et al*[103], and Batten *et al*[77], the last four being extensions of Fu *et al*'s model and the very last being a compressibility-generalised variant suitable for shock-affected flows. The models differ in detail and in respect of the order of terms included, but all have arisen from the common approach of proposing non-linear expansions, in terms of components of the Reynolds-stress tensor $\overline{u_i u_j}$ (or rather the anisotropy tensor a_{ij}), to second- and fourth-rank tensors which arise in the most general relationship for the pressure-strain term prior to its approximation:

$$\Phi_{ij} = \varepsilon A_{ij}\left(a_{ij}\right) + kM_{ijkl}\left(a_{ij}\right)\frac{\partial U_k}{\partial x_l} \qquad \ldots (74)$$

in which the two groups of terms correspond, respectively, to Φ_{ij1} and Φ_{ij2}. The coefficients of the various terms in the expansions for A_{ij} and M_{ijkl} are then determined by imposing necessary kinematic constraints (continuity, symmetry, etc.). Realisability is introduced into some model forms by sensitising the pressure strain model to invariants of the stress anisotropy. The most elaborate model is that of Craft and Launder and is quadratic in Φ_{ij1} and cubic in Φ_{ij2}, the latter containing six distinct groups of terms and associated coefficients. This model has recently been modified by Batten *et al*[77] to apply to shock-affected flows, in view of experience which had revealed that the parent form responds incorrectly to shocks.

In common with linear models, the above cubic forms also rely on wall corrections (or inhomogeneity terms), albeit much weaker. To at least avoid reliance on the wall distance, efforts have thus been made to replace the wall-distance parameter $\dfrac{k^{3/2}/\varepsilon}{c_\mu^{-3/4}\kappa y}$ in Equation (71) by local turbulence-structure parameters which indicate the wall proximity by implication. Examples for such parameters are those proposed by Craft and Launder[96] and Jakirlic[104],

$$f^w = \frac{1}{c_\mu^{-3/4}\kappa}\frac{\partial l}{\partial x_n} \quad \text{or} \quad f^w = \frac{1}{c_\mu^{-3/4}\kappa}\frac{\partial A^{1/2} l}{\partial x_n} \qquad \ldots (75)$$

where $l = k^{3/2}/\varepsilon$.

Stress diffusion (which is rarely a dominant process) is usually approximated by the 'generalised gradient diffusion hypothesis' (GGDH) of Daly and Harlow[105], already encountered in Equation (67):

$$d_{ij} = \frac{\partial}{\partial x_k}\left(c_s \overline{u_k u_l}\frac{k}{\varepsilon}\frac{\partial \overline{u_i u_j}}{\partial x_l}\right) \qquad \ldots (76)$$

More complex forms of Equation (76) exist, but are not demonstrably superior (see, for example, Demuren and Sarkar[106] and Younis *et al*[107] for reviews) and have rarely been used. The rationale of the GGDH may be understood by reference to the exact transport equations for the triple correlations $\overline{u_i u_j u_k}$ (see Hanjalic and Launder[108]). In the exact Equation (62), the dominant fragment (at high Reynolds numbers) is $\partial(\overline{u_i u_j u_k})/\partial x_k$, with pressure diffusion being sub-ordinate (estimated by Lumley[109] at around 20%). It turns out that the triple-moment equations contain production terms that are formed as products of stresses and stress gradients. A simple algebraic model for the triple moments is one that is based on the assumption that these moments are proportional to the their rate of generation multiplied by a turbulent time scale (k/ε). This notional relationship is reflected by Equation (76) (and also Equation (67)).

Little has been said so far about accommodating the effects of viscosity in the context of low-Re modelling. Most recent models, among them those of Shima[110], Launder and Tselepidakis[82], Launder and Shima[93], So *et al*[94], Jakirlic and Hanjalic[57] and Craft and Launder[96], are low-Re variants, allowing an integration through the viscous sublayer. This is an area in which much reliance is placed on recent DNS data for near-wall flows. In essence, different model elements, especially the dissipation equation (via $C_{\varepsilon 1}$, $C_{\varepsilon 2}$ and additive corrections to the equation), are sensitised to viscosity by way of damping functions with subjects being forms of the turbulent Reynolds number. As the near-wall structure is substantially affected by both inertial and viscous damping, the former provoking strong anisotropy via pressure reflections, low-Re extensions involve a functionalisation on anisotropy invariants, Equation (64), as well as viscosity, each expressing a different physical process. In fact, the dissipation invariants, Equation (65), can also be used, as has been done by Jakirlic and Hanjalic[57]. Because the functionalisation process is non-rigorous, essentially aiming to make the model return a phenomenological behaviour consistent with experimental or DNS data, there is a considerable amount of ambiguity in extending models to low-Re conditions, and thus each model features its own individual sets of functions derived along different routes. Such extensions are not, therefore, considered in detail here.

Although low-Re second-moment-closure models are beginning to be applied to quite complex 2D and even 3D flows, the desire for relative simplicity and the uncertainties associated with near-wall modelling have encouraged the application of somewhat 'simpler' hybrid models which combine high-Re second-moment closure with low-Re EVMs, the latter applied to the viscous near-wall layer (Lien and Leschziner[111, 112]), or even with wall functions (Lien[113], Leschziner and Ince[114], Hanjalic *et al*[115]). Justification, especially for the former option, is provided by the observation that stress transport is usually uninfluential very close to the wall and that the principal function of the near-wall model is to provide the correct level of the shear stress and wall-normal heat flux.

3.3.3 Non-linear eddy-viscosity and explicit algebraic stress models (NLEVM, EARSM)

NLEVMs are based on the general tensorial expansion:

$$a_{ij} = \sum_\lambda \alpha_\lambda T_{ij}^\lambda \qquad \ldots (77)$$

where T_{ij} is a function of the strain and vorticity tensors:

$$S_{ij} \equiv \frac{1}{2}\left(\frac{\partial U_i}{\partial x_j} + \frac{\partial U_j}{\partial x_i} - \frac{2}{3}\frac{\partial U_k}{\partial x_k}\right), \quad \Omega_{ij} \equiv \frac{1}{2}\left(\frac{\partial U_i}{\partial x_j} - \frac{\partial U_j}{\partial x_i} - 2\varepsilon_{ijk}\Omega_k\right) \qquad \ldots (78)$$

in which Ω_k represents any system rotation and α_λ depend on the turbulent time scale (e.g. k/ε) and, in general, also on invariants of strain and vorticity. Linear models follow, evidently, upon setting $\lambda = 1$, $T_{ij} = S_{ij}$, $\alpha_1 = -2\mu_t/k = -2c_\mu k/\varepsilon$. Following particular choices of Equation (77), subject to tensorial constraints, the coefficients of the non-linear terms are determined by reference to experimental and DNS data for key baseline flows.

EARSM turn out to have the same form as Equation (77), but arise from an inversion of simplified forms of the Reynolds-stress-transport models discussed in the previous section. The key simplification is Rodi's[116] 'algebraic' approximation of the convective and diffusive stress transport:

$$\frac{\mathrm{D}\overline{u_i u_j}}{\mathrm{D}t} - d_{ij} \approx \frac{\overline{u_i u_j}}{k}\left(\frac{\mathrm{D}k}{\mathrm{D}t} - d_k\right) = \frac{\overline{u_i u_j}}{k}\left(P_k - \varepsilon\right) \qquad \ldots (79)$$

which leads to an implicit set of algebraic equations for the stresses, with the k- and ε-equation providing P_k and ε. The algebraic approximation for convection in Equation (79) is equivalent to:

$$\frac{\mathrm{D}a_{ij}}{\mathrm{D}t} = 0 \qquad \ldots (80)$$

that is, the rate of change of the anisotropy vanishes and the turbulence structure is thus assumed to be in equilibrium.

Pope[117] was the first to show that the algebraic set arising from the insertion of Equation (79) into the model of Launder *et al*[118] could be arranged in the explicit form in Equation (77) (although P_k, which includes the stresses, was retained in its implicit form). The route by which EARSMs are derived will be further discussed below. What should be clear already is the fact that both NLEVMs and EARSMs are inevitably less general and less fundamentally secure than full Reynolds-stress models. A particular problem arises from the fact that stress convection can be a substantial contributor to the stress balance in curved and swirling flows, and that, in such circumstances, turbulence-energy convection is not a good representation of the convection of stresses (see Fu *et al*[119]). Generally, the adequacy of Equation (79) is strongly dependent of the co-ordinate system adopted and the orientation of the flow relative to that co-ordinate system. Stress convection is only low in the streamwise direction, but the co-ordinates are very rarely well aligned with the flow in practically relevant cases. Some recent proposals designed to address this problem may be found in Girimaji[120], Rumsey *et al*[121] and Wallin and Johansson[122].

The derivation of expansions of the form (77) is constrained by the Cayley-Hamilton theorem, which dictates that there are at most ten tensorially independent, symmetric, traceless, second-rank tensor products of S_{ij} and Ω_{ij} (Pope[117]). No model contains all groups. Cubic models use the first six groups:

$$\begin{aligned}\mathbf{a} = {} & \alpha\mathbf{s} \\ & + \beta_1\left(\mathbf{s}^2 - \frac{1}{3}\{\mathbf{s}^2\}\mathbf{I}\right) + \beta_2(\mathbf{ws} - \mathbf{sw}) + \beta_3\left(\mathbf{w}^2 - \frac{1}{3}\{\mathbf{w}^2\}\mathbf{I}\right) \\ & - \gamma_1\{\mathbf{s}^2\}\mathbf{s} - \gamma_2\{\mathbf{w}^2\}\mathbf{s} - \gamma_3\left(\mathbf{w}^2\mathbf{s} + \mathbf{sw}^2 - \{\mathbf{w}^2\}\mathbf{s} - \frac{2}{3}\{\mathbf{wsw}\}\mathbf{I}\right) \\ & - \gamma_4\left(\mathbf{ws}^2 - \mathbf{s}^2\mathbf{w}\right)\end{aligned} \qquad \ldots (81)$$

where bold type is used for a second-rank tensor, {} indicates its trace, and $\mathbf{I} \equiv (\delta_{ij})$. Products are, for example, $\mathbf{ws} = \Omega_{ik}S_{kj}$ and $\mathbf{w}^2\mathbf{s} = \Omega_{ik}\Omega_{kl}S_{lj}$. The first term on the right-hand side corresponds to a linear eddy-viscosity model (stress $\propto$ strain). For simple shear, $\sigma = (k/\varepsilon)(\partial U/\partial y)$, Equation (81) simplifies to:

$$\begin{aligned} a_{11} &= \frac{1}{12}(\beta_1 + 6\beta_2 - \beta_3)\sigma^2, \quad a_{22} = \frac{1}{12}(\beta_1 - 6\beta_2 - \beta_3)\sigma^2 \\ a_{33} &= -\frac{1}{6}(\beta_1 - \beta_3)\sigma^2 \end{aligned} \qquad \ldots (82)$$

and this shows that the quadratic terms allow normal-stress anisotropy to be captured. These terms make no contribution to the production of k in two-dimensional incompressible flow. The requirement that pure rotation should not generate anisotropy requires that β_3 is either identically zero or vanishes as $\mathbf{s} \to 0$. The terms with coefficients γ_1 and γ_2 are tensorially linear (proportional to $\mathbf{s}$) and are responsible for an important sensitivity to curvature, since in a curved shear layer,

$$\{\mathbf{s}^2\} + \{\mathbf{w}^2\} = -2\left(\frac{k}{\varepsilon}\right)^2 \frac{\partial U}{\partial R}\frac{U}{R} \qquad \ldots (83)$$

where R is the local radius of curvature. The γ_3-related term imparts a sensitivity to swirl. Both this and the γ_4-related term vanish in two-dimensional incompressible flow.

EARSMs are derived, in principle, by inserting Equation (81) (or a variant thereof) into the implicit set of algebraic Reynolds-stress equations, which can be written in the form†:

$$\mathbf{a} = f(\mathbf{a}, \mathbf{w}, \mathbf{s}) \qquad \ldots (84)$$

where the right-hand side contains groups which are linear in $\mathbf{a}$, provided the pressure-strain process has been approximated by a linear model (e.g. Equation (69)). This insertion then leads to a set of equations which can be solved for the set of coefficients in Equation (81) (see, for example, Jongen and Gatski[123], Wallin and Johansson[124]). Closure is then provided by equations for the turbulence scales, k and ε or ω. Apart from being constrained to linear pressure-strain models, EARSMs rely on the linearity of the dissipation on the stresses. This is irrelevant if the dissipation is assumed isotropic. However, more refined near-wall approximations such as Equation (66), with f_ε being a function of the stresses, present EARSMs with problems. These are addressed by Xu and Speziale[125] and Johansson *et al*[126].

There are now some dozen NLEVMs and EARSMs. A first generation of quadratic models emerged through contributions by Saffman[127], Wilcox and Rubesin[128] and Speziale[129]. In Speziale's model, for example, the coefficients were simply taken to be powers of the time scale k/ε, so as to achieve dimensional consistency. Since then, a number of models of various complexity and derived along quite different routes have emerged (Yoshizawa[130], Shih *et al*[131], Rubinstein and Barton[132], Gatski and Speziale[133], Craft *et al*[134], Lien and Durbin[135], Lien *et al*[136], Taulbee *et al*[137], Wallin and Johansson[124,138], Rung *et al*[139] and Apsley and Leschziner[140]). Most NLEVMs are quadratic, while those of Craft *et al*, Lien *et al* and Apsley and Leschziner are cubic. These differences in order are of considerable significance, especially in three-dimensional flows. In particular, the cubic fragments play an important role in capturing the strong effects of curvature on the Reynolds stresses‡. The models by Shih *et al*, Lien *et al* and Craft *et al* are NLEVMs and start from the generic expansion (81), while those of Gatski and Speziale, Apsley and Leschziner, Taulbee *et al*, Wallin and Johansson and Rung *et al* start from an algebraic Reynolds-stress model and are EARSMs. Other routes involve the 'Direct Interaction' approximation adopted by Yoshizawa and the 'Renormalisation Group' (RNG) approach taken by Rubinstein and Barton. Most models depend on two turbulence scales (usually k and ε), as well as strain and vorticity invariants. In contrast, one variant of Craft *et al*'s cubic model makes use of a transport equation for the stress invariant $A_2 = a_{ij}a_{ij}$, while Lien and Durbin's quadratic model depends on the Reynolds stress normal to the streamlines, which is also obtained from a related transport equation.

The predictive quality with which any particular NLEVM resolves anisotropy depends significantly on the calibration of the model's coefficients. This is demonstrated in Table 1 and Fig. 1, taken from Loyau *et al*[141]. Table 1 compares, against experimental data by Tavoularis and Corrsin[142], levels of normal-stress anisotropy in homogeneous shear predicted by the non-linear models of Wilcox and Rubesin[128], Shih *et al*[131], Craft *et al*[134] and Apsley and Leschziner[140]. Figure 1 compares model solutions with DNS data for the normal stresses in a fully-developed channel flow.

As demonstrated through Equations (82) and (83), NLEVMs are able to represent turbulence anisotropy and sensitivity to curvature.

†While implicit algebraic stress models can be and have been used directly, in which case they need to be inverted iteratively during the solution process, they tend to display numerical stiffness and have also been observed to generate more than one solution for one and the same flow, reflecting some ill-posedness.

‡In 2D flow, the genuinely cubic fragments make no contribution. However, the quasi-cubic (strictly linear) terms in Equation (81), associated with γ_1 and γ_2, are active. Indeed, these are responsible for imparting sensitivity to curvature, as reflected by Equation (83).

Table 1
Equilibrium values of non-dimensional anisotropy and shear stress predicted by several models for homogeneous turbulent shear flow

	$a_{11,\infty}$	$a_{12,\infty}$	$a_{22,\infty}$	$a_{33,\infty}$	$(Sk/\varepsilon)_\infty$
Expt	0·403	–0·284	–0·295	–0·108	6·08
Linear $k-\varepsilon$ EVM	0	–0·434	0	0	4·82
WR	0·3	–0·434	–0·3	0	4·82
SZL	0·313	–0·318	–0·19	–0·112	6·56
CLS	0·53	–0·273	–0·307	–0·223	7·66
AL	0·449	–0·276	–0·353	–0·095	6·81

However, one problem they do not alleviate, without intervention, is the excessive generation of turbulence at high strain rates, explained by reference to Equations (29) to (33). This problem is rooted in the form of the linear term in Equation (81) if the coefficient α is taken to be $\alpha = -2c_\mu k/\varepsilon$, as would be consistent with the linear eddy-viscosity framework. This is not, of course, an issue relevant to EARSM, because they determine the coefficients from the Reynolds-stress model which represents far better the sensitivity of the stresses and turbulence energy to the strain. A constant value of c_μ (= 0·09) gives the wrong response to high strain rates (see (29) *vs* (33) and also the last equation in set (6) relative to set (3)). The correct response implies the need for $c_\mu \propto [(k/\varepsilon)(\partial U/\partial y)]^{-1}$ or $c_\mu \propto [(k/\varepsilon)S]^{-1}$. Substitution of the former into Equation (33) shows $\overline{uv} \propto k$ (or a_{12} = const), which is consistent with Bradshaw's expression in Equation (29) and Menter's modelling proposal in Equation (59) for high strain rates. Loyau *et al*[141] show variations of c_μ with the non-dimensional strain in simple shear, $(k/\varepsilon)(\partial U/\partial y)$, built into three non-linear models. All three models incorporate a similar functional dependence, especially at strain rates exceeding the equilibrium value. In most model variants, c_μ is sensitised to both strain and vorticity invariants so as to also avoid the excessive generation of turbulence energy in stagnation flow. Such sensitisation may, of course, also be applied to linear EVMs, and this has indeed been done by Liou *et al*[62]. Here again, EARSMs handle this type of sensitivity without special intervention.

3.4 Compressibility effects

Compressibility manifests itself, first, through mean-density effects in all transport equations and, second, through turbulence correlations, associated with density fluctuations, which only arise in the presence of compressibility and require additional modelling assumptions. The approach taken has thus almost invariably been one of extending models formulated and calibrated for incompressible flow to compressible conditions.

Mean-density variations are accounted for explicitly, as matter of course, in the computation of the convective as well as diffusive fluxes, the latter through dilatation terms in the constitutive stress-strain relation in Equation (1). What is normally not accounted for, however, are implicit effects of density variations on the numerical values of the turbulence-model coefficients. Thus, Huang *et al*[143] show that satisfaction of the van Driest compressible log-law of the wall depends on the use of the ratio of local-to-wall densities in deriving the universal velocity. This has implications to the manner in which numerical constants in the turbulence-transport equations are derived by reference to experiments for incompressible flows. For example, the turbulence-equilibrium relation in Equation (43), which is used to fix $C_{\varepsilon 1}$, depends, in compressible conditions, on the density gradients, and failure to account for this link leads to errors in the representation of the boundary-layer structure. One difficulty here is that every model variant, even within the same model category, exhibits a different level of sensitivity to the density gradient. Marvin and Huang[144] show, for example, that the $k-\omega$ model is much less sensitive than the $k-\varepsilon$ model to the density gradient, at least in terms of the log-law of the wall. Another problem is that the interaction of mean-density gradients with turbulence-model constants cannot really be divorced from other interactions associated with density fluctuations, for which explicit compressibility corrections are usually introduced. Hence, the effects of mean-density gradients need to be investigated in models which are complete, i.e. with all compressibility corrections included. Fortunately, implicit mean-density effects appear to be relatively unimportant when the Mach number is below 2-3.

The effects of compressibility on turbulence transport, via density fluctuations, emerges upon a consideration of the equations governing the Reynolds stresses. This is normally done using density-weighted averaging:

$$\widetilde{\Phi} = \frac{\overline{\rho\Phi}}{\bar{\rho}} \qquad \ldots (85)$$

where Φ is any flow variable. The associated decomposition:

$$\Phi = \widetilde{\Phi} + \phi'' \quad \left(= \bar{\Phi} + \phi\right) \qquad \ldots (86)$$

then implies:

$$\begin{aligned} &\widetilde{\phi''} = 0 \\ &\bar{\rho}\overline{\phi''} = -\overline{\rho'\phi} \\ &\bar{\rho}\widetilde{\phi''\psi''} = \overline{\rho\phi''\psi''} \end{aligned} \qquad \ldots (87)$$

where ψ'' is the density weighted fluctuation of a fluid property Ψ different from Φ.

The inclusion of compressibility leads, principally, to the appearance of dilatational pressure-strain and dilatational dissipation fragments in the Reynolds-stress equations:

$$\begin{aligned} &\Phi_{ij}^{(d)} = \frac{2}{3}\overline{p\frac{\partial u_k}{\partial x_k}}\delta_{ij} \\ &\varepsilon_{ij}^{(d)} = \frac{8}{3}\nu\overline{s_{kk}s_{ij}} \end{aligned} \qquad \ldots (88)$$

where s_{ij} identifies strain fluctuations, as well as source-like pressure-work terms which contain $\overline{u_k''}$ (interpretable as a turbulent mass flux),

$$\bar{\rho}S_{ij}^{(P)} = -\bar{\rho}\overline{u_i''}\frac{\partial P}{\partial x_j} - \bar{\rho}\overline{u_j''}\frac{\partial P}{\partial x_i} \qquad \ldots (89)$$

Moreover, there are covert influences which appear upon the expansion of density-weighted correlations in terms of conventional Reynolds averages. For example, the mean-momentum and energy equations contain:

$$\begin{aligned} &\bar{\rho}\widetilde{u_i''u_j''} = \bar{\rho}\overline{u_iu_j} - \bar{\rho}\overline{u_i''}\overline{u_j''} + \overline{\rho' u_iu_j} \\ &\bar{\rho}\widetilde{u_i''T''} = \bar{\rho}\overline{u_iT'} - \bar{\rho}\overline{u_i''}\overline{T''} + \overline{\rho' u_iT'} \end{aligned} \qquad \ldots (90)$$

where

$$\overline{u_k''} = -\frac{\overline{\rho' u_k}}{\bar{\rho}}; \quad \overline{T''} = -\frac{\overline{\rho' T'}}{\bar{\rho}} \qquad \ldots (91)$$

as well as triple correlations associated with density fluctuations.

Morkovin's[145] hypothesis suggests, and an analysis of DNS data by Huang *et al*[146] for compressible boundary layers confirms, that the correlations in Equation (91) can be safely ignored for M < O(5), which simplifies Equation (90) and removes Equation (89) altogether. Huang *et al*[146] also show that $\overline{\rho' u_iu_j}$ and $\overline{\rho' u_iT'}$ in Equation

(90) are of order 5% of $\overline{\rho u_i'' u_j''}$ and, $\overline{\rho u_i'' T}$ respectively, over most parts of boundary layers at M = 3, with somewhat higher maxima in the viscous sublayer, so that these terms can also be neglected, unless M >> 3. This leaves open the question of the importance of the dilatational pressure and dissipation terms, which are — it is important to point out — pertinent not only to second-moment closure, but also eddy-viscosity models.

There have been several proposals, over the past decade, for modelling the dilatational dissipation terms (Zeman[147], Sarkar *et al*[148], Wilcox[149], Fauchet *et al*[150]) and the pressure-strain fragments (Aupoix *et al*[151], Sarkar[152], Zeman[153], El-Baz and Launder[154]). Some further, mostly *ad hoc* corrections are given in Coakley *et al*[155]. While the models differ substantially in detail, most feature the turbulent Mach number (usually squared) as a key indicator of the importance of compressibility. All models, were derived by reference to flows unaffected by walls (homogeneous or free-shear flows), in which the principal manifestation of compressibility is a reduction in turbulent fluctuations with increasing Mach number and hence a decrease in spreading rate of shear flows. Their applicability to near-wall flows was unclear until the analysis of DNS data by Huang *et al*[146] for supersonic boundary layers at M = 1·5 and 3 demonstrated that the dilatational terms are insignificant in near-wall flows, in marked contrast to free flows. Huang *et al*[146] also showed that all major models for the dilatational terms grossly over-estimate their actual influence, and that the assumption of the dilatational dissipation being correlated with the turbulent Mach number is incorrect. Indeed, the effect of most compressibility corrections on turbulent boundary layers is in the wrong direction (Huang[156]). It is not surprising, therefore, that the use of these models to predict compressible boundary layers gives disappointing results. Thus, the outcome of extensive validation studies in the 1990s at NASA for shock-affected boundary layers is encapsulated by the statement by Marvin and Huang[144] that "indeed experience has shown that for the prediction of subsonic and supersonic flows, these two modifications degrade the results and are not recommended."

While the profound difference in the level of contribution of the dilatational terms in free and wall-bounded flows is not fully understood, Friedrich and Bertolotti[157] conjecture, on the basis of a linear analysis of Coleman *et al*'s[158] DNS data, that the primary source is the impermeability constraint of the wall and its damping influence on wall-normal velocity fluctuations. A parameter which appears to be particularly influential is the gradient Mach number Sl/c, where S is the strain, l is the integral length scale of turbulence and c is the speed of sound, which is one order of magnitude higher in free-shear layers than in boundary layers. DNS studies by Sarkar[159] confirm this and also indicate that the compressibility-related reduction of turbulence is not associated with explicit dilatational effects, but is due to a reduced level of energy production. This suggests that the models proposed for Equation (88), while phenomenologically effective, are fundamentally wrong, even for free shear layers.

The principal conclusion offered on the basis of the above considerations is that there is no tenable argument for including any explicit compressibility models in computations of near-wall flows up to M = O(5). What to do beyond this value is unclear, at present. For free shear layers, current dilatation-related corrections are effective, but must be used with considerable caution in view of their probably serious fundamental flaws.

4.0 NUMERICAL IMPLEMENTATION

4.1 Introductory remarks

Turbulence models consist, in general, of systems of coupled, non-linear algebraic and differential equations. These systems are numerically stiff, and their effective implementation into viscous-flow solvers is a non-trivial task. Indeed, in the case of the most complex class of second-moment-closure models, which lack the numerically advantageous viscosity-related second-order derivative terms, the manner in which the model equations are treated can dictate the numerical properties of the solution algorithm as a whole to the extent of causing or preventing catastrophic instability.

In the case of compressible flows, a wide variety of explicit and implicit time-marching algorithms have been developed to solve the hyperbolic conservation laws. Most schemes used for computing incompressible flows are based on the pressure-Poisson method, originally proposed by Harlow and Welch[160] and recast by Patankar and Spalding[161], the latter being the most widely known of many variations. Other popular approaches for incompressible flows include the projection method (Chorin[162]) and the artificial-compressibility method (Chorin[163]). Both projection and artificial compressibility methods advance a velocity field by some convenient means whilst disregarding the solenoidal nature of **V** and then recover the solenoidal velocity field by a second step. The projection method accomplishes this through the 'Hodge and Helmholtz decomposition' (Chorin and Marsden[164]) in which the velocity field is decomposed into divergence-free and curl-free parts. In the case of the artificial-compressibility method, the incompressible-flow equations are cast in a pseudo-compressible form by adding a pseudo-pressure-time derivative to the continuity equation. The classical formulation of Chorin[163], suitable for steady-state problems, can also be extended to transient flows (Merkle *et al*[166], Rogers[165], Drikakis[167]) via an approach often referred to as 'dual-time stepping'.

The purpose of this section is to discuss specific issues of turbulence-model implementation within the types of numerical framework outlined above.

An appropriate starting point is the two-dimensional Navier-Stokes equations, supplemented by the relevant turbulence-transport equations, written here in a conservative, matrix form in terms of the general spatial coordinates (ξ, ζ),

$$\frac{\partial \mathbf{U}}{\partial t}+\frac{\partial \mathbf{E}}{\partial \xi}+\frac{\partial \mathbf{G}}{\partial \zeta}=\frac{\partial \mathbf{R}}{\partial \xi}+\frac{\partial \mathbf{S}}{\partial \zeta}+\mathbf{H} \qquad \ldots (92)$$

$$\mathbf{U}=\left(\rho,\rho U,\rho W,e,\rho k,\rho\varepsilon,\rho\overline{u_i u_j}\right)^T \qquad \ldots (93)$$

where **E** and **G** contain the advective terms, **R** and **S** contain the viscous terms and **H** contains source-like terms in the turbulence-model equations which do not fit into the flux terms.

It is widely accepted that numerical accuracy is dictated, principally, by the approximation of the advective terms. The most well-founded class of methods for discretising these terms are Riemann solvers (also known as high-resolution methods). Such methods aim to maximise accuracy by solving the Riemann problem at the cell faces of a computational volume. Implementations of Riemann solvers have been proposed in conjunction with both upwind and centred approximations of variables on the characteristics defining the directions of propagation of acoustic and scalar-property changes. The design of these schemes is based on the mathematical theory of hyperbolic conservation laws.

The addition of turbulence-transport equations leads to a number of specific solution difficulties, the most important of which are rooted in the weak coupling of these equations to the aerodynamic set. In the case of eddy-viscosity models, the link between the fluid-flow and turbulence-transport equations is established through the eddy viscosity, which is not, however, a solution (transported) variable. In the case of second-moment closure, the link is effected directly through the Reynolds stresses which are solution variables in **U** and occur explicitly in the momentum-flux components of **R** and **S**.

In the case of eddy-viscosity models, implemented in hyperbolic-system solvers, inter-equation coupling can be strengthened through: (*i*) the development of non-linear high-resolution methods that encompass the characteristics of the turbulence equations and (*ii*) an implicit-coupled solution of the equations, including an implicit treatment of the source terms. Apart from relatively minor rearrange-

ments in the source terms of the turbulence equations (e.g. their linearisation), no special measures are generally adopted in pressure-based schemes which solve the equations as a segregated, sequential set. Second-moment closure is considerably more challenging, however, and its stable implementation relies, in both numerical environments, on a whole range of stability-promoting measures, designed to strengthen the coupling between the equations. These issues are discussed in the following sections.

4.2 Schemes originating from hyperbolic conservation laws

4.2.1 Numerical reconstruction of advective terms

A seemingly minor, though influential implementation aspect to highlight first is that the turbulence energy featuring in most turbulence-transport models should be included in the total-energy budget. This can be particularly important for the accuracy of supersonic- and hypersonic-flow simulations. It certainly affects the efficiency of the computations, especially when implicit schemes are employed, in which case the turbulence energy contributes implicitly to the elements of the inverse matrix of the system in Equation (93).

Since the turbulence energy is a solution variable in both eddy-viscosity and second-moment closure models (in the latter through) $k = 0{\cdot}5(\overline{u^2} + \overline{v^2} + \overline{w^2})$ one can include the equation for the turbulence energy in the solution of the Riemann problem. The solution variables can then be re-constructed at the cell faces as functions of their corresponding characteristic values, i.e. those which are dependent on the three wave speeds. The latter are defined by the eigenvalues of the Jacobi matrices of the advective fluxes. Barakos and Drikakis[168] have developed a Riemann solver along these lines for the compressible Navier-Stokes equations in conjunction with two- and three-equation eddy-viscosity models. In their method, the solution to the Riemann problem relates the cell-face turbulence energy to the values of the turbulence energy on the three characteristics, as well as to the corresponding characteristic values of the conservative flow variables. The values on the characteristics are subsequently calculated by second- or third-order MUSCL-type interpolation schemes. The above advective method provides a direct coupling between turbulence-transport and fluid-flow equations, regardless of whether explicit or implicit time-discretisation is employed.

While the turbulence energy can be reconstructed as a function of its three characteristics values, the same does not apply to the subject of the second turbulence-transport equation, i.e. the equation for the turbulence dissipation or any other variable employed as a surrogate of the turbulence length scale. This is due to the fact that the length-scale variable does not appear explicitly in the fluxes of other equations and cannot be coupled to them. For incompressible flow, neither the turbulence energy nor the length-scale variable appears explicitly in the flux terms of the fluid-flow equations, and both can therefore be re-constructed only as a function of their first characteristic value (Drikakis and Goldberg[169]).

Although the eigenstructure of the equations allows for inter-equation coupling via the flux terms, it does not account for the coupling established through the source terms of the turbulence-transport equations. These terms, which are often dominant and hence numerically influential, must therefore be treated by other numerical means which are discussed below.

4.2.2 Implicit implementation

Many schemes devised originally for non-turbulent flow have been used to solve turbulent-flow problems through the addition of eddy-viscosity models implemented in a decoupled fashion, in which the Navier-Stokes set is solved first and the turbulence equations are then integrated sequentially to update the eddy viscosity (Kunz and Lakshminarayana[170], Liou and Shih[171], Sahu and Danberg[172]). This approach is straightforward and hence popular. However, it results in slow numerical convergence, as will be demonstrated later. It is especially disadvantageous in unsteady flows, because it tends to require, for stability reasons, different time steps for the mean-flow and turbulence-transport equations.

The implicit-coupled solution of the Navier-Stokes and turbulence-transport equations has been pursued in a number of schemes (Gerolymos and Vallet[173], Lin *et al*[174], Barakos and Drikakis[168]). Gerolymos and Vallet[173] have adopted an implicit implementation of the Launder-Sharma[41] $k - \varepsilon$ model using a fully coupled, approximately factored, implicit-backward Euler method. They applied this method to transonic flow with shock-boundary layer interaction and found it to be robust and stable for Courant-Friedrichs-Lewy (CFL) numbers up to 50. Lin *et al*[174] also presented an implicit-coupled solution in conjunction with Chien's[44] $k - \varepsilon$ model, using a biconjugate gradient method with incomplete lower-upper factorisation as pre-conditioner. They concluded that this method (denoted Bi-CGSTAB) was more efficient than other conjugate-gradient variants.

Implicit unfactored methods, based on Newton sub-iterations and Gauss-Seidel relaxation (IUNGS), have been successfully used both for the Euler[175-177] and Navier-Stokes[178-181] equations, the latter in conjunction with algebraic turbulence models. These studies demonstrate that the method allows very high CFL numbers to be reached, while the numerical solution is less sensitive to the choice of the time step than approximate-factorisation methods. Other studies[182, 183] have shown that implicit unfactored methods are also well-suited to efficient parallel implementation on multi-processor platforms.

The success of unfactored methods in inviscid and viscous-flow computations has encouraged their adoption in conjunction with two-equation eddy-viscosity models[168, 184]. This requires the calculation of the Jacobian and eigenvector matrices with the turbulence variables included (see below). In the case of two-equation eddy-viscosity models, these are 6×6 and 7×7 matrices for two- and three-dimensional flows, respectively. When turbulence is represented via second-moment closure, a fully-coupled solution is a formidable task, since the system then consists of 12×12 Jacobian and eigenvector matrices.

Morrison[185] has presented a coupled, approximate-factored solution for second-moment closure. However, his scheme was not fully implicit, in that the source terms of the turbulence equations associated with production, redistribution and dissipation were only point-coupled. Further simplifications introduced by Morrison led to a scheme in which the turbulence-model equations were coupled only through the presence of the turbulence energy (normal stresses) in the Jacobian flux matrices; thus, the turbulence-transport equations were, in effect, decoupled from those describing the mean flow.

A more elaborate scheme for second-moment closure was employed by Vallet[186] who adopted a flux-vector-splitting scheme in conjunction with a point-implicit method. The coupling among the fluxes as well as source terms was accounted for across the entire set of twelve equations. Coupling was mainly established through a full linearisation of all sources with respect to all turbulence quantities. The subset could then be solved by sub-iterations, rather than full inversion (which would require very large amounts of computer storage). There is no unambiguous evidence, however, that this level of strong coupling is beneficial to stability and convergence. For example, Vallet[186] reports convergence results for a transonic channel flow, which show convergence stalls after a reduction in residuals by less than two orders of magnitude.

A somewhat simpler approach for implementing second-moment closure in compressible Navier-Stokes methods was adopted by Batten *et al*[187]. They solved the mean-flow equations by means of a block-coupled implicit scheme and the turbulence-transport equations as a segregated set. Thus, the fluxes of any turbulence variable were assembled by reference to the contact-wave velocity and the interface state of the density, and then an implicit decoupled equation was derived by including only diagonal components of the convective, diffusive and source Jacobians in the equation, while the remaining terms were treated explicitly.

Other routes to obtaining coupled solution schemes rely on the use of explicit multistage algorithms, for example, the Runge-Kutta method. This can also be combined with the implementation of advanced solvers such as multigrid acceleration. Liu[188] has presented such a coupling approach for the $k - \omega$ model, and reported results for steady-flow computations around cascade geometries. In the explicit-coupled approach, residual smoothing and multigrid acceleration are uniformly applied to both the Navier-Stokes and turbulence-model equations, with the eddy viscosity being updated at each stage of the multi-stage Runge-Kutta scheme. The corresponding loosely-coupled approach, based on the combination of the multi-stage Runge-Kutta scheme and multigrid solver, has been employed by Liu and Zheng[189]. In this case, the turbulence-model equations were 'frozen' while the Navier-Stokes equations were being solved, and *vice versa*. Within the loosely-coupled approach, the eddy viscosity need not be updated at every stage of the explicit iterative process, but only at the first and last stages, the advantage being a gain in economy. The loosely-coupled approach generally leads to different convergence rates for the Navier-Stokes and turbulence-model equations.

In order to convey, in specific terms, an impression of the implementation issues that need to be addressed in implicit density-based solvers, details are presented below for the particular fully-coupled approach of Barakos and Drikakis[168], which includes a two-equation eddy-viscosity model (EVM). In particular, the Jacobian matrices are derived, the Newton iteration is outlined, and the treatment of the source-term matrix associated with the turbulence-model equations is explained. Attention is restricted to the 2D set Equation (92). In the case of the $k - \omega$ model, the dissipation rate ε in **U** is obviously replaced by ω. Two-equation EVMs contain source terms which are included in the matrix **H** in Equation (92). These terms must also be treated implicitly if a fully-coupled, implicit implementation is to be obtained.

The implicit form of Equation (92) is written as follows:

$$\frac{U^{n+1}-U^n}{\Delta t}+E_\xi^{n+1}+G_\varsigma^{n+1}=R_\xi^{n+1}+S_\varsigma^{n+1}+H^{n+1} \quad \ldots (94)$$

Next, the fluxes are linearised around the time-level n, e.g.,

$$E^{n+1}=E^n+\left(\frac{\partial E}{\partial U}\right)^n \Delta U \quad \ldots (95)$$

where

$$\Delta U = U^{n+1}-U^n \quad \ldots (96)$$

Using Equation (95), Equation (94) is written:

$$\begin{aligned}&\frac{\Delta U}{\Delta t}+\left(A_{inv}^n\Delta U\right)_\xi+\left(C_{inv}^n\Delta U\right)_\varsigma-\left(A_{inv}^n\Delta U\right)_\xi\\&-\left(C_{inv}^n\Delta U\right)_\varsigma-\frac{\partial H}{\partial U}\left(U^{n+1}-U^n\right)=RHS\end{aligned} \quad \ldots (97)$$

The right-hand-side terms (RHS) are:

$$RHS=-\left(E_\xi^n+G_\varsigma^n-R_\xi^n-S_\varsigma^n-H^n\right) \quad \ldots (98)$$

and

$$A_{inv}=\frac{\partial E}{\partial U},\quad C_{inv}=\frac{\partial G}{\partial U},\quad A_{vis}=\frac{\partial R}{\partial U},\quad C_{vis}=\frac{\partial S}{\partial U} \quad \ldots (99)$$

are the Jacobi matrices of the inviscid and viscous fluxes. Note that the Jacobians contain terms from all equations, incuding those describing turbulence transport. In the case of Reynolds-stress models, these are 12×12 matrices. On the left-hand-side (LHS) of Equation (97), the thin-layer viscous Jacobian matrices can be used instead of the full ones (Barakos and Drikakis[168]). Numerical experiments have shown, however, that for steady flows, the number of iterations remains virtually unchanged if the full Jacobians are utilised[178, 179]. The above system can be solved by an approximate factorisation or unfactored method. The former restricts the CFL number to lower values than the latter, especially on highly-skewed grids. Therefore, the implicit-unfactored method is preferred in turbulent-flow computations.

The implicit-unfactored method can be combined with efficient iterative solvers such as a Newton-type method. The latter can be obtained if a sequence of approximations† q^v such that $\lim_{v>1} q^v \rightarrow U^{n+1}$ is defined between the two time levels n and $n+1$. In the case of steady flow, a fixed Newton sub-iteration is utilised, whereas for unsteady flow, Newton sub-iterations are carried out until convergence is achieved at each real time step. The inversion of the final discretised system of equations can be obtained by line- or point-Gauss-Seidel relaxation techniques.

From Equation (97) it is obvious that the eigenstructure of Equation (92) is taken into account in the implicit part of the discretised equations through the inviscid Jacobian matrices. The inviscid Jacobians A and C are written in terms of their eigenvector and eigenvalue matrices,

$$A_{inv}=T\Lambda T^{-1} \quad \ldots (100)$$

where Λ is the eigenvalue matrix and T, T^{-1} are the left and right eigenvector matrices, respectively. In the case of two-equation models, these are 6×6 matrices and include the contributions from the turbulence-model equations (Barakos and Drikakis[168]). It is sufficient for accuracy and efficiency to obtain second-order accurate discretisation for the terms $(A_{inv}^n\Delta U)_\xi$, $(C_{inv}^n\Delta U)_\varsigma$, $(A_{vis}^n\Delta U)_\xi$ and $(C_{vis}^n\Delta U)_\varsigma$.

The implicit-coupled implementation can be employed for all types of two- and three-equation EVMs, both linear and non-linear. The Jacobians of the inviscid and viscous fluxes remain the same for all two-equation turbulence models. The treatment of source terms in the matrix **H** is discussed below.

4.2.3 Treatment of source terms

For present purposes, it is sufficient to consider the reduced system,

$$\frac{\partial U}{\partial t}=H\equiv H\left(U,U_\xi,U_\varsigma\right) \quad \ldots (101)$$

where

$$U=\begin{pmatrix}\rho k\\ \tilde{\rho\varepsilon}\end{pmatrix},\quad H=\begin{pmatrix}h_k\\ h_{\tilde{\varepsilon}}\end{pmatrix} \quad \ldots (102)$$

and H_k and $H_{\tilde{\varepsilon}}$ are the source terms associated with the transport equations for k and $\tilde{\varepsilon}$, respectively. The implicit discretisation of Equation (101) is:

$$U^{n+1}=U^n+\Delta t H^{n+1} \quad \ldots (103)$$

After linearisation of the matrix H^{n+1} with respect to U, Equation (103) is written as

$$\left(U^{n+1}-U^n\right)\left(I-\Delta t\frac{\partial H}{\partial U}\right)=\Delta t H^n \quad \ldots (104)$$

A stability analysis of Equation (101) shows that the implicit discretisation in Equation (104) is unstable if $H > 0$. In order to increase the diagonal dominance of the inversion matrix, only terms

†q denotes the conservative solution vector **U** at each Newton sub-iteration.

with negative sign may be moved to the LHS of Equation (104) and similarly to the LHS of Equation (97). For the case of the Launder-Sharma[41] $k-\varepsilon$ model, the negative source terms are given by:

$$H_k = -\rho\tilde{\varepsilon}, \quad H_{\tilde{\varepsilon}} = -C_{\varepsilon 2} f_2 \frac{(\rho\tilde{\varepsilon})^2}{\rho k} \qquad \ldots (105)$$

where $C_{\varepsilon 2}$ is a coefficient and f_2 is a damping function. Using $\mu_t = c_\mu f_\mu [(\rho k)^2/\rho\tilde{\varepsilon}]$ for the eddy viscosity (c_μ is a numerical coefficient and f_μ is a damping function), the source terms are written as:

$$H_k = -c_\mu f_\mu \frac{(\rho k)^2}{\mu_t}, \quad H_{\tilde{\varepsilon}} = -C_{\varepsilon 2} f_2 \frac{(\rho\tilde{\varepsilon})^2}{\mu k} \qquad \ldots (106)$$

and the Jacobian matrix $\partial H/\partial U$ is given by:

$$\frac{\partial H}{\partial U} = \begin{bmatrix} -2\dfrac{c_\mu f_\mu}{\mu_t}(\rho k) & 0 \\ c_{\varepsilon 2} f_2 \dfrac{(\rho\tilde{\varepsilon})^2}{(\rho k)^2} & -2c_{\varepsilon 2} f_2 \dfrac{\rho\tilde{\varepsilon}}{\rho k} \end{bmatrix} \qquad \ldots (107)$$

The diagonal elements of Equation (107) are added to the diagonal elements of the inversion matrix of the system in Equation (97).

A similar analysis to that above can also be followed for the case of incompressible flows computed with the artificial-compressibility method (Merci *et al*[190]).

4.2.4 Performance examples

Barakos and Drikakis[168] have contrasted the efficiency of the implicit-coupled method against those of the implicit-decoupled and fully explicit strategies. In the implicit-decoupled approach, the implicit solution is used only for the mean-flow equations, while the turbulence-transport equations are solved in a segregated fashion by an explicit (Runge-Kutta) method. Table 2 shows the work units required for the three solution strategies for the case of a transonic flow over the axisymmetric bump of Bachalo and Johnson[191] (see also Johnson *et al*[192]). The flow features shock–boundary-layer interaction and separation and has been identified as Case 8611 in Klein *et al*[193]. The work units (WU) in Table 2 relate to the Launder-Sharma[41] $k-\varepsilon$ model; one WU corresponds to one minute of CPU time on a HP9000/735/99 workstation using double precision computer arithmetic. The convergence results demonstrate that the implicit coupled implementation is the most efficient.

The implementation of non-linear EVMs can be undertaken in a similar fashion, as shown by Barakos and Drikakis[194]. Results for the CPU time (work units) of the fully-coupled, implicit implementation of several linear and non-linear (two- and three-equation) EVMs are shown in Table 3. The work units refer to computations for the Case 8611[190-192] as well as for Delery's[195] transonic channel-bump flow (Case C).

Table 2
Work units required by different implementation approaches of turbulence models; a WU corresponds to 1 minute of CPU time on a HP9000/735/99 machine, using double-precision arithmetic; results taken from Barakos and Drikakis[194]

Numerical approach	Work units (WU)	Convergence error
Implicit-coupled	1·0	10^{-7}
Implicit-decoupled	~1·55	10^{-7}
Explicit	~1·4	10^{-2} (stalled at this level)

Table 3
Work units required for linear and non-linear EVMs based on the fully-coupled, implicit implementation; a work unit corresponds to one minute of CPU time on a HP~9000/700/99 workstation; results taken from Barakos and Drikakis[194]

Model	Case 8611, Bachalo bump	Delery bump, Case C
LS	610	—
SST	738	1,090
NL $k-\varepsilon$	890	1,332
NL $k-\varepsilon-A_2$	1,028	1,803

The non-linear three-equation EVM ($k-\varepsilon-A_2$) of Craft *et al*[134] is the most expensive variant employed. The increased CPU time for this form, compared to the other models, is due to the presence of the equation for A_2 (the second invariant of Reynolds-stress anisotropy, Equation (64)). This can also be observed by reference to the CPU times required for the three-equation and two-equation NLEVMs (Craft *et al*[134]). As for linear models, the SST (shear-stress-transport) model of Menter[29] is slightly more CPU demanding than the Launder-Sharma (LS) form. An advantage of the SST model is that it can be used in conjunction with coarser grids in the near-wall region — with values of $y^+ \approx 2$ at the first grid point off the wall — without adverse effects on the accuracy of the results. On the other hand, the $k-\varepsilon$-based models, both linear and non-linear, only converge (Barakos and Drikakis[194]) if the wall-nearest y^+ value is of order 1 and below.

Figure 3, taken from Leschziner *et al*[78], shows the convergence histories for four models applied to a Langley jet/afterbody flow: two EVMs and two RSTMs (JH denoting the Jakirlic-Hanjalic model[57] and MCL a model documented in Batten *et al*[77]). The figure demonstrates that judicious implementation allows Reynolds-stress models to be converged at roughly the same rate as that for much simpler linear EVMs.

4.3 Pressure-based approach

Pressure-based schemes have emerged in the context of efforts to compute incompressible or weakly compressible flows and are much less popular in aerodynamics. In essence, the mass-conservation equation is replaced by a pressure Poisson (or pressure-correction)

†Similar extensions to the zero Mach number limit have been presented for methods originating from hyperbolic conservation laws[201-203].

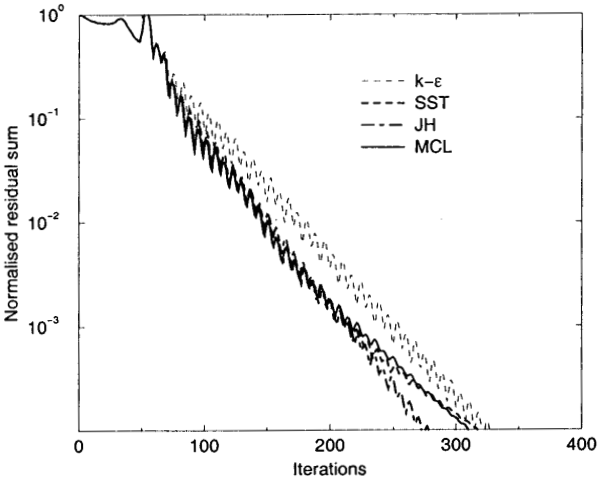

Figure 3. Convergence histories for four turbulence models, two of which are second-moment closures (JH[57], MCL[77]), applied to Langley jet-afterbody flow (taken from Leschziner *et al*[78]).

equation derived by combining the momentum and mass-conservation equations. A number of compressible-flow extensions (for M > 1) have been formulated[196-200] with the aim of deriving a solution framework for a broad range of Mach numbers†, from low subsonic to supersonic.

Pressure-based solvers are almost always only partially coupled, involving a sequential solution of the equations. Hence, the incorporation of transport models of turbulence usually entails little more than stringing the related differential equations to those governing the mean flow, with minimal implicit coupling, usually effected via a source-term linearisation and the use of negative fragments to enhance diagonal dominance, similar to that outlined in Section 4.2.3. This explicitness can be a disadvantage, but there is relatively little that can be done to address this.

An important exception arises in the case of Reynolds-stress-transport models. The distinction is rooted in the absence of the crucially important second-order viscosity-related terms, which changes the character of the momentum equations from elliptic to hyperbolic. In effect, turbulence transport in the mean-flow equations is represented by substantial source-like terms, which makes the equations extremely stiff. In this case, elaborate stability-promoting measures are needed, and these are documented in considerable detail in Lien and Leschziner[199] and Leschziner and Lien[204].

One key measure is the extraction of apparent (pseudo-) viscosities from the Reynolds-stress-transport equations, which then allows the introduction of stability-promoting second-order-gradient terms into the mean-flow equations. As shown by Lien and Leschziner[199], this can be done either at the differential (pre-discretisation) level or after discretisation. The latter option is indicated below in highly simplified terms to convey the essential idea.

With attention directed towards the normal stress $\overline{u^2}$, the discretised form of the stress-transport equation, integrated over a rectangular finite volume, may be written:

$$A_P\overline{u_P^2} = \sum_m A_m\overline{u_m^2} + \mu_{11}^P\frac{(U_+ - U_-)}{\Delta x} + S_{\overline{u^2}} \qquad \ldots (108)$$

where the subscript P denotes the cell-centre at which the normal stress is being computed, the RHS sum represents, through A_m, the influence of neighbouring cell-centre values on P (via the fluxes of the normal stress through the faces of the finite volume) and $S_{\overline{u2}}$ contains all fragments not included in other RHS terms. The crucial second term on the RHS contains an approximation of the x-wise U-velocity derivative across the cell. This term arises naturally in the discretisation process as a consequence of the presence of the stress-generation term $P_{\overline{u2}}$ (see Equation (3), for example) in the stress-transport equation. The premultiplier of the velocity difference, identified by μ_{11}, turns out to be an unconditionally positive group of terms of the form

$$\mu_{11}^P = \left(C\rho\overline{u^2}\right)_P \qquad \ldots (109)$$

where C is a function of model constants and geometric grid parameters. Upon insertion of Equation (108) into the U-momentum equation, there arises, quite naturally, a second-order (diffusive) velocity-derivative term which is associated with the (apparent) viscosity μ_{11}. The analogous treatment of other stress-transport equations gives rise to corresponding apparent viscosities μ_{22}, μ_{12} and μ_{21} (for 2D conditions), the overall result being a stabilisation of the iterative solution of the mean-flow equations.

Other important measures include the implicit introduction of artificial fourth-order stress diffusion into the discretised stress-transport equations (in fully-colocated finite-volume schemes) and a practice which allows diagonal dominance of the discretised stress-equation sets to be substantially enhanced, along the lines indicated in Section 4.2.3, through a linearisation of the stress-source terms with fragments being arranged to be unconditionally positive and negative. In the case of staggered-grid schemes (rarely used now for complex 3D problems), a staggered arrangement of the stresses contributes greatly to stability and convergence (Huang and Leschziner[205]). This arrangement involves locating stress nodes on the faces of momentum cells, midway between the velocity nodes used to approximate the associated 'driving' strain, the association being implied by the Bousinesq stress-strain relationships. The purpose of this is to secure, numerically, a strong coupling between the stress and strain fields. The introduction of fourth-order stress diffusion in collocated-cell schemes, already mentioned, serves a similar purpose.

With these measures in place, a number of quite complex aerodynamic flows, both compressible and incompressible, have been computed with RSTMs, among them separated flow over aerofoils and prolate spheroids at high incidence (Lien and Leschziner[206,207]), transonic bump flows (Lien and Leschziner[112], Hasan and McGuirk[208]), 3D subsonic and supersonic impinging jets (Leschziner and Ince[114]) and 3D transonic jet-afterbody flow (Hasan *et al*[209]). While in all cases, the resource requirements of the RSTM were larger that those for EVMs, the CPU overheads were relatively modest — typically, of order 1·5-3.

5.0 ASSESSMENT OF MODEL PERFORMANCE

5.1 Introduction

Any attempt at a definitive and secure assessment of the predictive performance of turbulence models over a wide range of flow conditions is fraught with difficulties, for this performance is sensitive to:

- even very minor changes to the turbulence model in terms of its numerical constants, flow-specific correction terms and limiters;
- details of the model's implementation into the numerical framework;
- numerical errors, grid topology and convergence criteria;
- the location of computational boundaries and the realism and completeness of boundary conditions;
- the sensitivity of the models to the boundary values of the transported turbulence scales;
- the accuracy and completeness of the experimental data, and the applicability of corrections (e.g. tunnel corrections for transonic flows).

In very many cases, a turbulence model or variant has only been tested by the originator of that model, most frequently for a narrow range of flow conditions. Often, no statement is given on numerical accuracy or boundary conditions. In many cases, especially in compressible flows, turbulence quantities are not available, and boundary conditions need to be inferred from the mean-flow data — for example, by way of the mixing-length or equilibrium considerations, see Equations (11)-(17). This can be done in a number of different ways and can have a significant influence on the predictions.

The most valuable sources of information on model performances are concerted and targeted validation programmes undertaken by teams, with the specific objective of identifying generic predictive characteristics of model types and highlighting broadly applicable differences. These studies are especially valuable if undertaken by several groups in parallel with more than one numerical method and if the results are demonstrated to be practically independent of the numerical framework. One such programme, or rather series of programmes, was undertaken by NASA Ames in the mid-1990s by Coakley, Marvin, Huang, Bardina and their colleagues. Some of the conclusions presented below arise from this work. Other useful sources are EU-funded validation projects such as EUROVAL (Haase *et al*[210]), ECARP (Haase *et al*[211]) and, to a lesser extent, ETMA (Dervieux *et al*[212]), although these (especially the last) were not as closely interactive as would be desirable for a secure assessment. The series of ERCOFTAC workshops on refined turbulence

modelling is potentially useful, but has focused mainly on internal flows and has included no over-arching quality-control framework for undertaking the computations submitted to the workshops. Finally, national validation programmes focusing on carefully selected test flows and involving a close collaboration between industrial and university groups offer some fairly reliable conclusions. Unfortunately, the amount of information on the performance of advanced anisotropy-resolving models is quite limited, partly because only a few groups are able to undertake computations with these models for complex flows. Some individual studies have been quite extensive, however, involving a rational sequence of test cases, from homogeneous to highly demanding 3D flows, and can be trusted to provide fairly reliable information on the performance of these models.

In what follows, the predictive performance of models is reviewed, for steady-flow applications, by model category. This is done, in most cases, by reference to studies involving what are held to be relatively reliable comparisons of several models contained within one and the same study. With few exceptions, isolated verifications of single models are not included, but these may be found, in most cases, within publications by the respective model originators which are referred to in Section 3. Results for turbulent unsteady flow are much rarer, and broad comparative studies are virtually non-existent. These are therefore reviewed separately, at the end, in sub-sections pertaining to the few application areas for which turbulence-modelling studies have been undertaken.

5.2 Algebraic models

There is relatively little that needs to be said about algebraic models. They are designed for attached flows and should only be applied to such (a fact disregarded with astonishing frequency, even as recently as 1997), in which case differences in the solutions they return are modest in most circumstances. This applies, in particular, to attached aerofoil flows, even those around multi-element high-lift configurations (e.g. NLR 7301 with flap) and wings (e.g. DLR-F4), where algebraic models return entirely adequate results, as long as the flow does not approach separation (see Haase *et al*[211]). An informative fundamental study undertaken within EUROVAL (Haase *et al*[210]) involved the application of the Cebeci-Smith and Baldwin-Lomax models, as well as two half-equation models, to five boundary layers at zero, favourable and adverse pressure gradients. In the most taxing retarded boundary layers, some differences between models did emerge, with the Baldwin-Lomax model underestimating the response to the adverse pressure gradient and the Cebeci-Smith model performing as well as the best of the half-equation models. In flows approaching or involving separation, algebraic models do not perform well, tending to predict excessive levels of eddy viscosity, inhibiting separation or returning a seriously erroneous representation of the separation process, if at all captured. This is illustrated, for example, by computations for the Aerospatiale 'A' aerofoil in Haase *et al*[210] and for NACA 4412 aerofoil in Haase *et al*[211]. In transonic flows, algebraic models provide a reasonable response in weak-interaction conditions, but misrepresent the interaction associated with shock-induced separation. There are several examples of this included in Haase *et al*[210] for the RAE2822 aerofoil (especially case 10) and for Delery's[213] transonic bump flows (especially the separated case C). Here again, algebraic models under-estimate the response to the adverse pressure gradient, prevent separation and return a shock position which is too far downstream. Poor performance is also observed in hypersonic, separated compression-corner flows for which Horstman[214] finds a widely varying, non-systematic level of agreement of algebraic-model solutions with experimental data (see also Dolling[215]).

5.3 Half-equation models

Half-equation models have hardly been used outside the area of external aerodynamics. Their main attraction is their simplicity and economy, based on a combination of an algebraic viscosity prescription across the flow with an evolution equation along it. This combination implies, or leads to the hope of, a favourable performance in attached flows that depart from equilibrium as a result of significant streamwise changes.

Among the group of one-equation models, that of Johnston and King[31] and its improved form by Johnson and Coakley[34] have been the two most extensively applied and tested, mainly in the industrial environment in which computational economy is of outstanding advantage. Several flows computed with these models are included in Haase *et al*[210, 211] and in Menter[216]. One flow is the RAE 2822 transonic aerofoil. For the most challenging separated Case 10, significant differences are reported in Haase *et al* between solutions arising from slight computor-specific variations of the models, and no firm conclusion can be drawn, except that most implementations result in defects not dissimilar to those observed with algebraic models. In contrast, Robinson and Hassan[217] report a close to excellent resolution of the shock–boundary layer interaction over the RAE 2822 (Case 10) aerofoil and data for the NACA 0012 aerofoil with the Johnson-King model. Substantial variability in performance is also observed in results for shock-induced separation over Delery's channel bump (Cases A & C), with only one implementation showing marked improvements relative to algebraic models in respect of capturing the separation (Case C). However, that same implementation gives an overly sensitive representation of the weak interaction on the plane wall opposing the bump and also in the weak-interaction case A. An outcome of a study, also reported in Haase *et al*[210], of five incompressible boundary layers is that both the Johnson-King and, to a lesser extent, the Johnston-Coakley models are not well suited to near-equilibrium conditions — a conclusion consistent with the performance of the models in weak shock–boundary-layer interaction. In particular, both give fairly poor results for skin-friction, shape-factor distributions and universal velocity profiles. Menter[216] reports computations for two decelerating boundary layers and a thin separated flow from a cylinder in a diffuser, and these show the Johnson-King model to perform well across all flows — indeed better than the $k - \omega$ model. Results for incompressible separation from two high-lift aerofoils, the Aerospatiale A and NACA 4412, both documented in Haase *et al*[211], are mixed. In the former, performance is unclear as there are inconsistencies between contributed solutions. However, in the latter geometry, good results are achieved with the Johnston-King model which returns the extensive suction-side separation observed experimentally. Overall, the performance of half-equation models is too variable to permit a definitive conclusion. Menter's observations, in particular, provide indications that the Johnson-King model has advantageous characteristics in retarded boundary layers and thin separated flows, through its lower eddy viscosity in strong non-equilibrium conditions. However, half-equation models, do less well in attached weakly non-equilibrium boundary layers.

5.4 Two-equation models

There have been numerous studies of two-equation models for external as well as internal flows. Gerolymos and Vallet[173] provide an overview table of over 30 computational studies of transonic flows with two-equation models (mostly $k - \varepsilon$). A broad conclusion emerging from these is that models of this type, unless corrected, tuned to specific conditions or used with different constants relative to the base-line formation, generally return disappointing results in separation (although much better than algebraic models). This is especially so in separation from curved surfaces, in decelerating boundary layers, in curved shear layers and in shock–boundary-layer interaction. Better performance is returned when separation is provoked by sharp edges, such as in backward-facing steps.

There is a fair number of studies that report relatively modest performance differences between basic $k - \varepsilon$ and $k - \omega$ formulations. A difficulty here is that any intrinsic differences between the ε- and

ω-equations are clouded by the strong dependence of performance on the precise value of the numerical constants in the ω-equation, the nature of the viscosity-related damping functions and the inclusion or omission of the fragment of mixed k- and ω-derivatives (see Equation (57)). For example, Jang *et al*'s[218] computations of separated flow behind a streamwise periodic channel constriction show that the $k - \omega$ model yields significantly stronger sensitivity to adverse pressure gradient, hence giving a longer recirculation zone, but this appears to be linked, principally, to the viscosity-dependent damping functions†. There is ample evidence pointing to excessive near-wall turbulence that is returned by both types of length-scale equation, thus hindering deceleration and separation, albeit to a different extent. Menter[216], Huang[219] and Bardina *et al*[76] show this for Driver's[220] incompressible separated boundary layer, the Bachalo-Johnson[191] transonic-bump flow and the RAE 2822 aerofoil; Rung *et al*[221] for Delery's separated bump flow, the RAE 2822 aerofoil and the ONERA M6 wing (Schmitt and Charpin[222]); Apsley and Leschziner[74] for the separated diffuser flow of Obi *et al*[223]; Barakos and Drikakis[224] for the Bachalo-Johnson[191] transonic-bump flow; Barakos *et al*[225] for the subsonic flow around the ONERA-A aerofoil[33] and the transonic flow around the RAE 2822 aerofoil[22]; Abid *et al*[226, 227] for Coles and Wadcock's[34] measurements of the flow around the NACA 4412 aerofoil, the RAE 2822 aerofoil and the axisymmetric bump flow. A similar message is conveyed in a compilation by Dolling[215] of computational studies for compression-ramps. Finally, Robinson and Hassan[217] report a poor performance of the $k - \omega$ model for transonic flow over the RAE 2822 (Case 10) and NACA 0012 aerofoils and subsonic separation over the NACA 4412 aerofoil. These defects are partly rooted in fundamental weaknesses of the eddy-viscosity formulation and partly in the tendency of the length-scale equation to give excessive values for this scale. To this must be added the strong sensitivity of the $k - \omega$ model to the free-stream level of ω (Menter[75], Bardina *et al*[76]), which makes the model perform especially badly in free shear layers (Bardina *et al*[76]). The use of the time scale τ as a surrogate length-scale equation in the models of Speziale *et al*[69] and Kalitzin *et al*[70] offers only marginal benefits, if judged on the basis of solutions for the separated flow over the Aerospatiale 'A' high-lift aerofoil (Haase *et al*[211]). In a study by Coakley and Huang[48], six two-equation models have been applied to strong shock-wave boundary-layer interaction on a cylinder-flare geometry and compression corners at Mach 2·84-9·22 (see also Dolling[215]). While the models were found to give a wide range of performance in terms of separation and reattachment behaviour, the basic $k - \omega$ model was demonstrated to offer no intrinsic advantages over the $k - \varepsilon$ framework. Similar conclusions are offered by Haidinger and Friedrich[228, 229], again for supersonic ramp flows, although Coratekin *et al*[230] show that the inclusion of compressibility corrections to the $k - \omega$ can substantially improve the model's predictive capabilities for ramp flows. The performance of various $k - \varepsilon$ models for shock-induced separation in transonic bump, aerofoil and jet-afterbody flows is also deficient, as shown in Haase *et al*[210], Lien and Leschziner[112], Zhou *et al*[231], Barakos and Drikakis[224], Gerolymos and Vallet[173] and Leschziner *et al*[78], among many others. All models again under-estimate the strength of the interaction, failing to resolve separation and misplacing the shock. Broadly consistent conclusions also emerge from many studies of three-dimensional flows — for example in separated fuselage-like flows (Lien and Leschziner[207]) and wing-body/junction flows, both subsonic (Apsley and Leschziner[79]) and supersonic (Batten *et al*[77]). Interestingly, the predictive defects in three-dimensional flows occasionally appear to be less serious than in two-dimensional ones, despite the added strain complexities involved (e.g. Robinson and Hassan's[217] computations of shock–boundary-layer interaction over a cylinder/offset-flare juncture). This can be attributed, at least in some cases, to the larger contribution of convection to the balance of processes governing momentum transport, arising from generally much larger flow curvature.

The addition of corrections to the basic two-equation-model forms can have major consequences to the predicted behaviour. One modification routinely adopted is the 'Yap' correction (Equation (44)), and this tends to slightly improve the prediction of $k - \varepsilon$ models in adverse pressure gradients. The most influential correction is that of Menter (see Equation (59)), which limits the shear stress by linking it to the turbulence energy, thus over-riding the eddy-viscosity relation. It will be recalled that Menter's model is a hybrid, combining the $k - \varepsilon$ and $k - \omega$ models. This combination is not, in itself, a key feature. Of much greater importance is the shear-stress limiter, and several studies show the introduction of this limiter to result in a much improved behaviour in separated flows, including shock-induced separation in several transonic aerofoil and wing configurations (Huang[219], Marvin and Huang[144], Batten *et al*[77], Haase *et al*[211]), jet-afterbody flows (Leschziner *et al*[78]), incompressible aerofoil flows (e.g. Aerospatiale A and NLR 7301 two-element configuration, Haase *et al*[211]) and dynamic stall in oscillating aerofoils (Srinivasan *et al*[232], Ekaterinaris and Menter[233]). Excessive sensitivity of SST (shear-stress-transport)-model solutions to adverse pressure gradient for transonic-bump and supersonic compression-ramp flows is reported, however, by Liou *et al*[62]. Flows in which the SST model does not work well include some complex three-dimensional configurations — for example, incompressible wing/body-junction flow (Apsley and Leschziner[79]) and strong three-dimensional shock–boundary-layer interaction in a channel with a skewed bump (Leschziner *et al*[234]). In both cases, the SST model appears to return too low level of stresses, resulting either in excessive separation or insufficient post-shock recovery, the latter leading to grossly excessive transverse motion in the recovery region.

5.5 One-equation models

Of the group of one-equation models the variant most extensively investigated for aeronautical flows is the Spalart-Almaras model[24]. In particular, Bardina *et al*[76] have included this model in their wide-ranging investigations of two-equation models mentioned earlier. Not surprisingly, in view of the details of the calibration process, the model performs well in thin shear flows, except for the round jet. It also does well in a 3D (close to infinitely) swept-bump boundary layer examined by Wu and Squires[235], although the 3D distortion in this flow is relatively benign. In the more demanding separated flows (Driver[220], Bachalo-Johnson[191], Cook *et al*[22]) the model is generally observed to return rather indifferent solutions (though better than some arising from two-equation formulations!), often under-estimating the separation region and the separation-related pressure plateau on the surface. Liou *et al*[62] report, in contrast, examples in which the model returns excellent performance for the Bachalo and Johnson transonic bump flow and even excessive sensitivity to strong oblique shocks impinging on a flat-plate boundary layer. That the model can give acceptable performance for separated flows is remarkable, as it relies on an explicit prescription of the length scale, by reference to the wall-normal distance. This favourable behaviour is due mainly to the fact that the separation zones in the test cases considered are elongated and rather thin, so that the turbulence structure within the separated zone and the separated shear layer above it is dominated by the wall.

Menter's one-equation equivalent of his SST two-equation model is a second formulation of particular interest in aerodynamic applications, because of the favourable performance of the SST form. It is recalled that the one-equation variant has been derived by combining the k- and ε-equations and inserting Bradshaw's shear-stress/turbulence-energy relationship into the result. Applications of the model to Driver's separated boundary layer and to a separated backward-facing step by Menter are, unsurprisingly, found to be close to the

†Substantial sensitivity has been observed to whether the 1988[67] or 1994[68] version of the ω-equation is used.

k – ε-model solutions, although use of the Bradshaw relation results in slight improvements, as would be expected in view of the previously noted performance of the two-equation SST model. This observation and those made in relation to the Spalart-Almaras model lead to the conclusion that, for relatively benign, two-dimensional flows featuring moderate separation, some one-equation models are preferable to basic two-equation models which have a poor record of resolving separation.

Other one-equation models examined in Haase *et al*[211] for the separated Aerospatiale 'A' aerofoil flow are two variants of Wolfshtein's model and the Baldwin-Barth model. Only one variant returned a separated boundary layer, none can be said to have performed satisfactory, and none is therefore recommended for general separated flows.

5.6 Reynolds-stress models

Early applications of Reynolds-stress models (RSTMs) to aerospace-related problems were directed, principally, towards predicting shock–boundary-layer interaction and were motivated by the poor performance returned by two-equation eddy-viscosity models. Studies by Vandrome and Ha Minh[236], Benay *et al*[237], Leschziner *et al*[238], Lien and Leschziner[112] and Morrison *et al*[239], all concerned with shock-induced separation over nominally two-dimensional channel bumps and/or the RAE 2822 aerofoil, conveyed a broadly positive message on the predictive advantages gained from RSTMs relative to k – ε eddy-viscosity models. Thus, separation was found to be predicted at the correct position, the lambda-shock structure and the extent of the recirculation zone were better resolved, and the characteristic surface-pressure plateau associated with the separation zone was captured. It must be said that this outcome was no surprise to those familiar with the much more extensive earlier experience with RSTMs in predicting incompressible, mostly internal flows.

Over the past decade, there has been a steady, albeit slow, broadening in the range of conditions and problems computed with RSTMs and, more recently, with non-linear eddy-viscosity models (NLEVMs). Some of the most complex flows investigated over the past three years with RSTM variants include shock–boundary-layer interaction in a Mach 2 fin–body-junction flow (Batten *et al*[77]) and in a Mach 1·8 jet injected into a Mach 3 cross-flow (Chenault and Beran[240], Chenault *et al*[241]), shock-induced separation in two- and three-dimensional jet-afterbody configurations (Leschziner *et al*[78]) and over a swept bump in a channel (Gerolymos and Vallet[242]), shock–boundary-layer interaction over a full body–wing–fin model of a generic fighter configuration (Leschziner *et al*[78]) and dynamic stall flows around aerofoils (Drikakis and Barakos[243]). The additional challenge of predicting heat transfer with RSTMs, especially in hypersonic flow, has been addressed by Huang[156] and Huang & Coakley[244].

The rather subdued rate of uptake of RSTMs for aerodynamic flows is rooted, on the one hand, in the perception that this level of modelling is too complex and resource-intensive for practical applications, and, on the other hand, in the observation that many, if not most, flows in aerodynamic practice can be adequately computed with modified or corrected forms of two-equation models, such as Menter's[29] SST model. There is also the view that the variability in performance among different variants of RSTM contradicts the notion of RSTM being an intrinsically superior modelling framework, and that a great deal depends upon the precise model form and its calibration. None of these arguments can be categorically negated or dismissed. RSTMs are undoubtedly more demanding than two-equation models. However, the availability of a whole range of stability and convergence-promoting measures (Leschziner and Lien[204]) now allows the resource overheads of RSTM computations, relative to two-equation models, to be kept to within 20-50%, even in the case of complex three-dimensional flows. Indeed, Leschziner *et al*[78] demonstrate that, in certain circumstances, RSTMs converge faster than two-equation models. The argument that simpler models can be made to return equally adequate solutions is not disputed either, but it must be borne in mind that these models are not general and can fail badly in conditions outside those encountered in relatively thin near-wall flows (with or without separation). This emerges with some force from studies by Batten *et al*[77] and Apsley and Leschziner[79], the former on an impinging jet and the latter on a subsonic wing–body-junction flow. In both cases, the SST model returns indifferent or even poor results. Hence, the key distinction relates to model generality. If width of applicability is not a high-priority issue then the adoption of a simple, non-general, but well-tuned model is entirely defensible. However, in complex flows remote from walls, simple models can be seriously inadequate. One example is a whole range of flows involving multiple impinging jets in cross-flow, pertinent to VSTOL flight. In such cases, as well as supersonic jet injection into supersonic cross-flow (Chenault and Beran[240], Chenault *et al*[241]), RSTMs yield a distinctly better representation of jet, fountain and ground-vortex structure (Leschziner and Ince[114]). Moreover, in the case of underexpanded impinging jets, a RSTM is virtually the only type of model capable of returning the correct response of turbulence to the series of compression and expansion waves in the jet as it develops towards the strong stand-off shock above the impingement plane.

Regrettably, there are very few broad comparative studies in which several RSTM solutions have been included and contrasted with other model classes. The compilations of Haase *et al*[210] and Haase *et al*[211] contain a few RSTM or implicit-ASM contributions for the Delery[213] channel bumps, Cook *et al*'s[22] transonic RAE 2822 aerofoil, Piccin and Cassoudessale's[33] high-lift 'Aerospatiale A' aerofoil and Meier *et al*'s[245] 6:1 prolate spheroid. In most cases, a single RSTM solution, or at most two, are contrasted with those of simpler models, and are generally shown to give a superior representation of separation-related processes. Much more extensive expositions of studies contributing to the above compilations are those of Leschziner *et al*[238] and Davidson[246], both on shock-induced two-dimensional separation, Lien and Leschziner[206] on the separated 'Aerospatiale A' aerofoil flow, and Lien and Leschziner[207] on separation from a sprolate spheroid at 10° as well as 30° incidence. A compilation by Hasan and McGuirk[208] of 12 solutions for Bachalo and Johnson's axisymmetric bump, contributed by a number of collaborating investigators, includes RSTM results which are entirely consistent with others mentioned earlier. A particularly challenging flow is that involving shock-induced separation over the skewed (swept) channel bump of Pot *et al*[247]. This is a generic model of a swept transonic wing flow, but is much more complex and demanding, because the interaction between the shock and all four walls is important. This flow was modelled with a RSTM by Gerolymos and Vallet[242], with some modest improvements being obtained relative to the solution with a k – ε model. This same flow was also computed by Leschziner *et al*[234] with NLEVM variants, a study which will be revisited in the next section.

5.7 Non-linear eddy-viscosity and explicit algebraic Reynolds-stress models

Although NLEVMs and EARSMs are simpler than RSTMs, their application to aeronautical flows is considerably rarer, mainly because they have emerged more recently, as a significant model category, in response to the desire of practitioners for formulations that combine some of the predictive properties of RSTM with the numerical advantages of EVMs. An overall conclusion arising from a variety of studies on all types of flow, not only those pertinent to external aerodynamics, is that the performance of NLEVMs and EARSMs is more variable than that of RSTMs. This is rooted, on the one hand, in major fundamental differences, in terms of derivation, between NLEVMs and EARSMs (see Section 3.3.3), and, on the other hand, in the high sensitivity of NLEVMs to the calibration process for the coefficients of the non-linear fragments in the stress-strain/vorticity relations. In addition, the performance of a NLEVM

depends greatly on the order of terms included and the dependence of c_μ (or lack of it) on the strain and vorticity invariants, the latter being highly influential in relation to the response of the model to high strain rates. In fact, some studies suggest that the precise form of the dissipation-rate equation (especially the coefficients therein) and the form of c_μ carry more weight than the inclusion or exclusion of the higher-order terms that are responsible for the resolution of anisotropy and the sensitivity to curvature.

Some applications of NLEVMs to aeronautical flows are those of Lien and Leschziner[206, 207], Loyau *et al*[141], Leschziner *et al*[234, 248], Hasan *et al*[208], Barakos and Drikakis[224] and Apsley and Leschziner[79]. Lien and Leschziner's two studies focus, respectively, on the 'Aerospatiale A' aerofoil and a 6:1 prolate spheroid at high incidence, and include computations with variants of Shih *et al*'s[131] quadratic NLEVM. The results demonstrate that the NLEVMs can reproduce the behaviour of RSTMs (for which solutions are also included), but that the predictions are quite sensitive to the precise functional dependence $c_\mu(S, \Omega)$. Loyau *et al*'s concern is with shock-induced separation over Delery's channel bumps, Bachalo and Johnson's axi-symmetric bump and Pot *et al*'s swept channel bump, while Barakos and Drikakis[224] consider Bachalo and Johnson's case. In their first study, Loyau *et al* examine four NLEVMs and show that, while all return improvements relative to the $k - \varepsilon$ framework, owing mainly to their greater sensitivity to adverse pressure gradient, agreement with experiment varies significantly. There are also major differences among models in respect of their ability to resolve normal-stress anisotropy, reflecting the different approaches to calibration taken by the models' respective originators. Barakos and Drikakis[224] present conclusions on the performance of two variants of Craft *et al*'s[134] cubic NLEVM that are broadly consistent with those of Loyau *et al*'s. Loyau *et al*'s other study, concerned with the swept-bump flow, reveals some major predictive weaknesses in all three NLEVMs investigated for this very challenging flow. While all models return a much better resolution of the shock–boundary-layer interaction process itself, relative to the $k - \varepsilon$ model, the post-shock recovery is too slow, reflecting insufficient turbulent mixing and accompanied by a seriously excessive level of transverse motion. Very similar defects are also displayed by Menter's[29] SST model which tends, as noted in the previous section, to yield predictions that are often close to those arising from RSTMs. Thus, in this flow, Reynolds-stress modelling appears to be distinctly superior to NLEVMs, if Gerolymos and Vallet's[242] results are accepted as being correct. Hasan *et al*'s[209] study focuses on shock-induced separation over Putnam and Mercer's[250] rectangular jet-afterbody configuration, and it includes computational solutions with Craft *et al*'s[134] cubic NLEVMs, which are much closer to the experimental data than those arising from the $k - \varepsilon$ model (a subset of these results can also be found in Leschziner *et al*[234]). These solutions are also close to those obtained by Leschziner *et al*[77] with a RSTM. Apsley and Leschziner's[79] study investigates the performance of 12 turbulence models for Fleming *et al*'s[251] wing–body-junction flow, including two cubic NLEVMs. For this flow, in contrast to all other cases, the NLEVMs fail to give solutions which are clearly superior to simpler models, and this is conjectured to be due to a partial cancellation of the contributions arising from the quadratic and cubic fragments. This case is one that illustrates the background to an observation made in the introductory comments in this section about the variability in the predictions emerging from NLEVMs.

As noted in Section 3.4, EARSMs differ fundamentally from NLEVMs in so far as the former have been derived from particular Reynolds-stress models, with the transport of the anisotropy neglected. An important implication of this fact is that, unless stress convection makes a significant contribution to the stress balance, the performance of a EARSM should be close to that of the baseline Reynolds-stress model from which it was derived. It is arguable, therefore, that an EARSM may be viewed as a Reynolds-stress model, except in terms of the different computational implementation and solution both entail. Abid *et al*[226, 227] report the application of an EARSM, derived from the RSTM of Speziale *et al*[100], to the RAE 2822 aerofoil (though only to the attached Case 9), the NACA 4412 aerofoil, Bachalo and Johnson's axisymmetric bump and the ONERA M6 wing. In all three 2D cases, impressive improvements are reported relative to Wilcox's $k - \omega$ model which performs poorly for the separated flows. Results achieved for the ONERA M6 wing are also good, but are not compared with other models. Impressive performance is also demonstrated by Rung *et al*[221] who apply their EARSM, again in comparison with Wilcox's $k - \omega$ model, to Delery's transonic bump flow, the RAE 2822 transonic aerofoil flow and the ONERA M6 wing. This outcome may be argued to add weight to arguments made earlier in favour of RSTMs. In attached flow over multi-element aerofoils Rumsey *et al*[252] show that EARSMs offer no particular advantages over NLEVMs, or even linear EVMs, but in that case transition dominates as the feature dictating model performance.

5.8 Unsteady flows

5.8.1 Application needs

In the context of aerodynamics, the numerical prediction of unsteady, turbulent and compressible flows around moving bodies is motivated by the need to understand flow phenomena associated with the behaviour of aircraft during manoeuvres and around helicopter rotors. The above applications involve (unsteady) separation, transition, relaminarisation and shock–boundary-layer, viscous–inviscid, vortex–body and vortex–vortex interactions. A better understanding of the fundamental flow physics in the above applications will allow, among others, better prediction methods for flow control to be developed, thus enhancing the performance of aircraft and helicopters.

The cost of wind-tunnel or flight experiments in unsteady conditions is exceptionally high. Moreover, the information obtained through experiments is inevitably restricted to global quantities, surface distribution and, at best, a few sets of data for cross-flow structure. The numerical prediction of unsteady flows is a promising alternative, providing far more detailed information than experiments, but it is especially challenging and involves uncertainties over and above those arising in computations for statistically steady flow.

5.8.2 Fundamental studies

Algebraic eddy-viscosity models have been used extensively in unsteady viscous-flow codes because of their simplicity. However, investigations of oscillating turbulent boundary layers using algebraic models have shown that these models result in substantial inaccuracies with respect to the evolution of unsteady integral parameters and the phase shift of the wall shear stress[253, 254].

Two-equation EVMs, primarily the $k - \varepsilon$ model, have been extensively used in simulating unsteady turbulent boundary layers[253-256]. An instantaneous representation of the logarithmic law of the wall does not generally exist in unsteady flow. Hence, simple wall functions, based on the log law and the turbulence-equilibrium assumption, are bound to be erroneous. Cousteix and Houdville[253] have used a steady wall function in conjunction with a high-Reynolds-number $k - \varepsilon$ model[30], to simulate periodic turbulent boundary layers. A similar approach was taken by Mankbadi and Mobark[255] to predict pipe and boundary-layer flows. These studies demonstrate that high-Re models, combined with wall functions, do not yield adequate predictions of the wall shear stress.

The applicability of low Reynolds number $k - \varepsilon$ models to unsteady flows has also been investigated by Justesen and Spalart[256] for an oscillatory turbulent boundary layer under a free stream that varied sinusoidally in time around a zero mean. Two different low-Re $k - \varepsilon$ models were used[30]. Comparison with direct numerical simulations by Spalart and Baldwin[262] showed that the Jones-Launder model[30] performed better than Chien's[44] model. Fan *et al*[257] applied their own variant of distance-free, low-Re $k - \varepsilon$

model to oscillating boundary layers for a range of frequencies, and Dafa'Alla *et al*[258] did likewise with their own $q - \varsigma$ model. Their calculations, compared with DNS and experimental data, showed that the unsteady wall shear stress is not predicted satisfactorily.

Applications of full Reynolds-stress models to unsteady turbulent wall flows are rare. Shima[259] employed a second-moment closure — a modified version of Launder and Shima's[93] model — to compute boundary layers with periodic pressure gradient, demonstrating good agreement with experiments and direct numerical simulations. In particular, the tendencies towards re-laminarisation and re-transition in the oscillating boundary layer were faithfully reproduced, and the effect of the turbulent length scale in the free-stream was correctly captured.

Ha Minh *et al*[260] and Hanjalic *et al*[261] have also used second-moment closures to compute the oscillating boundary layers investigated by Jutesen and Spalart[256] with $k - \varepsilon$ models, covering a range of transitional and high-Re flows. The computations yielded a satisfactory representation of the sudden turbulence bursts at the start of the deceleration phase and the subsequent relaminarisation phenomena at the lower range of Reynolds numbers. To a degree, this illustrates the validity of the argument made in the introduction in favour of including Reynolds-stress transport. However, the unavoidable penalty is a significant increase in computational time, which may be regarded as unacceptable in aerospace practice. Recently, non-linear eddy-viscosity models have also been investigated[263] in oscillating pipe and channel flows[264, 265], yielding promising results.

As regards aerodynamic phenomena, unsteady RANS computations have been performed mainly for dynamic stall, buffet and vortical flows around missiles and wings at high lift, some in the context of flow-structure interaction. Validation studies of turbulence models for some of these flows are documented in[184, 232, 233, 243, 249, 266] and references therein. Some illustrative examples are shown below for the cases of dynamic stall and buffet.

5.8.3 Dynamic stall

The phenomenon of dynamic stall (DS) appears in high-angle manoeuvres and is caused by the development of a vortical structure known as dynamic-stall vortex (DSV). The DSV leads to a significant (instantaneous) lift increase. Accurate prediction and, possibly, control of the DS would enhance the performance in various aeronautical applications. For example, the manoeuvrability of fighter aircraft could be enhanced if the unsteady airloads generated by DS are utilised in a controlled manner. Effective stall control of the retreating blade of a helicopter rotor could also increase the maximum flight speed by reducing rotor vibrations and power requirements. Similarly, by controlling DS the maximum speed of wind generators and turbine rotors can increase, thus resulting in more electrical energy and reduced rotor vibration. The numerical simulation of the above flow phenomena imposes both numerical and physical challenges. This requires the development of accurate and efficient CFD methods in conjunction with turbulence models.

Dynamic stall can be studied by considering the pitching motion of an aerofoil beyond its static-stall incidence angle. There are several phenomena associated with the pitching motion of the aerofoil, the most important being the generation of intense vorticity on the suction surface around the leading edge of the aerofoil. A discrete vortex is formed, detaches from the body and convects along the suction surface. This leads to large variations in lift, drag and pitching moment. The phenomenon continues either with the generation of weaker vortices, if the aerofoil remains above its static angle of attack, or terminates if the aerofoil returns to an angle sufficiently small that allows re-attachment of the flow. Dynamic-stall flows have been under investigation for about three decades, and significant progress has been made towards understanding the physical phenomena associated with the rapid pitching motion of an aerofoil beyond its static-stall incidence angle.

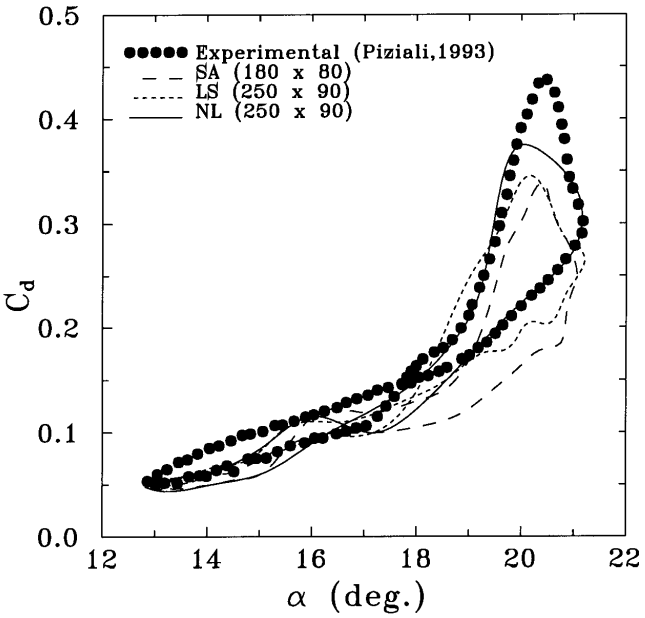

Figure 4. Unsteady drag coefficient predicted by Barakos and Drikakis[249] using the Spalart-Allmaras (SA)[24], Launder-Sharma (LS)[41] and Craft *et al* [134] models for the oscillating NACA-0015 aerofoil, M = 0·29, $Re_c = 1{\cdot}95 \times 10^6$, amplitude of oscillation 4·2° and mean incidence 17°. The experiments are from Piziali[277].

In the 1970s, a number of experimental and theoretical investigations were performed. Telionis[267] discussed the flow in unsteady boundary layers, including the derivation of analytic and semi-analytic solutions. The first computational investigations of dynamic stall were presented by Mehta[268], Gulcat[269] and McCroskey *et al*[270]. In the 1980s, the rapid progress in computer technology allowed researchers to simulate unsteady flows by solving the full Navier-Stokes equations[271, 272], while a comprehensive set of experimental data for the light-stall regime was also published[273]. The papers by McCroskey *et al*[274], Carr[275] and Visbal[276] also provide a comprehensive description of the DS processes. In the 1990s, the effects of turbulence on dynamic stall have been the subject of extensive experimental[277] and numerical studies[184, 232, 233, 243, 249, 266, 278]. These studies have shown that the accuracy of simulations depends strongly on the realism of the turbulence model employed. Experience with algebraic models has shown that such approximations do not provide satisfactory results in most cases. Linear low-Re, two-equation models seem to offer a reasonable balance between accuracy and computational cost, but are not able to capture effects arising from normal-stress anisotropy.

Recently, non-linear EVMs and second-moment closures have been used[232, 249] in dynamic-stall simulations. Figure 4 shows comparisons of different model predictions with experiments[277] for the unsteady airloads around an oscillating NACA 0015 aerofoil. The models are the one-equation turbulence model of Spalart and Allmaras (SA)[24], the linear low-Re EVM of Launder and Sharma (LS)[41], and the cubic EVM of Craft *et al*[134]. The computations shown in Fig. 4 are for deep-stall conditions: the free stream conditions correspond to Reynolds number of $1{\cdot}95 \times 10^6$ and Mach number of 0·29; the amplitude of the oscillation is 4·2°, the mean incidence is 17° and the reduced frequency of oscillation is $k_f = 0{\cdot}1$. The predictions of the cubic $k - \varepsilon$ and SA models are comparable for some parts of the unsteady cycle, but at larger incidence angles the former model gives better results. Linear models, such as the Launder-Sharma model, have been found[249] to be, in general, more dissipative than the Spalart-Allmaras and non-linear EVMs. Computations using second-moment closures[232] have not shown any

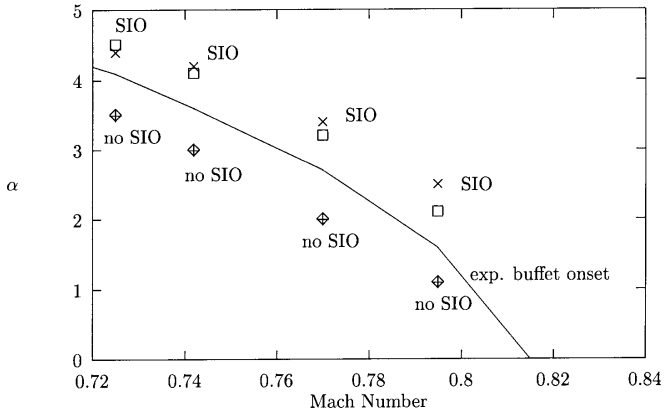

Figure 5. Transonic buffet onset for the NACA-0012 aerofoil as predicted by the Spalart-Allmaras model (crosses) and a non-linear $k-\omega$ model[281] (squares); solid line represents experimental data; SIO stands for shock-induced oscillations (reprinted from *Int J Heat and Fluid Flow*, **21**, Barakos, G. and Drikakis, D. [266], Numerical simulation of transonic buffet flows using various turbulence closures, pp 620-626, 2000).

substantial improvements compared to non-linear models. This is in contrast to experience on simpler oscillating boundary layers. It must be said, however, that the mere inclusion of stress transport is not in itself sufficient to procure satisfactory predictions. A great deal depends, also in second-moment closure, on the details of the closure assumptions and the particular form of the length-scale equation used.

5.8.4 Transonic buffet

Transonic buffet arises in many aeronautical applications, such as wing flow and internal flows around turbomachinery blades. The aerodynamic performance in these applications depends strongly on the unsteady shock–boundary-layer interaction. The latter may change position around the aerofoil due to self-excited shock oscillations. Accurate prediction of buffet is dictated by both the accuracy/properties of the numerical discretisation scheme and the accuracy of the turbulence model.

Experiments have been conducted by McDevitt and Okuno[279] for the NACA-0012 aerofoil at Mach numbers between 0·7 and 0·8, angles of incidence less than 5° and Reynolds number in the range of 10^6 and $1{\cdot}4 \times 10^7$. McDevitt and Okuno[279] identified the incidence angle and Mach number as the most important parameters for the buffet onset. Their wind-tunnel results are particularly suitable for validating CFD codes, because they are free from wall effects, in contrast to previous experimental studies[280].

Figure 5 shows comparisons of numerical[266] with experimental results[280] for the buffet onset around a NACA 0012 aerofoil. There is a well-defined region of Mach number and incidence angle where buffet occurs. Initially, four computations were performed at conditions below the experimentally reported buffet onset, and steady-state solutions were achieved (symbols in Fig. 5 labelled 'no SIO'). Afterwards, the incidence-angle was slowly increased to obtain unsteadiness, and it was found that after the initial peak of the curve the computations resulted either in periodic loads, thus indicating buffet (symbols in Fig. 5 labelled 'SIO'), or in steady-state flow. In the latter case, the computations were repeated for a higher incidence angle until buffet was captured. Once buffet was predicted, the incidence angle was again decreased, and the computation was repeated to check whether the experimental boundary (solid line in Fig. 5) for buffet onset could be approached with greater precision. Figure 5 shows that very similar predictions are obtained with the linear Spalart-Allmaras[24] and non-linear $k-\omega$ models[281].

6.0 CONCLUDING REMARKS

This article started with a somewhat provocative statement on the importance given to turbulence modelling within the spectrum of topics constituting aerodynamics for aeronautical engineering. Yet, it proceeded to identify close to 300 pertinent papers — perhaps only 50% of the total, and excluding studies on simulation — providing ample evidence of substantial research into turbulence modelling for aerodynamics and the use of models in challenging aeronautical flows. In considering the apparent contadiction contained therein, one has to ask the question as to what the impact of the research has been on aeronautical practice.

The majority of design-related computations performed by industry, especially those for lifting surfaces along an evolutionary family of designs, are still based on viscous-inviscid interaction methods, within which the effects of boundary layers are represented by well-tuned integral relations. These methods are cheap, robust and produce perfectly adequate results for attached flows corresponding to near-cruise (design) conditions. In this context, turbulence modelling does not arise explicitly and is a non-issue. Navier-Stokes methods have been developed aggressively in recent years for more challenging applications, and these are now being used for component design and even full configurations, but mostly with 'simple' eddy-viscosity models, often algebraic and at most two-equation forms. Although it is recognised that complex flows, especially those involving separation and strong vortical features, cannot be predicted adequately with such models, the emphasis on simplicity, computational speed and robustness in an industrial context militates against the adoption of more advanced models. An equally important factor has been, however, a great deal of uncertainty (indeed, confusion) on the prospect of advanced turbulence models providing adequate return for the added complexity. It is certainly true to say that the current body of knowledge arising from numerous validation studies does not provide unambiguous recommendations.

This review has provided evidence that eddy-viscosity models are fundamentally flawed and often perform poorly in flows featuring separation, strong shock–boundary-layer interaction and 3D vortical structures. More seriously, perhaps, the models do not display a consistent behaviour across a wide range of conditions. In relatively simple flows, which develop slowly and in which a single shear stress (expressed in wall-oriented coordinates) is wholly dominant, eddy-viscosity models can be crafted to give the correct level of this stress and thus yield adequate solutions. This applies to near-wall flows, thin wakes and even separated flows in which the separated region is long and thin and hugs the wall. Another type of flow in which eddy-viscosity models are adequate is one in which inviscid features (pressure gradient, advection) dictate the mean flow, so that the Reynolds stresses are largely immaterial, however wrong they may be. The fact that many flows are an amalgam of shear layers and regions in which turbulence is dynamically uninfluential explains, in part, the moderate level of success of eddy-viscosity models. Among two-equation eddy-viscosity models, SST forms perform fairly well (at least in 2D flow), due to the limiter which prevents the shear stress from responding to the strain to the extent dictated by the stress-strain relationship. The length-scale equation is a key area of uncertainty and its precise form greatly affects model performance. There is some evidence that models using the turbulent vorticity as a length-scale variable near the wall perform (marginally) better than models based on the dissipation-rate equation, although it must be stressed that performance depends greatly on the nature of viscosity-related damping functions and the numerical constants in the length-scale equation.

Much of the recent research in turbulence modelling has focused on the development of anisotropy-resolving models. Of these, Reynolds-stress-transport models are the most 'complete' and fundamentally secure forms, in the sense that they come closest to the exact representation within the constraints of closure at second-moment level. These models are complex and pose particular numer-

ical challenges, but are now used to compute flows around practical configurations. The weak elements of such models are the length-scale equation and the (influential) pressure-strain model. While Reynolds-stress models often give better predictions than eddy-viscosity models in many complex 'laboratory' flows, they cannot be said to guarantee better solutions in practice. Current forms are therefore unlikely to be adopted in general industrial methods, except for analysing a narrow range of complex flow problems in a pre-design environment. Non-linear eddy-viscosity models are, at best, approximations of Reynolds-stress transport models — these forms being referred to as Explicit Algebraic Reynolds-stress Models (EARSM). Hence, clearly, their performance cannot be superior to that of their parents. In particular, EARSMs ignore stress transport and are based on relatively simple (linear) closure forms for the dissipation rate and pressure-strain process. They are, however, numerically simpler and more economical than stress-transport closure and are therefore gaining in popularity.

Numerical aspects play an important role in turbulent-flow computations in terms of both accuracy and efficiency. Numerical methods encompass numerical dissipation which acts to regularise the flow, thereby allowing shock propagation to be captured physically realistically even if it is not fully resolved on the computational mesh. One develops numerical schemes with two competing criteria in mind: a desire for high accuracy coupled with protections against catastrophic failure due to nonlinear wave steepening or unresolved features. Nonlinear limiter mechanisms in high-resolution methods guard the methods from such catastrophic failures by triggering entropy-producing mechanisms that safeguard the calculation when the need arises. The two key questions are: (*i*) what criteria should be used to design the nonlinear mechanism that triggers the entropy production, and (*ii*) to what extent numerical dissipation double-counts effects which are supposed to be captured by turbulence modelling.

The algorithmic implementation of turbulence models can significantly affect the efficiency of turbulent-flow computations. Slow convergence rates or convergence stall have been experienced by many researchers in the implementation of linear and non-linear EVMs, as well as second-moment closure. Implicit methods seem to offer better stability properties and covergence rates than explicit schemes, but they make the code development more complicated. Additionally, in unsteady flows the physical time scales ultimately decide about the magnitude of the time step, thus using implicit schemes in this case may be pointless. In general, the CPU overheads of non-linear EVM and RSTM against linear models are typically of order 1·2-1·8 and 1·5-3, respectively.

It is not easy to predict the future of turbulence modelling in aeronautics. It is most likely that progress will be highly incremental, with a trend being towards using well-validated models or model types for different problems (a 'horses-for-courses' approach). The most complex approaches likely to be used practice are EARSMs which need, however, to include approximate treatments of stress transport. Such approximations are emerging, but need to be verified for 3D conditions.

Large eddy simulation (LES) beckons in the distance as an alternative approach to RANS modelling, but poses substantial challenges in high-Re near-wall flows, especially in the presence of separation from gently curved surfaces, where resolution and thus computing-cost issues are critical. LES is certainly likely to be a useful (though expensive) approach in flows that are not strongly affected by viscous near-wall features.

Over the past decade, there has also been an increasing amount of evidence that high-resolution numerical methods for hyperbolic partial differential equations have an embedded (or 'implicit') turbulence model (see Rider and Drikakis[282], and references therein). It has been shown[282] that 'implicit' modelling (or monotone integrated LES (MILES)[283]) includes elements of nonlinear eddy viscosity, modelling scale-similarity and an effective dynamic subgrid-scale model. The MILES approach may be particularly useful in the context of coarsely resolved LES (very large eddy simulation (VLES)[284]). However, further development and validation is required, especially in relation to viscous near-wall features.

Finally, the detached eddy simulation (DES) method of Spalart *et al*[285], or a related strategy, may be a possible route to economically tenable simulations for complex configurations, but there are several important fundamental and practical questions that need to be addressed and resolved in relation to the coupling of near-wall RANS models to the outer LES region, on which DES is based.

REFERENCES

1. ANDERSON, J.D. *A History of Aerodynamic*s, 1997, Cambridge University Press.
2. REYNOLDS, O. On the dynamical theory of incompressible viscous fluids and the determination of the critertion, 1894, Phil Trans Roy Soc, 1895, **186**, pp 123-164.
3. MELLEN, P., FROEHLICH, J. and RODI, W. Lessons from the European LESFOIL project on LES of flow around an airfoil, 2002, AIAA 2002-0111.
4. JONES, W.P. and MANNERS, A. The calculation of the flow through a two-dimensional faired diffuser, *Turbulent Shear Flows 6*, ANDRÉ, J.C. ET AL, (Eds), 1989, pp 18-31, Springer.
5. LAI, Y.G. Computational method of second-moment turbulenbce closures in complex geometries, *J AIAA*, 1995, **33**, pp 1426-1432.
6. DURBIN, P. Separated flow computations with the $k - \varepsilon - v^2$ model, *J AIAA*, 1995, **33**, pp 659-664.
7. PARNEIX, S., DURBIN, P.A. and BEHNIA, M. Computation of 3D turbulent boundary layers using the V2F model, *Flow, Turbulence and Combustion*, 1998, **60**, pp 19-46.
8. KASSINOS, S.C., LANGER, C.A., HAIRE, S.L. and REYNOLDS, W.C. Structure-based modelling for wall-bounded flows, *Int J Heat and Fluid Flow*, 2000, **21**, pp 599-605.
9. CAMBON, C. and SCOTT, J.F. Linear and nonlinear models of anisotropic turbulence, *Ann Rev Fluid Mech*, 1999, **31**, pp 1-53.
10. SCHIESTEL, R. Multiple time scale modelling of turbulent flows in one point closures, *Phys Fluids,* 1987, **30**, pp 722.
11. WILCOX, D.C. Multi-scale model for turbulent flows, *AIAA J*, 1988, **26**, pp 1311-1320.
12. PRANDTL, L. Bericht ueber die Enstehung der Turbulenz, *Z Angew Math Mech*, 1925, **5**, pp 136-139.
13. VON KARMAN, T. Mechanische Aenlichkeit und Turbulenz, 1930, Proc of Third Int Congress App Mech, Stockholm, pp 85-105.
14. CEBECI, T. and SMITH, A.M.O. Analysis of turbulent boundary layers, *Ser in Appl Math & Mech XV*, 1974, Academic Press, London.
15. BALDWIN, B.S. and LOMAX, H. Thin-layer approximation algebraic model for separated turbulent flows, 1978, AIAA Paper 78-0257.
16. GRANVILLE, P.S. Baldwin-Lomax factors for turbulent boundary layers in pressure gradients, *J AIAA*, 1987, **25**, pp 1624-1627.
17. GOLDBERG, U.C. Separated flow treatment with a new turbulence model, *J AIAA*, 1986, **24**, pp 1711-1713.
18. WOLFSHTEIN, M. The velocity and temperature distribution in one-dimensional flow with turbulence augmentation and pressure gradient, *Int J Heat Mass Transfer*, 1969, **12**, p 139.
19. NORRIS, L.H. and REYNOLDS, W.C. Turbulence channel flow with a moving wavy boundary, 1975, Rep FM-10, Dept of Mech Eng, Stanford University.
20. HASSID, S. and POREH, M. A turbulence energy model for flows with drag reduction, *ASME J of Fluids Eng*, 1975, **97**, pp 234-241.
21. MITCHELTREE, R.A., SALAS, M.D. and HASSAN, H.A. One equation turbulence model for transonic airfoil flows, *J AIAA*, 1990, **28**, pp 1625-1632.
22. COOK, P.H., MCDONALD, M.A. and FIRMIN, M.C.P. Aerofoil 2822 — Pressure distributions, boundary layer and wake measurements, 1979, AGARD AR-138.
23. BALDWIN, B.W. and BARTH, T.A. One-equation turbulence transport model for high Reynolds number wall-bounded flows, 1991, AIAA Paper 91-0610.
24. SPALART, P.R. and ALLMARAS, S.R. A one-equation turbulence model for aerodynamic flows, 1992, AIAA Paper 92-0439.
25. MENTER, F.R. Eddy viscosity transport equations and their relation to the k-ε model, *ASME J Fluids Eng*, 1997, **119**, pp 876-884.
26. GOLDBERG, U.C. Hypersonic flow heat transfer prediction using single equation turbulence models, *ASME J Heat Transfer*, 2001, **123**, pp 65-69.

27. GOLDBERG, U.C. and RAMAKRISHNAN, S.V. A pointwise version of the Baldwin-Barth turbulene model, *Int J Comp Fluid Dynamics*, 1994, **1**, pp 321-338.
28. BRADSHAW, P., FERRIS, D.H. and ATWELL, N.P. Calculation of boundary layer development using the turbulent energy equation, *J Fluid Mech*, 1967, **23**, pp 31-64.
29. MENTER, F.R. Two equation eddy viscosity turbulence models for engineering applications, *J AIAA*, 1994, **32**, pp 1598-1605.
30. JONES, W.P. and LAUNDER, B.E. The prediction of laminarisation with a two-equation model of turbulence, *Int J Heat and Mass Transfer*, 1972, **15**, pp 301-314.
31. JOHNSON, D.A. and KING, L.S. A mathematical simple turbulence closure model for attached and separated turbulent boundary layers, 1985, AIAA Paper 84-0175.
32. COLES, D. and WADCOCK, A.J. Flying hot-wire study of flow past a NACA 4412 airfoil at maximum lift, *J AIAA*, 1979, **17**, pp 321-328.
33. PICCIN, O. and CASSOUDESALLE, D. Etude dans la soufflerie F1 des profils AS239 et AS240, 1987, ONERA Technical Report, PV 73/1685 AYG.
34. JOHNSON, D.A. and COAKLEY, T.J. Improvements to a non-equilibrium algebraic turbulence model, *J AIAA*, 1990, **28**, pp 2000-2003.
35. ABID, R., VATSA, V.N., JOHNSON, D.A. and WEDAN, B.W. Prediction of separated transonic wing flows with a non-equilibrium algebraic model, 1989, Paper AIAA 89-0558.
36. DAVIDOV, B.I. On the statistical dynamics of an incompressible turbulent fluid, *Dokl Akad Nauk S S S R*, 1961, **136**, pp 47-50.
37. RODI, W. and MANSOUR, N.N. Low Reynolds number k-ε modelling with the aid of direct numerical simulation data, *J Fluid Mech*, 1993, **250**, pp 509-529.
38. RICHARDSON, L.F. *Weather Prediction by Numerical Process*, 1992, University Press, Cambridge.
39. HARLOW, F.H. and NAKAYAMA, P.I. Transport of turbulence energy decay rate, 1968, University of California Report LA-3854, Los Alamos Science Laboratory.
40. HANJALIC, K. Two-Dimensional Asymmetric Flows in Ducts, 1970, PhD Thesis, University of London.
41. LAUNDER, B.E. and SHARMA, B.I. Application of the energy-dissipation model of turbulence to the calculation of flow near a spinning disc, Letters in *Heat and Mass Transfer*, 1974, **1**, p 131.
42. HOFFMAN, G.H. Improved form of low Reynolds-number k-ε turbulence model, *Physics of Fluids*, 1975, **18**, pp 309-312.
43. LAM, C.K.G. and BREMHORST, K. A modified form of the k-ε model for predicting wall turbulence, *J Fluids Eng*, 1981, **103**, pp 456-460.
44. CHIEN, K.Y. 1982, Predictions of channel and boundary-layer flows with a low-Reynolds-number turbulence model, *J AIAA*, 1982, **20**, (1) pp 33-38.
45. NAGANO, Y. and HISHIDA, M. Improved form of the k-ε model for turbulent shear flows, 1987, Trans of ASME, **109**, p 156.
46. MYONG, H.K. and KASAGI, N. A new approach to the improvement of k-ε turbulence model for wall bounded shear flows, *JSME Int J*, Series II, 1990, **33**, pp 63-72.
47. SO, R.M.C., ZHANG, H.S. and SPEZIALE, C.G. Near-wall modelling of the dissipation rate equation, *J AIAA*, 1991, **29**, pp 2069-2076.
48. COAKLEY, T.J. and HUANG, P.G. Turbulence modelling for high speed flows, 1992, Paper AIAA 92-0436.
49. ORSZAG, S.A., YAKHOT, V., FLANNERY, W.S., BOYSAN, F., CHOUDHURY, D., MARUZEWSKI, J. and PATEL, B. Renormalisation group modelling and turbulence simulations, *Near-Wall Turbulent Flows*, SO, R.M.C., SPEZIALE, C.G. and LAUNDER, B.E. (Eds), 1993, Elsevier, pp 1031-1046.
50. KAWAMURA, H. and KAWASHIMA, N. A proposal for a k-ε model with relevance to the near-wall turbulence, Paper IP.1, Proc Int Symp on Turbulence, *Heat and Mass Transfer*, 1994, Lisbon.
51. LIEN, F.S. and LESCHZINER, M.A. 1994, Modelling the flow in a transition duct with a non-orthogonal FV procedure and low-Re turbulence-transport models, 1994, Proc ASME FED Summer Meeting, Symposium on Advances in Computational Methods in Fluid Dynamics, pp 93-106.
52. MOSER, R., KIM, J. and MANSOUR, N.N. Direct numerical simulation of turbulent channel flow up to $Re_\tau = 590$, *Physics of Fluids*, 1999, **11**, pp 943-945.
53. PATEL, C.V., RODI, W. and SCHEUERER, G. Turbulence models for near-wall and low Reynolds number flows: A review, *J AIAA*, 1985, **23**, pp 1308-1319.
54. MICHELASSI, V. and SHIH, T-H. Low Reynolds number two equation modelling of turbulent flows, 1991, Report NASA TM-104368, ICOMP-91-06.
55. MANSOUR, N.N., KIM, J. and MOIN, P. Near-wall k-ε turbulence modelling, *J AIAA*, 1989, **27**, pp 1068-1073.
56. YAP, C.R. Turbulent Heat and Momentum Transfer in Recirculating and Impinging Flows, 1987, PhD thesis, University of Manchester.
57. JAKIRLIC, S. and HANJALIC, K. A second-moment closure for non-equilibrium and separating high- and low-Re-number flows, 1995, Proc 10th Symp on Turbulent Shear Flows, Pennsylvania State University, 23.25.
58. IACOVIDES, H. and RAISEE, M. Computation of flow and heat transfer in 2D rib roughened passages, 1997, Proc 2nd Int Symp on Turbulence, Heat and Mass Transfer, HANJALIC, K. and PETERS, T.W.J. (Eds), Delft University Press, pp 21-30.
59. HANJALIC, K. and LAUNDER, B.E. Sensitising the dissipation equation to irrotational strains, *ASME J Fluids Eng*, 1980, **102**, pp 34-40.
60. YAKHOT, V., ORSZAG, S.A., THANGHAM, S., GATSKI, T.B. and SPEZIALE, C.G. Development of turbulence models for shear flows by a double expansion technique, *Phys Fluids A4,* 1992, p 1510.
61. KATO, M. and LAUNDER, B.E. The modelling of turbulent flow around stationary and vibrating square cylinders, 1993, Proc 9th Symp on Turbulent Shear Flows, Kyoto, 10.4.1-10.4.6.
62. LIOU, W.W., HUANG, G and SHIH, T-H. Turbulence model assessment for shock wave/turbulent boundary-layer interaction in transonic and supersonic flow, *Computers and Fluids*, 2000, **29**, pp 275-299.
63. LAUNDER, B.E., PRIDDIN, C.H. and SHARMA, B. The calculation of turbulent boundary layers on curved and spinning surfaces, *ASME J Fluids Eng*, 1977, **98**, p 753.
64. RODI, W. Influence of buoyancy and rotation on equations for the turbulent length scale, 1979, Proc 2nd Symp on Turbulent Shear Flows, London, 10.37-10.42.
65. RODI, W. and SCHEUERER, G. Calculation of curved shear layers with two-equation turbulence models, *Physics of Fluids*, 1983, **26**, p 1422.
66. LESCHZINER, M.A. and RODI, W. Calculation of annular and twin parallel jets using various discretisation schemes and turbulence models, *ASME J Fluids Eng*, 1981, **103**, pp 352-360.
67. WILCOX, D.C. 1988, Reassessment of the scale-determining equation for advanced turbulence models, *J AIAA*, 1988, **26**, pp 1299-1310.
68. WILCOX, D.C. Simulation transition with a two-equation turbulence model, *J AIAA*, 1994, **32**, pp 247-255.
69. SPEZIALE, C.G., ABID, R. and ANDERSON, E.C. Critical evaluation of two-equation models for near-wall turbulence, *J AIAA*, 1992, **30**, pp 324-331.
70. KALITZIN, G., GOULD, A.R.B. and BENTON, J.J. Application of two-equation turbulence models in aircraft design, 1996, AIAA Paper 96-0327.
71. GIBSON, M.M. and DAFA'ALLA, A.A. Two-equation model for turbulent wall flow, *J AIAA*, 1995, **33**, pp 1514-1518.
72. GOLDBERG, U.C. Towards a pointwise turbulence model for wall-bounded and free shear flows, *ASME J Fluids Eng*, 1994, **116**, p 72.
73. BENAY, R. and SERVEL, P. Two-equation k-σ turbulence model: application to supersonic base flow, *J AIAA*, 2001, **39**, pp 407-416.
74. APSLEY, D.D. and LESCHZINER, M.A. Advanced turbulence modelling of separated flow in a diffuser, *Flow, Turbulence and Combustion*, 2000, **63**, pp 81-112.
75. MENTER, F.R. Influence of freestream values on k-ω turbulence model predictions, *J AIAA*, 1992, **30**, pp 1657-1659.
76. BARDINA, J.E., HUANG, P.G. and COAKLEY, T.J. Turbulence modelling validation, 1997, Paper AIAA 97-2121.
77. BATTEN, P., CRAFT, T.J., LESCHZINER, M.A. and LOYAU, H. Reynolds-stress-transport modelling for compressible aerodynamic flows, *J AIAA*, 1999, **37**, pp 785-796.
78. LESCHZINER, M.A., BATTEN, P. and CRAFT, T.J. Reynolds-stress modelling of afterbody flows, *Aeronaut J*, 2001, **105**, (1048), pp 297-306.
79. APSLEY, D.D. and LESCHZINER, M.A. Investigation of advanced turbulence models for the flow in a generic wing-body junction, *Flow, Turbulence and Combustion*, 2001, **167**, pp 25-55.
80. ZEIERMAN, S. and WOLFSHTEIN, M. Turbulent time scale for turbulent flow calculations, *J AIAA*, 1986, **24**, pp 1606-1610.
81. GILBERT, N. and KLEISER, L. Turbulence model testing with the aid of direct numerical simulation results, 1991, Proc 8th Symp on Turbulent Shear Flows, Munich, 26.1.1-26.1.6.
82. LAUNDER, B.E. and TSELEPIDAKIS, D.P. Contribution to the modelling of near-wall turbulence, *Turbulent Shear Flows 8*, DURST, F. *et al* (Eds), 1993, Springer Verlag, **81**.
83. HALLBAECK, M., GROTH, A. and JOHANSSON, A.V. Anisotropic dissipation rate — implications for Reynolds-stress models, *Advances in Turbulence*, JOHANSSON, A.V. and ALFREDSON, P.H. (Eds), Springer, pp 414-421.

84. HANJALIC, K. and JAKIRLIC, S. A model of stress dissipation in second moment closures, *Appl Scientific Research*, 1993, **51**, pp 513-518.
85. LAUNDER, B.E. and REYNOLDS, W.C. Asymptotic near-wall stress dissipation rates in turbulent flow, *Phys of Fluids*, 1983, **26**, p 1157
86. HANJALIC, K. Advanced turbulence closure models: a view of current status and future prospects, *Int J Heat Fluid Flow*, 1994, **15**, pp 178-203.
87. OBERLACK, M. Non-isotropic dissipation in non-homogeneous turbulence, *J Fluid Mechanics*, 1997, **350**, pp 351-374.
88. ROTTA, J.C. Statistische theory nichhomogener turbulenz, *Zeitschrift der Physik*, 1951, **129**, p 547.
89. GIBSON, M.M. and LAUNDER, B.E. Ground effects on pressure fluctuations in the atmospheric boundary layer, *J Fluid Mech*, 1978, **86**, p 491.
90. FU, S., LESCHZINER, M.A. and LAUNDER, B.E. Modelling strongly swirling recirculating jet flow with Reynolds-stress transport closure, 1987, Proc 6th Symposium on Turbulent Shear Flow, Toulouse, 17.6.1.
91. SHIR, C.C. A preliminary numerical study of atmospheric turbulent flows in the idealised planetary boundary layer, *J Atmos Sci*, 1973, **30**, p 1327.
92. CRAFT, T.J. and LAUNDER, B.E. New wall-reflection model applied to the turbulent impinging jet, *J AIAA*, 1992, **30**, p 2970.
93. LAUNDER, B.E. and SHIMA, N. Second-moment closure for the near-wall sublayer, *J AIAA*, 1989, **27**, pp 1319-1325.
94. SO, R.M.C., LAI Y.G., ZHANG, H.S. and HWANG, B.C. Second-order near-wall turbulence closures: A review, *J AIAA*, 1991, **29**, pp 1819-1835.
95. INCE, N.Z., BETTS, P.L. and LAUNDER, B.E. Low Reynolds number modelling of turbulent buoyant flows, 1994, Proc EUROTHERM Seminar 22, Turbulent Natural Convection in Cavities, Delft, Editions européenes Thermique et Industrie, Paris, HENKES, R.A.W.M. and HOOGENDOORN, C.J. (Eds) p 76.
96. CRAFT, T.J. and LAUNDER, B.E. 1996, A Reynolds stress closure designed for complex geometries, *Int J Heat Fluid Flow*, 1996, **17**, p 245.
97. DURBIN, P.A. A Reynolds stress model for near-wall turbulence, *J Fluid Mech*, 1993, **249**, p 465.
98. SHIH, T.H. and LUMLEY, J.L. Modelling of pressure correlation terms in Reynolds-stress and scalar-flux equations, 1985, Report FDA-85-3, Sibley School of Mech. and Aerospace Eng, Cornell University.
99. FU, S., LAUNDER, B.E. and TSELEPIDAKIS, D.P. Accommodating the effects of high strain rates in modelling the pressure-strain correlation, 1987, Report TFD/87/5 Mechanical Engineering Dept, UMIST, Manchester.
100. SPEZIALE, C.G., SARKAR, S. and GATSKI, T.B. Modelling the pressure-strain correlation of turbulence: an invariant dynamical systems approach, *J Fluid Mech*, 1991, **227**, p 245.
101. CRAFT, T.J., GRAHAM, L.J.W. and LAUNDER, B.E. Impinging jet studies for turbulence model assessment — II. An examination of the performance of four turbulence models, *Int J Heat Mass Transfer*, 1993, **36**, p 2685.
102. CRAFT, T.J. Developments in a low-Reynolds-number second-moment closure and its application to separating and reattaching flows, *Int J Heat and Fluid Flow*, 1998, **19**, pp 541-548.
103. PFUNDERER, D.G., EIFERT, C. and JANICKA, J. Nonlinear second moment closure consistent with shear and strain flows, *J AIAA*, 1997, **35**, pp 825-831.
104. JAKIRLIC, S. Reynolds-Spannungs-Modellierung Komplexer Turbulenter Stroemungen, 1997, PhD thesis, University of Erlangen-Nuernberg.
105. DALY, B.J. and HARLOW, F.H. Transport equations in turbulence, *Phys of Fluids*, 1970, **13**, pp 2634-2649.
106. DEMUREN, A.O. and SARKAR, S., Perspective: Systematic study of Reynolds-stress closure models in the computation of plane channel flows, *ASME J Fluids Eng*, 1993, **115**, pp 5-12.
107. YOUNIS, B.A., GATSKI, T.B. and SPEZIALE, C.G. Towards a rational model for the triple velocity correlations of turbulence, Proc Royal Soc London A, 2000, **456**, pp 909-920.
108. HANJALIC, K. and LAUNDER, B.E. A Reynolds stress model and its application to thin shear flows, *J Fluid Mechanics*, 1972, **52**, pp 609-638.
109. LUMLEY, J.L. Computational modelling of turbulent flows, *Adv Appl Mech*, 1978, **18**, pp 123-176.
110. SHIMA, N. A Reynolds-stress model for near-wall and low-Reynolds-number regions, *ASME J Fluids Engineering*, 1988, **110**, pp 38-44.
111. LIEN, F-S, and LESCHZINER, M.A. Modelling 2D and 3D separation from curved surfaces with variants of second-moment closure combined with low-Re near-wall formulations, 1993, Proc 9th Symposium Turbulent Shear Flows, Kyoto, 13.1.1-13.1.6.
112. LIEN, F.S. and LESCHZINER, M.A. A pressure-velocity solution strategy for compressible flow and its application to shock–boundary-layer interaction using second-moment turbulence closure, *J Fluids Engineering*, 1993, **115**, pp 717-725.
113. LIEN, F.S. Computational Modelling of 3D Flow in Complex Ducts and Passages, 1992, PhD thesis, University of Manchester.
114. LESCHZINER, M.A. and INCE, N.Z. Computational modelling of three-dimensional impinging jets with and without cross flow using second-moment closure, Computers and Fluids, 1995, **24**, pp 811-832.
115. HANJALIC, K., HADZIC, I. and JAKIRLIC, S. Modelling the turbulent wall flows subjected to strong pressure variations, *ASME J Fluids Engineering*, 1999, **121**, pp 57-64.
116. RODI, W. A new algebraic relation for calculating the Reynolds stresses, *Z Angew Math Mech*, 1976, **56**, pp 219-221.
117. POPE, S.B. A more general effective-viscosity hypothesis, *J Fluid Mech*, 1975, **72**, pp 331-340.
118. LAUNDER, B.E., REECE, G.J. and RODI, W. Progress in the development of Reynolds-stress turbulence closure, *J Fluid Mech*, 1975, **68**, pp 537-566.
119. FU, S., LESCHZINER, M.A. and LAUNDER, B.E. Modelling strongly swirling recirculating jet flow with Reynolds-stress transport closure, 1987, Proc 6th Symposium on Turbulent Shear Flow, Toulouse, 17.6.1-17.6.6.
120. GIRIMAJI, S.S. A Galilean invariant explicit algebraic Reynolds stress model for turbulent curved flows, *Physics of Fluids*, 1997, pp 1067-1077.
121. RUMSEY, C.L., GATSKY, T.L. and MORRISON, J.H. Turbulence model predictions of extra strain rate effects in strongly curved flows, 1999, Paper AIAA 99-157.
122. WALLIN, S. and JOHANSSON, A.V. Modelling of streamline curvature effects on turbulence in explicit algebraic Reynolds stress turbulence models, 2001, Proc Second Int Symp on Turbulence and Shear Flow Phenomena, Stockholm, pp 223-228.
123. JONGEN, T. and GATSKI, T.B. General explicit algebraic stress relations and best approximation for three-dimensional flows, 1998, *Int J Engineering Science*, **36**, pp 739-763.
124. WALLIN, S. and JOHANSSON, A.V. An explicit algebraic Reynolds stress model for incompressible and compressible turbulent flows, *J Fluid Mech*, 2000, **403**, pp 89-132.
125. XU, X-H. and SPEZIALE, C.G. Explicit algebraic stress model of turbulence with anisotropic dissipation, *J AIAA,* 1996, **34**, pp 2186-2189.
126. JOHANSSON, M.C., KNOELL, J. and TAULBEE, D.B. Monlinear stress-strain model accounting for dissipation anisotropies, *J AIAA*, 2000, **38**, pp 2187-2189.
127. SAFFMAN, P.G. Results of a two-equation model for turbulent and development of a relaxation stress model for application to straining and rotating flows, Proc Project SQUID Workshop on Turbulence in Internal Flows, MURTHY, S. (Ed), Hemisphere Press, 1977, pp 191-231.
128. WILCOX, D.C. and RUBESIN, M.W. Progress in turbulence modelling for complex flow field including effects of compressibility, 1980, NASA TP1517.
129. SPEZIALE, C.G. On nonlinear $K - l$ and $K - \varepsilon$ models of turbulence, *J Fluid Mech*, 1987, **178**, pp 459-475.
130. YOSHIZAWA, A. Statistical analysis of the derivation of the Reynolds stress from its eddy-viscosity representation, *Phys of Fluids*, 1987, **27**, pp 1377-1387.
131. SHIH, T-H., ZHU, J. and LUMLEY, J.L. A realisable Reynolds stress algebraic equation model, 1993, NASA TM105993.
132. RUBINSTEIN, R. and BARTON, J.M. Non-linear Reynolds stress models and the renormalisation group, *Phys Fluids A*, 1990, **2**, pp 1472-1476.
133. GATSKI, T.B. and SPEZIALE, C.G. On explicit algebraic stress models for complex turbulent flows, *J Fluid Mech*, 1993, **254**, pp 59-78.
134. CRAFT, T.J., LAUNDER, B.E. and SUGA, K. Development and application of a cubic eddy-viscosity model of turbulence, *Int J Num Meth in Fluids*, 1996, **17**, pp 108-115.
135. LIEN, F.S. and DURBIN, P.A. 1996, Non-linear k-v2 modelling with application to high-lift, Proc Summer Prog, Centre For Turbulence Research, Stanford University, pp 5-22.
136. LIEN, F.S., CHEN, W.L. and LESCHZINER, M.A. Low-Reynolds-number eddy-viscosity modelling based on non-linear stress-strain/vorticity relations, *Engineering Turbulence Modelling and Measurements 3,* RODI W. and BERGELES, G. (Eds), 1996, Elsevier, pp 91-100.
137. TAULBEE, D.B., SONNENMEIER, J.R. and WALL, K.M. 1993, Application of a new non-linear stress-strain model to axisymmetric turbulent swirling flows, *Engineering Turbulence Modelling and Experiments 2*, RODI W. and MARTELLI, F.A. (Eds), 1993, Elsevier, pp 103-112.
138. WALLIN, S. and JOHANSSON, A.V. 1997, A new explicit algebraic Reynolds stress turbulence model for 3D flows, Proc 11th Symp. on Turbulent Shear Flows, DURST, F. *et al*, (Eds), 1997, Grenoble, 13.13-13.17.
139. RUNG, T., FU, S. and THIELE, On the realisability of non-linear stress-strain relation for Reynolds-stress closures, *Flow, Turbulence and Combustion*, 1999, **60**, pp 333-359.

140. APSLEY, D.D. and LESCHZINER, M.A. A new low-Reynolds-number nonlinear two-equation turbulence model for complex flows, *Int J Heat and Fluid Flow*, 1998, **19**, pp 209-222.
141. H. LOYAU, H., BATTEN, P. and LESCHZINER, M.A. Modeling shock–boundary-layer interaction with nonlinear eddy-viscosity closures, *Flow, Turbulence and Combustion*, 1998, **60**, pp 257-282.
142. TAVOULARIS, S. and CORRSIN, S. Experiment in nearly homogeneous turbulent shear flow with a uniform mean temperature gradient, Part I, *J Fluid Mech*, 1981, **104**, pp 311-347.
143. HUANG, P.G. BRADSHAW, P. and COAKLEY, T.J. Turbulence models for compressible boundary-layers, *J AIAA*, 1994, **32**, pp 735-740.
144. MARVIN, J.G. and HUANG, P.G. Tubulence modelling — progress and future outlook, 1996, Proc of 15th Conf on Numerical Methods in Fluid Dynamics, Monterey, California.
145. MORKOVIN, M.V. 1962, Effects of compressibility on turbulent flows, *Mecanique de la Turbulence*, FAVRE, A. (Ed), Gordon and Breach, NY, pp 367-380.
146. HUANG, P.G., COLEMAN, G.N. and BRADSHAW, P. Compressible turbulent channel flows — DNS results and modelling, *J Fluid Mech*, 1995, **305**, pp 185-218.
147. ZEMAN, O. Dilatation disspation: the concept and application in modelling compressible mixing layers, *Phys Fluids*, 1990, **2**, pp 178-188.
148. SARKAR, S., ERLEBACHER, G., HUSSAINI, M.Y. and KREISS, H.O. The analysis and modelling of dilatational terms in compressible turbulence, *J Fluid Mech*, 1991, **227**, pp 473-493.
149. WILCOX, D.C. *Turbulence Modelling for CFD*, 1993, DCW Industries, La Canada, California.
150. FAUCHET, G., SHO, L., WUNENBERGER, R. and BERTOGLIO, J.P. An improved two-point closure for weakly compressible turbulence and comparison with large-eddy simulations, *Appl Sci Research*, 1997, **57**, pp 165-194.
151. AUPOIX, B., BLAISDELL, G.A., REYNOLDS, W.C. and ZEMAN, O. Modelling the turbulent kinetic energy equation for compressible homogeneous turbulence, *J AIAA*, 1986, **24**, pp 437-443.
152. SARKAR, S. The pressure-dilatation correlation in compressible flows, *Phys Fluid*, 1992, **282**, pp 163-186.
153. ZEMAN, O. New model for super/hypersonic turbulent boundary layers, 1993, Paper AIAA 93-0897.
154. EL BAZ, A.M. and LAUNDER, B.E. Second-moment modelling of compressible mixing layers, *Engineering Turbulence Modelling and Experiments 3*, 1993, Elsevier, pp 63-70.
155. COAKLEY, T.J., HORSTMAN, C.C., MARVIN, J.G., VIEGAS, J.R., BARDINA, J.E., HUANG, P.G. and KUSSOY, M.I. Turbulence compressibility corrections, 1994, NASA TM-108827.
156. HUANG, P.G. Modelling hypersonic boundary layers with second moment closure, 1990, CTR, University of Stanford, Annual Research Briefs, pp 1-13.
157. FRIEDRICH, R. and BERTOLOTTI, F. Ompressibility effects due to turbulent fluctuations, *Appl Sci Research*, 1997, **57**, pp 165-194.
158. COLEMAN, G.N., KIM, J. and MOSER, R.D. A numerical study of turbulent supersonic isothermal wall channel flow, *J Fluid Mech*, 1995, **30**, pp 159-183.
159. SARKAR, S. The stabilising effect of compressibility in turbulent shear flow, *J Fluid Mech*, 1995, **282**, pp 163-186.
160. HARLOW, F.H. and WELCH, J.E. Numerical calculation of time-dependent viscous incompressible flow of fluid with free surface, *Phys Fluids*, 1965, **8**, pp 2182-2189.
161. PATANKAR, S.V. and SPALDING, D.B. *Heat and Mass Transfer in Boundary Layers*, 1970, Second Edition, Intertext, London.
162. CHORIN, J. Numerical solution of the Navier-Stokes equations, *Mathematics of Computation*, 1968, **22**, pp 745-762.
163. CHORIN, J. A numerical method for solving incompressible flow problems, *J Comp Phys*, 1967, **2**, pp 12-26.
164. CHORIN, A.J. and MARSDEN, G. *A Mathematical Introduction to Fluid Mechanics*, 1993, Springer-Verlag.
165. ROGERS, S.E., KWAK, D. and KIRIS, C. Steady and unsteady solutions of the incompressible Navier-Stokes equations, *J AIAA*, 1991, **29**, pp 603-610.
166. MERKLE, C.L. and ATHAVALE, M. Time-accurate unsteady incompressible flow algorithms based on artificial compressibility, 1987, AIAA Paper 87-1137.
167. DRIKAKIS, D. Uniformly high-order methods for unsteady incompressible flows, In *Godunov Methods: Theory and Applications*, TORO, E.F. (Ed), 2001, Kluwer Academic Publishers, pp 263-283.
168. BARAKOS, G. and DRIKAKIS, D. Implicit-coupled implementation of two-equation turbulence models in compressible Navier-Stokes methods, *Int J Num Meth Fluids*, 1998, **28**, pp 73-94.
169. DRIKAKIS, D. and GOLDBERG, U. Wall-distance-free turbulence models applied to incompressible flows, *Int J of Comput Fluid Dyn*, 1998, **10**, pp 241-253.
170. KUNZ, R.F. and LAKSHMINARAYAMA, B. Explicit Navier-Stokes computation of cascade flows using the turbulence model, *J AIAA*, 1992, **30**, pp 13-22.
171. LIOU, W.W. and SHIH, T.H. Transonic turbulent flow predictions with two-equation turbulence models, NASA, Lewis, CR, ICOMP (1996).
172. SAHU, J. and DANBERG, J. Navier-Stokes computations of transonic flows with a two equation turbulence model, *J AIAA*, 1986, **24**, pp 1744-1751.
173. GEROLYMOS, G.A. and VALLET, I. Implicit computation of three-dimensional compressible Navier-Stokes equations using k-ε closure, *J AIAA*, 1996, **34**, pp 1321-1330.
174. LIN *et al.*
175. CHAKRAVARTHY, S.R. High resolution upwind formulations for the Navier-Stokes equations, 1988, VKI Lecture Series, *Comp Fluid Dyns*, 1988-05.
176. EBERLE, A. 3D Euler calculations using characteristic flux extrapolation, 1985, Paper AIAA-85-0119.
177. ZOLTAK, J. and DRIKAKIS, D. Hybrid upwind methods for the simulation of unsteady shock-wave diffraction over a cylinder, *Computer Methods in Appl Mech & Eng*, 1998, **162**, pp 165-185.
178. SCHMATZ, M.A., BRENNEIS, A. and EBERLE, A. Verification of an implicit relaxation method for steady and unsteady viscous flow problems, 1988, AGARD CP 437, 15.1-15.33.
179. DRIKAKIS, D and DURST, F. Investigation of flux formulae in transonic shock wave/Turbulent boundary layer interaction, *Int J Num Meth Fluids*, 1994, **18**, pp 385-413.
180. CHEN, J.P. and WHITFIELD, D.L. Navier-Stokes calculations for the unsteady flowfield of turbomachinery, 1993, Paper AIAA-93-0676.
181. EBERLE, A., Rizzi, A. and HIRSCHEL, E.H. Numerical solutions of the Euler equations for steady flow problems, *Notes on Numerical Fluid Mechanics*, 1992, **34**, Vieweg Verlag.
182. DRIKAKIS, D. SCHRECK, E., and DURST, F. Performance analysis of viscous flow computations on various parallel architectures, *ASME J of Fluids Eng*, 1994, **116**, pp 835-841.
183. DRIKAKIS, D. and DURST, F. Parallelisation of inviscid and viscous flow solvers, *Int J of Comp Fluid Dyn*, 1994, **3**, pp 101-121.
184. BARAKOS, G. and DRIKAKIS, D. An implicit unfactored method for unsteady, turbulent compressible flows with moving boundaries, *Computers & Fluids*, 1999, **28**, pp 899-921.
185. MORRISON, J.H. A compressible Navier-Stokes solver with two-equation and Reynolds stress closure models, 1992, NASA CR 4440.
186. VALLET, I. Aerodynamique Numerique 3D Instationnaire avec Fermature bas-Renolds au Second Ordre, 1995, Doctoral Thesis, Universite Paris 6.
187. BATTEN, P., LESCHZINER, M.A. and GOLDBERG, U.G. Average state Jacobians and implicit methods for compressible viscous and turbulent flows, *J Comp Phys*, 1997, **137**, pp 38-78.
188. LIU, F. Multigrid Solution of the Navier-Stokes Equations with a two-equation turbulence model, *Frontiers of Computational Fluid Dynamics*, CAUGHEY, D.A. and HAFEZ, M.M. (Eds), 1994, John Wiley and Sons, pp 339-359.
189. LIU, F. and ZHENG, X. A staggered finite volume scheme for solving cascade flow with a two-dimensional model of turbulence, 1993, Paper AIAA 93-1912.
190. MERCI, B., STEELANT, J., VIERENDEELS, J., RIEMSLAGH, K. and DICK, E. Computation treatment of source terms in two-equation turbulence models, *J AIAA*, 2000, **38**, pp 2085-2093.
191. BACHALO, W.D. and JOHNSON, D.A. Transonic turbulent boundary layer separation generated on an axisymmetric flow model, *J AIAA*, 1986, **24**, pp 437-443.
192. JOHNSON, D.A., HORSTMAN, C.C. and BACHALO, W.D. Comparison between experiment and prediction for a transonic turbulent separated flow, *J AIAA*, 1982, **20**, pp 737-744.
193. KLINE, S.J., CANTWELL, B.J. and LILLEY, G.M. Proc 1980-81 AFSOR-HTTM-Stanford Conference on Complex Turbulent Flows, 1981, Stanford University, Stanford, California.
194. BARAKOS, G. and DRIKAKIS, D. Investigation of non-linear eddy-viscosity models in shock–boundary-layer interaction, *AIAA J*, 2000, **38**, pp 461-469.
195. DÉLERY, J.M. Experimental investigation of turbulence properties in transonic shock–boundary-layer interactions, *J AIAA*, 1983, **21**, pp 180-185.
196. KARKI, K.C. and PATANKAR, S.V. A pressure-based calculation procedure for viscous flows at all speeds in arbitrary configurations, *J AIAA*, 1989, **27**, pp 1167-1174.

197. MCGUIRK, J.J. and PAGE, G.J. Shock-capturing using a pressure-correction method, 1989, AIAA Paper, 27th Aerospace Sciences Meeting, Reno.
198. KOBAYASHI, M.H. and PEIRERA, J.C.F. Prediction of compressible viscous flows at all Mach numbers using pressure correction, collocated primitive variables and non-orthogonal meshes, 1992, Paper AIAA-92-0548.
199. LIEN, F-S. and LESCHZINER, M.A. A general non-orthogonal finite volume algorithm for turbulent flow at all speeds incorporating second-moment closure. Part I: Numerical implementation, *Comp Meth Appl Mech Eng*, 1994, **114**, pp 123-148.
200. SHYY, W., CHEN, M-H. and SUN, C-S. A pressure-based FMG/FAS algorithm for flow at all speeds, 1992, Paper AIAA-92-0426.
201. KLEIN, R. Semi-implicit extension of a Godunov-type scheme based on low Mach number asymptotics, *J Comp Phys*, 1995, **121**, pp 213-237.
202. SESTERHENN, J., MUELLER, B. and THOMANN, H. On the cancellation problem in calculating compressible low Mach number flows, *J Comp Phys*, 1999, **151**, pp 597-615.
203. DRIKAKIS, D. and BAGABIR, A. On Godunov-type methods for low Mach number flows, 2000, CD-ROM Proceedings of the ECCOMAS 2000 Conference, Barcelona.
204. LESCHZINER, M.A. and LIEN, F-S. Numerical aspects of applying second-moment closure to complex flows, *Closure Strategies for Turbulent and Transitional Flows*, 2001, LAUNDER, B.E. and SANDHAM, N.D. (Eds), Cambridge University Press.
205. HUANG, P.G. and Leschziner, M.A. Stabilisation of recirculating flow computations performed with second-moment closure and third-order discretisation, 1985, Proc 5th Symp on Turbulent Shear Flow, Cornell University, 20.7-20.12.
206. LIEN, F-S. and LESCHZINER, M.A. Modelling 2D separation from high-lift aerofoils with a non-linear eddy-viscosity model and second-moment closure, *Aeronaut J*, April 1995, **99**, (984), pp 125-144.
207. LIEN, F-S. and LESCHZINER, M.A. 1997, Computational modelling of separated flow around streamlined body at high incidence, *Aeronaut J*, June/July 1997, **101**, (1006), pp 269-275.
208. HASAN, R.G.M. and MCGUIRK, J.J. Assessment of turbulence model performance for transonic flow over an axisymmetric bump, *Aeronaut J*, January 2001, **105**, (1043), pp 17-31.
209. HASAN, R.G.M., MCGUIRK, J.J., APSLEY, D.D. and LESCHZINER, M.A. A turbulence model study of separated 3D jet/afterbody flow, *Aeronaut J*, January 2004, **108**, (1079), pp 1-14.
210. HAASE, W., BRANDSMA, F., ELSHOLZ, E., LESCHZINER, M.A. and SCHWAMBORN, D. (Eds). EUROVAL — A European Initiative on Validation of CFD Codes — Results of the EC/BRITE-EURAM Project EUROVAL, 1990-1992, *Notes on Numerical Fluid Mechanics*, 1993, **42**, Vieweg Verlag.
211. HAASE, W., CHAPUT, E., ELSHOLZ, E., LESCHZINER, M.A. and MÜLLER, U.R. (Eds) ECARP: European Computational Aerodynamics Research Project. II: Validation of CFD Codes and Assessment of Turbulent Models, *Notes on Numerical Fluid Mechanics*, 1996, **58**, Vieweg Verlag.
212. DERVIEUX, A., BRAZA, F. and DUSSAUGE, J-P. (Eds), Computation and Comparison of Efficient Turbulence Models for Aeronautics – European Research Project ETMA, *Notes on Numerical Fluid Mechanics*, 1998, **65**, Vieweg Verlag.
213. DELERY, J. Investigation of strong turbulent boundary-layer interaction in 2D flows with emphasis on turbulence phenomena, 1981, Paper AIAA 81-1245.
214. HORSEMAN, C.C. Prediction of hypersonic shock wave/turbulent boundary layer interaction flows, 1987, Paper AIAA 87-1367.
215. DOLLING, D.S. High-speed turbulent separated flows: consistency of mathematical models and flow physics, *J AIAA*, 1998, **36**, pp 725-732.
216. Menter, F.R., Performance of popular turbulence models for attached and separated adverse pressure gradient flows, *J AIAA*, 1992, **30**, pp 2066-2072.
217. ROBINSON, D.F. and HASAN, H.A. Further developments of the k-ζ (enstrophy) turbulence closure model, *J AIAA*, 1998, **36**, pp 1825-1833.
218. JANG, Y-J., TEMMERMAN, L. and LESCHZINER, M.A. Investigation of anisotropy-resolving turbulence models by reference to highly-resolved LES data for separated flow, 2001, CD-ROM proc ECCOMAS 2001 conf, Swansea.
219. HUANG, P.G. Validation of turbulence model – uncertainties and measures to reduce them, 1997, Proc ASME FED Summer Meeting, 22-26 June 1997.
220. DRIVER, D.M. Reynolds shear stress measurements in a separated boundary layer, 1991, Paper AIAA 91-1787.
221. RUNG, T., LUEBKE, H., FRANKE, M., XUE, L., THILE, F. and FU, S. Assessment of explicit algebraic stress models in transonic flows, *Engineering Turbulence Modelling and Experiments 4*, 1999, RODI, W. and LAURENCE, D. (Eds), Elsevier, 659-668.
222. SCHMITT, V. and CHARPIN, F. Pressure distributions on the ONERA M6 wing at transonic Mach numbers, AGARD AR-138 (179).
223. OBI, S., AOKI, K. and MASUDA, S. Experimental and computational study of turbulent separated flow in an asymmetric diffuser, Proc 9th Symp on Turbulent Shear Flows, Kyoto, 1993, pp 305-307.
224. BARAKOS, G. and DRIKAKIS, D. Assessment of various low-Re turbulence models in shock boundary layer interaction, *Computer Methods in Applied Mechanics and Engineering*, 1998, **160**, pp 155-174.
225. BARAKOS, G., DRIKAKIS, D. and LEFEBRE, W. Improvement to numerical predictions of aerodynamic flows using experimental data assimilation, *J Aircr*, 1999, **36**, (3), pp 611-614.
226. ABID, R., RUMSEY, C. and GATSKI, T.B. Prediction of non-equilibrium turbulent flows with explicit algebraic stress models, *J AIAA*, 1995, **33**, pp 2026-2031.
227. ABID, R., MORRISON, J.H., GATSKI, T.B. and SPEZIALE, C.G. Prediction of aerodynamic flows with a new explicit algebraic stress model, *J AIAA*, 1996, **34**, pp 2632-2635.
228. HAIDINGER, F.A. and FRIEDRICH, R. Computation of shock wave–boundary layer interactions using a two-equation model with compressibility corrections, *Appl Scientific Research*, 1993, **51**, pp 501-505.
229. HAIDINGER, F.A. and FRIEDRICH, R. Numerical simulation of strong shock/turbulent boundary layer interaction using a Reynolds stress model, *Zeitschrift der Flugwissenschaften und Weltraumforschung*, 1995, **19**, pp 10-18.
230. CORATEKIN, T. SCHUBERT, A. and BALLMANN, J. Assessment of eddy-viscosity models in 2D and 3D shock–boundary-layer interactions, *Engineering Turbulence Modelling and Experiments 4*, RODI, W. and LAURENCE, D. (Eds), Elsevier, pp 649-658.
231. ZHOU, G., DAVIDSON, L. and OLSSON, E. Turbulent transonic airfoil flow simulation using a pressure-based algorithm, *J AIAA*, 1995, **33**, pp 42-47.
232. SRINIVASAN, G.R., EKATERINARIS, J.A. and MCCROSKEY, W.J. Dynamic stall of an oscillating wing, 1993, Part 1: Evaluation of turbulence models, Paper AIAA 93-3403.
233. EKATERINARIS, J.A. and MENTER, F.R. Computation of oscillating airfoil flows with one and two-equation turbulence models. *J AIAA*, 1994, **32**, pp 2359-2365.
234. LESCHZINER, M.A., LOYAU, H. and APSLEY, D.D. Prediction of shock–boundary-layer interaction with non-linear eddy-viscosity models, 2000, CD-ROM Proc European Congress on Computational Methods in Applies Sciences and Engineering, ECCOMAS 2000, Barcelona.
235. WU, X. and SQUIRES, K.D. Prediction of the three-dimensional turbulent boundary layer over a swept bump, *J AIAA*, 1998, **36**, pp 505-514.
236. VANDROMME, D. and HAMINH, H. Physical analysis for turbulent boundary-layer–shock-wave interactions using second-moment closure predictions, *Turbulent Shear-Layer/Shock-Wave Interactions*, DELERY, J. (Ed), 1985, Springer, pp 127-136.
237. BENAY, R., COET, M.C. and DELERY, J. A study of turbulence modelling in transonic shock-wave/boundary-layer interactions, 1987, Proc of 6th Symp on Turbulent Shear Flows, Toulouse, 8.2.1-8.2.6.
238. LESCHZINER, M.A., DIMITRIADIS, K.P. and PAGE, G. Computational modelling of shock wave–boundary layer interaction with a cell-vertex scheme and transport models of turbulence, *Aeronaut J*, February 1993, **97**, (962), pp 43-61.
239. MORRISON, J.H., GATSKI, T.B., SOMMER, T.P. and SO, R.M.C. Evaluation of a near-wall turbulent closure model in predicting compressible ramp flows, *Near-Wall Turbulent Flows*, SO, R.M.C., SPEZIALE, C.G. and LAUNDER, B.E. (Eds), 1993, Elsevier, pp 239-250.
240. CHENAULT, C.F. and BERAN, P.S. K-ε and Reynolds stress turbulence model comparisons for two-dimensional injection flows, *J AIAA*, 1998, **36**, pp 1401-1412.
241. CHENAULT, C.F., BERAN, P.S. and BOWERSOX, R.D.W. Numerical investigation of supersonic injection using a Reynolds-stress turbulence model, *J AIAA*, 1999, **37**, pp 1257-1269.
242. GEROLYMOS, G.A. and VALLET, I. Near-wall Reynolds-stress three-dimensional transonic flow computation, *J AIAA*, 1997, **35,** pp 228-236.
243. DRIKAKIS, D. and BARAKOS, G. Numerical developments in unsteady aerodynamic flows, 2000, CD-ROM Proc ECCOMAS Conference, Forum: CFD in Aeronautics, Industrial Technology Session organised by EU, Barcelona, 2000.

244. HUANG, P.G. and COAKLEY, T.J. Modelling hypersonic flows with second-moment closure, *Near-Wall Turbulent Flows*, SO, R.M.C., SPEZIALE, C.G. and LAUNDER, B.E. (Eds), 1993, Elsevier, pp 199-208.
245. MEIER, H.U., KREPLIN, H.P., LANDHAUSER, A. and Baumgarten D. Mean velocity distribution in 3D boundary layers developing on a 1:6 prolate spheroid with artificial transition, 1984, DFVLR Report IB 222-84 A11.
246. DAVIDSON, L. Reynolds stress transport modelling of shock induced separated flow, *Computers & Fluids*, 1995, **24**, pp 253-268.
247. POT, T., DELERY, J. and QUELIN, C. Interaction choc-couche limite dans un canal tridimensionnel — nouvelles experiences en vue de la validation du code CANARI, 1991, ONERA TR-92/7078 AY.
248. LESCHZINER, M.A., BATTEN, P. and LOYAU, H. Modelling shock-affected near-wall flows with anisotropy-resolving turbulence closures, *Int J Heat and Fluid Flow*, 2000, **21**, pp 239-251.
249. BARAKOS, G. and DRIKAKIS, D. Unsteady separated flows over manouvring lifting surfaces, Phil Trans Royal Soc London. A, 2000, **358**, pp 3279-3291.
250. PUTNAM, L.E. and MERCER, C.E. Pitot-pressure measurements in flow fields behind a rectangular nozzle with exhaust jet for free-stream Mach numbers of 0, 0·6 and 1·2. 1986, NASA TM 88990.
251. FLEMING, J.L., SIMPSON, R.L., COWLING, J.E. and DEVENPORT, W.J. An experimental study of wing-body junction and wake flow, *Experiments in Fluids*, 1993, **14**, pp 366-378.
252. RUMSEY, C.L., GATSKY, T.B., YING, S.X. and BERTELRUD, A. Prediction of high-lift flows using turbulent closure models, *J AIAA*, 1998, **36**, pp 765-774.
253. COUSTEIX, J. and HOUDEVILLE, R. Effects of unsteadiness on turbulent boundary layers, 1983, von Karman Inst for Fluid Dynamics, Lecture Series 1983-03.
254. POWER, G.D., VERDON, J.M. and KOUSEN, K.A. Analysis of unsteady compressible viscous layers, Tran *ASME J Turbomachinery*, 1991, **133**, pp 644-653.
255. MANKBADI, R.R. and MOBARAK, A. Quasi-steady turbulence modelling of unsteady flows, *Int J Heat and Fluid Flow*, 1991, **12**, pp 122-129.
256. JUSTESEN, P. and SPALART, P.R. Two-equation turbulence modelling of oscillating boundary layers, 1990, Paper AIAA 90-0496.
257. FAN, S., LAKSHMINARAYANA, B. and BARNETT, M. Low-Reynolds-number k-ε model for unsteady turbulent boundary layers, *J AIAA*, 1993, **31**, pp 1777-1784.
258. DAFA'ALLA, A.A., JUNTASARO, E. and GIBSON, M.M. Calculation of oscillating boundary layers with the q-ζ turbulence model, *Eng Turbulence Modelling and Experiments*, 1996, **3**, pp 141-150.
259. SHIMA, N. Prediction of turbulent boudary layers with a second-moment closure: Part 1, Tran *ASME J Fluids Eng*, 1993, **115**, pp 56-63.
260. HA MINH, H., VIEGAS, J.R., RUBESIN, M.W., VANDROMME, D.D. and SPALART, P. Physical analysis and second-order modelling of an unsteady turbulent flow: The oscillating boundary layer on a flat plate, 7th Symp on Turbulent Shear Flows, Stanford, CA, (1989), 11.5.1-11.5.6.
261. HANJALIC, K., JAKIRLIC, S. and HADZIC, I. Computation of oscillating turbulent flows at transitional Reynolds number, 1993, 9th Symp on Turbulent Shear Flows, Kyoto, Japan, 1.4.1 – 1.4.6.
262. SPALART, P.R. and BALDWIN, B.S. Direct numerical simulation of turbulent oscillating boundary layer, *Turbulent Shear Flows,* 1989, Springer, pp 417-440.
263. KANI, A.R. Investigation of Turbulence Models in Oscillating Turbulent Flows, 2000, PhD dissertation, Queen Mary, University of London.
264. JENSEN, B.L., SUMER, B.M. and FREDSOE, J. Turbulent oscillating boundary layers at high Reynolds numbers, *J Fluid Mech*, 1989, **206**, pp 265-297.
265. HINO, M., KASHIWAYANAGI, M., NAKAYAMA, A. and HARA, T. Experiments on the turbulence statistics and the structure of a reciprocating oscillatory flow, *J Fluid Mech*, 1983, **133**, pp 363-400.
266. BARAKOS, G. and DRIKAKIS, D. Numerical simulation of transonic buffet flows using various turbulence closures, *Int J Heat and Fluid Flow*, 2000, **21**, pp 620-626.
267. TELIONIS, D.P. Unsteady boundary layers, separated and attached, paper 16, AGARD CP-227, *Unsteady Aerodynamics*, 1977, Ottawa.
268. MEHTA, U.B. and LAVAN, Z. Starting vortex, separation bubbles and stall: A numerical study of laminar unsteady flow around an airfoil, *J Fluid Mechs*, 1975, **67**, pp 227-256.
269. GULCAT, U. Separate Numerical Treatment of Attached and Detached Flow Regions in General Viscous Flows, 1981, PhD thesis, Georgia Institute of Technology, Atlanta, Georgia.
270. MCCROSKEY, W.J., MCALISTER, K.W., CARR, L.W., LAMBERT, O. and INDERGRAND, R.F. Dynamic stall of advanced airfoil sections, *J American Helicopter Soc*, 1991, pp 40-50.
271. WU, J.C., WANG, C.M. and TUNCER, I.H. Unsteady aerodynamics of rapidly pitched airfoil, 1986, Paper AIAA 86-1105.
272. TUNCER, I.H., WU, J.C. and WANG, C.M. Theoretical and numerical studies of oscillating airfoils, *J AIAA*, 1990, **28,** pp 1615-1624.
273. AGARD Advisory Report No 702, *Compendium of Unsteady Aerodynamic Measurements*, 1982.
274. MCCROSKEY, W.J., MCALISTER, K.W., CARR, L.W. and PUCCI, S.L. An experimental study of dynamic stall on advanced airfoil sections, 1982 Vol 1: Summary of the experiment, NASA-TM-84245-VOL-1.
275. CARR, L.W. Progress in analysis and prediction of dynamic stall, *J Aircr*, 1988, **25**, pp 6-17.
276. VISBAL, M.R. Effect of compressibility on dynamic stall, 1988, Paper AIAA Paper 88-0132.
277. PIZIALI, R.A. An experimental investigation of 2D and 3D oscillating wing aerodynamics for a range of angle of attack including stall, 1993, NASA-TM-4632.
278. GUO, W.H., FU, D.X. and WA, Y.W. Numerical investigation of dynamic stall of an oscillating aerofoil, *Int J for Num Methods in Fluids*, 1994, **19**, pp 723-734.
279. MCDEVITT, J.B. and OKUNO, A.F. Static and dynamic pressure measurements on a NACA 0012 airfoil in the Ames High Reynolds Number Facility, 1985, NASA-TP-2485, NASA Ames, CA.
280. MCDEVITT, J.B., LEVY, L.L. and DEIWERT, G.S. Transonic flow about a thick circular-arc airfoil, *J AIAA*, 1976, **14**, pp 606-613.
281. SOFIALIDIS, D. and PRINOS, P. Development of a non-linear strain-sensitive k-ω turbulence model, 1997, Proc of the 11th TSF-11 Conference, Grenoble, France, 2-89 – 2-94.
282. RIDER, W. and DRIKAKIS, D. High resolution methods for computing turbulent flows, *Turbulent Flow Computation*, DRIKAKIS, D. and GEURTS, B. (Eds), 2002, Kluwer Academic Publisher, 2002, pp 43-74.
283. ORAN, E.S. and BORIS, J.P. *Numerical Simulation of Reactive Flow*, 2001, Elsevier.
284. DRIKAKIS, D. Numerical issues in very large eddy simulation. CD-ROM, 2001, Proc of the ECCOMAS CFD 2001 Conference, Swansea, UK.
285. SPALART, P.R., JOU, W-J., STRELETS, M. and ALLMARAS, S.R. Comments on the feasibility of LES for wings and on the hybrid RANS/LES approach, 1997, Advances in DNS/LES, 1st AFOSR Int Conf on NDS/LES, Greden Press.